UNCLASSIFIED
SECURITY CLASSIFICATION OF THIS PAGE

MASTER COPY - FOR REPRODUCTION PURPOSES

2

REPORT DOCUMENTATION PAGE

AD-A217 496

	1b. RESTRICTIVE MARKINGS
	3. DISTRIBUTION/AVAILABILITY OF REPORT Approved for public release; distribution unlimited.
4. PERFORMING ORGANIZATION REPORT NUMBER(S)	5. MONITORING ORGANIZATION REPORT NUMBER(S) ARO 26911.1-EL-CF
6a. NAME OF PERFORMING ORGANIZATION Palisades Inst for Res Services, Inc.	6b. OFFICE SYMBOL (If applicable)
	7a. NAME OF MONITORING ORGANIZATION U. S. Army Research Office
6c. ADDRESS (City, State, and ZIP Code) New York, NY 10014-4899	7b. ADDRESS (City, State, and ZIP Code) P. O. Box 12211 Research Triangle Park, NC 27709-2211
8a. NAME OF FUNDING/SPONSORING ORGANIZATION U. S. Army Research Office	8b. OFFICE SYMBOL (If applicable)
	9. PROCUREMENT INSTRUMENT IDENTIFICATION NUMBER DAAL03-89-G0097
8c. ADDRESS (City, State, and ZIP Code) P. O. Box 12211 Research Triangle Park, NC 27709-2211	10. SOURCE OF FUNDING NUMBERS PROGRAM ELEMENT NO. / PROJECT NO. / TASK NO. / WORK UNIT ACCESSION NO.

11. TITLE (Include Security Classification)
Workshop on Physics and Chemistry of Mercury Cadmium Telluride

12. PERSONAL AUTHOR(S)
Mark Goldfarb

13a. TYPE OF REPORT	13b. TIME COVERED	14. DATE OF REPORT (Year, Month, Day)	15. PAGE COUNT
Final	FROM 9/1/89 TO 8/31/90	Nov 89	

16. SUPPLEMENTARY NOTATION
The view, opinions and/or findings contained in this report are those of the author(s) and should not be construed as an official Department of the Army position, policy, or decision, unless so designated by other documentation.

17. COSATI CODES		
FIELD	GROUP	SUB-GROUP

18. SUBJECT TERMS (Continue on reverse if necessary and identify by block number)
Mercury Cadmium Telluride, II-VI Compounds, Compound Defects, Compounds Impurities, Novel Material

19. ABSTRACT (Continue on reverse if necessary and identify by block number)
The workshop was held as scheduled. A report containing extended abstracts of the workshop has been prepared and distributed.

20. DISTRIBUTION/AVAILABILITY OF ABSTRACT	21. ABSTRACT SECURITY CLASSIFICATION
☐ UNCLASSIFIED/UNLIMITED ☐ SAME AS RPT. ☐ DTIC USERS	Unclassified
22a. NAME OF RESPONSIBLE INDIVIDUAL	22b. TELEPHONE (Include Area Code) / 22c. OFFICE SYMBOL

DD FORM 1473, 84 MAR — 83 APR edition may be used until exhausted. All other editions are obsolete.

SECURITY CLASSIFICATION OF THIS PAGE
UNCLASSIFIED

ARO 26911.1-EL-CF

EXTENDED ABSTRACTS

THE 1989 U.S. WORKSHOP
on the PHYSICS and CHEMISTRY
of MERCURY CADMIUM TELLURIDE
and RELATED II-VI COMPOUNDS

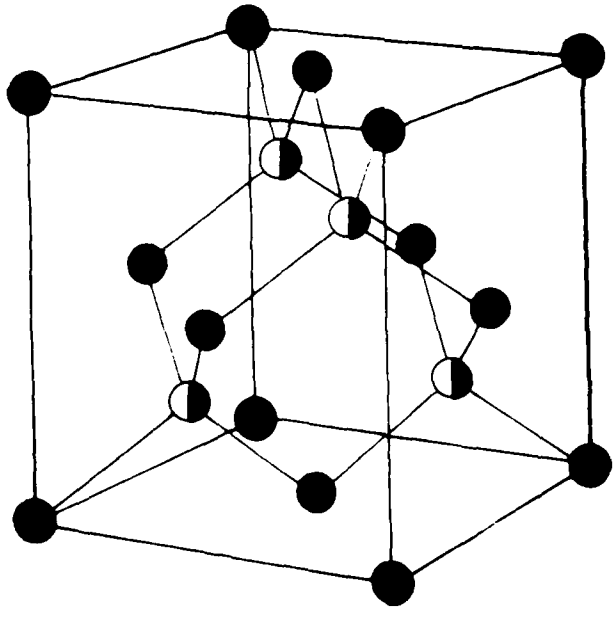

Sponsored by

[illegible]COM Center for Night Vision
and Electro-Optics
[illegible]el Technology
[illegible]search

"The views, opinions, and/or findings contained in this report are those of the author(s) and should not be construed as an official Department of the Army position, policy, or decision, unless so designated by other documentation."

ACKNOWLEDGEMENTS

The Workshop Committee would like to acknowledge the special contributions, pertinent to the success of the Workshop, which were made by the following institutions:

CALIFORNIA INSTITUTE OF TECHNOLOGY

ROCKWELL INTERNATIONAL

SANTA BARBARA RESEARCH CENTER

STANFORD UNIVERSITY

TEXAS INSTRUMENTS

CO-CHAIRMEN

T.N. Casselman
Santa Barbara Research Center
T.C. McGill
California Institute of Technology
C.G. Roberts
Texas Instruments
W.E. Spicer
Stanford University
W.E. Tennant
Rockwell International

PROGRAM COMMITTEE

R.L. Aggarwal
Massachusetts Institute of Technology
J.K. Furdyna
Notre Dame University
E.R. Gertner
Rockwell International
C.E. Jones
Santa Barbara Research Center
M.A. Kinch
Texas Instruments
P.M. Raccah
University of Illinois at Chicago
H.F. Schaake, Proceedings Editor
Texas Instruments
J.F. Schetzina
North Carolina State University
J.L. Schmit
Honeywell

GOVERNMENT ADVISORS

R.D. Graft
CECOM Center for NV&EO
G.H. Griffith
AFWAL
D.G. Seiler
NIST
R.J. Wagner
NRL
H. Wittmann
AFOSR

WORKSHOP COORDINATOR

J. Morreale
Palisades Institute for Research
Services, Inc.

WORKSHOP SPONSORS

CECOM Center for NV&EO
Office of Naval Technology
Air Force Office of Scientific Research
American Vacuum Society

PROGRAM

MONDAY, OCTOBER 2, 1989

7:00-10:00 pm	Pre-Workshop Check-In

TUESDAY, OCTOBER 3, 1989

7:00- 8:00 am	Workshop Check-In
8:00- 8:30 am	Invited Presentation
8:30- 9:50 am	I. Growth
9:50-10:20 am	BREAK
10:20-12:20 pm	I. Growth
12:20- 2:00 pm	LUNCH
2:00- 3:40 pm	I. Growth
3:40- 4:10 pm	BREAK
4:10- 5:50 pm	I. Growth
6:00- 7:30 pm	Wine and Cheese

WEDNESDAY, OCTOBER 4, 1989

7:00- 8:00 am	Workshop Check-In
8:00- 8:30 am	Invited Presentation
8:30-10:10 am	II. Defects and Impurities
10:10-10:40 am	BREAK
10:40-12:20 pm	II. Defects and Impurities
12:20- 1:50 pm	LUNCH
1:50- 3:10 pm	III. Surfaces and Interfaces
3:10- 3:40 pm	BREAK
3:40- 5:00 pm	III. Surfaces and Interfaces
5:00- 6:00 pm	Wine Cheese
6:00- 8:30 pm	Panel Discussion

THURSDAY, OCTOBER 5, 1989

7:00- 8:00 am	Workshop Check-In
8:00- 8:30 am	Invited Presentation
8:30-10:10 am	IV. Novel Materials and Structures
10:10-10:40 am	BREAK
10:40-12:20 pm	IV. Novel Materials and Structures
12:20- 2:00 pm	LUNCH
2:00- 4:00 pm	V. Electronic Properties

Partial Contents:

TABLE OF CONTENTS

Crystal Growth; Molecular Beam Epitaxy

PANEL DISCUSSION: INDUSTRY OF HgCdTe AND PRACTICAL IMPLICATIONS

MBE/ALE GROWTH PROCESSES OF WIDE-BAND-GAP II-VI COMPOUNDS

T. Yao, Z.Q. Zhu[a]. K. Uesugi[b], S. Kamiyama[b], and M. Fujimoto[b]
Electrotechnical Laboratory, 1-1-4 Umezono, Tsukuba, Ibaraki 305, Japan

Recently, thin film growth of wide-band-gap II-VI compounds has attracted considerable attention. One of the most important aims of this research would be achievement of good bipolar conductivity in II-VI compounds. Owing to the progress of thin film growth technology, successful control of electrical and optical properties of n-type ZnSe, which is a typical wide-band-gap II-VI compound, has been achieved [1,2]. Very recently, the growth of p-type ZnSe has been reported. However, there still remains difficult and severe problems in terms of controllability and reproducibility of growth[3-5], although extensive study on incorporation of p-type impurities under various growth conditions has been made so far. We believe that in order to solve these problems, the growth conditions and incorporation procedures of impurities should be examined based on comprehensive understanding of growth processes.

This paper describes comprehensive understanding of growth processes of wide-band-gap II-VI compounds by atomic layer epitaxy (ALE) and MBE. The growth processes have been investigated both experimentally and theoretically. "In situ" RHHED technique has been employed to investigate the growth processes. The surface processes during growth have been analyzed in terms of a simple kinetic model in which the adsorption/desorption processes of impinging constituent molecules (atoms) onto/from the surface takes place via precursor states [6].

The paper consists of 7 parts:

(1) First, RHEED investigation conditions are examined, since RHEED intensity variation is strongly sensitive to the investigation conditions. The relevant surface events are derived through a proper investigation condition. By taking a suitable observation condition, we have observed more than 100 periods of RHEED intensity oscillation during MBE growth of ZnTe (Fig. 1).

(2) The effect of growth interruption is investigated. It is found that a proper timing of growth interruption smooth surface.

(3) Two dimensional layer-by-layer growth manifests in RHEED intensity oscillations during MBE growth. RHEED intensity variation during MBE growth of ZnTe and ZnSe are investigated at various substrate temperatures and molecular beam fluxes. Figure 2 shows RHEED intensity oscillations during MBE growth of ZnSe at various substrate temperatures. Two

dimensional layer-by-layer growth is achieved for substrate temperature range of 120 - 475 °C.

(4) At high substrate temperature, sublimation takes place during MBE or ALE growth. Fig. 3 shows an example of RHEED intensity oscillation during growth interruption of ZnTe at 470 °C. The period of RHEED intensity oscillation corresponds to the sublimation time for a ZnTe mono-molecular layer.

(5) One of the most important findings in this study is that a stabilized RHEED intensity is strongly correlated with surface coverage or surface stoichiometry. Figure 4 shows the dependence of RHEED intensity oscillation on molecular beam flux ratio during MBE growth of ZnSe. When the growth condition is on the Zn rich side, where a c(2x2) reconstruction pattern appears, the RHEED intensity stabilizes near the RHEED intensity level of Zn-covered surface. On going from the Zn rich side to the Se rich side, the RHEED intensity goes from near the Zn-covered surface to the Se-covered surface. Thus, it is possible to characterize rather quantitatively surface stoichiometry during growth by RHEED intensity level.

(6) RHEED intensity variation with time is observed during ALE growth. Adsorption and desorption processes of surface atoms have been investigated. It is found that adsorbed excess atoms (molecules), which may be physisorbed in precursor states, influence considerably ALE growth processes.

(7) Most of the observed results are analyzed in terms of a kinetic model in which the adsorption and desorption processes occur via precursor states.

In conclusion, we have investigated experimentally and theoretically growth processes of MBE/ALE of Zn chalcogenides. It is found that RHEED technique gives rich information on growth processes and surface coverage. The understanding of growth processes are expected to open a way to a good controllability of bipolar conductivity in II-VI compounds.

One of the authors (Z.Q.Z) would like to thank Professor M. Hagino of Shizuoka University for his support and encouragement.

References

a) on leave form Research Institute of Electronics, Shizuoka University, Hamamatsu 432, Japan.

b) on leave from Faculty of Engineering, Tokai University, Hiratsuka 259-12, Japan.

1) T. Yao, in *The Technology and Physics of Molecular Beam Epitaxy*, edited by E.H.C. Parker (Plenum, New York, 1985), Chap. 10.

2) W. Stutius, J. Appl. Phys. 53, 284 (1982).

3) J. Nishizawa, R. Suzuki, and Y. Okuno, J. Appl. Phys. 59, 2256 (1986).
4) T. Yasuda, I. Mitsuishi, and H. Kukimoto, Appl. Phys. Lett. 52, 57 (1988).
5) K. Akimoto, T. Miyajima, and Y. Mori, Phys. Rev. B39, 3138 (1989).
6) Z.Q. Zhu, T. Nomura, M. Miyao, and M. Hagino, J. Cryst. Growth 95, 529 (1989).

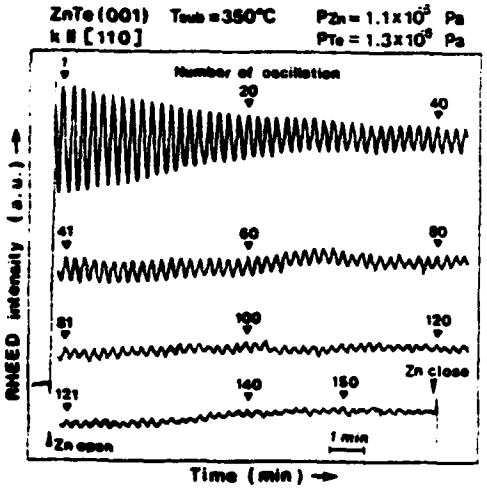

Fig. 1 RHEED intensity oscillations during MBE growth of ZnTe on ZnTe predeposited layer on GaAs (001) with k// [110]. The growth is initiated by impinging Zn flux on the Te-covered surface. The substrate temperature is 350°C, and the Te-to-Zn pressure ratio is 1.

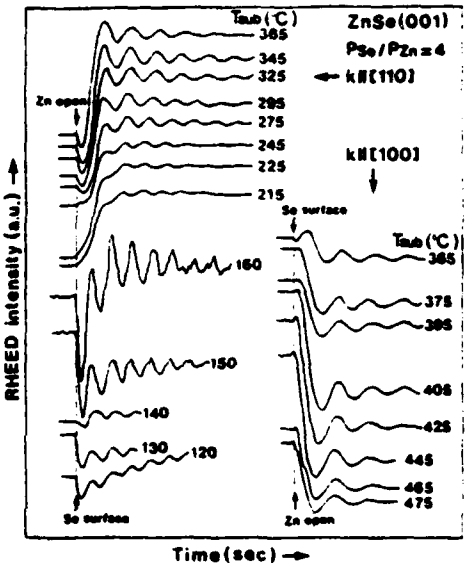

Fig. 2 RHEED intensity oscillations during MBE growth of ZnSe at various substrate temperatures. The Se-to-Zn pressure ratio is 4.

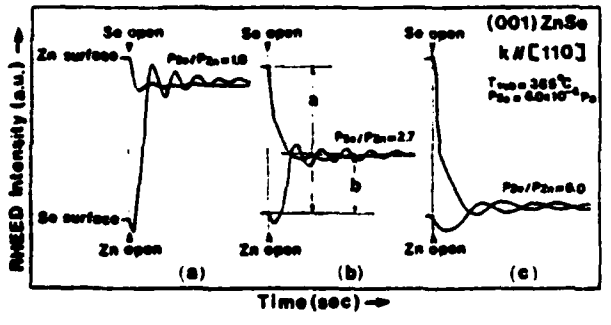

Fig. 3 The dependence of RHEED intensity oscillation on growth condition.

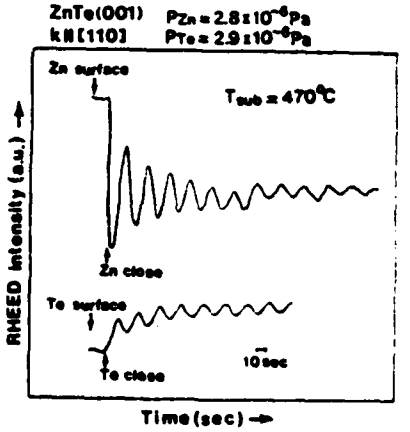

Fig. 4 RHEED intensity oscillation behaviors during sublimation of ZnTe at the substrate temperature of 470°C, initiated from Zn- and Te- covered surfaces respectively.

IN-SITU CALIBRATION OF SURFACE GROWTH TEMPERATURE FOR HgCdTe AND CdTe MOLECULAR BEAM EPITAXIAL GROWTH BY TELLURIUM CONDENSATION

D. Rajavel, J.D. Benson and C.J. Summers
Microelectronics Research Center, Georgia Tech Research Institute, Atlanta, GA 30332.

The properties of HgCdTe and CdTe are very sensitive to the substrate temperature during the growth of these materials by molecular beam epitaxy. Measurements of substrate surface growth temperature by conventional techniques is both inconvenient and often unreliable, and thus does not ensure reproducibility. We report in this paper a new in-situ technique which directly measures the substrate surface growth temperature and which can be used to calibrate substrate holders. The method exploits the fact that the condensation temperature for an incident stream of diatomic tellurium molecules is directly dependent on the flux density. Because of the exponential dependence of this relationship, very accurate surface temperature measurements are in principle possible. Experimental determination of the Te_2 condensation temperature on CdTe surfaces between 150-200°C confirm that condensation occurred when the pressure of the Te_2 flux incident on the substrate exceeded the vapor pressure of Te_2 over CdTe (Fig. 1). In these experiments, the substrate temperature at which condensation occurred for a measured flux of Te_2, was calculated from the equilibrium pressure versus temperature relationship of tellurium. Experimentally, the onset of Te_2 condensation was determined by a pronounced change in the reflection high-energy electron diffraction pattern of the substrate.

This technique was found to be applicable for CdTe substrate temperature measurements in the technologically important 150-200°C range for HgCdTe and CdTe growth. The temperature measurement by this method is accurate on an absolute scale to less than 5°C and reproducible to within 3°C. Recent results using a monomer tellurium gas-source will also be discussed, and compared with results obtained by using a conventional solid dimer tellurium source.

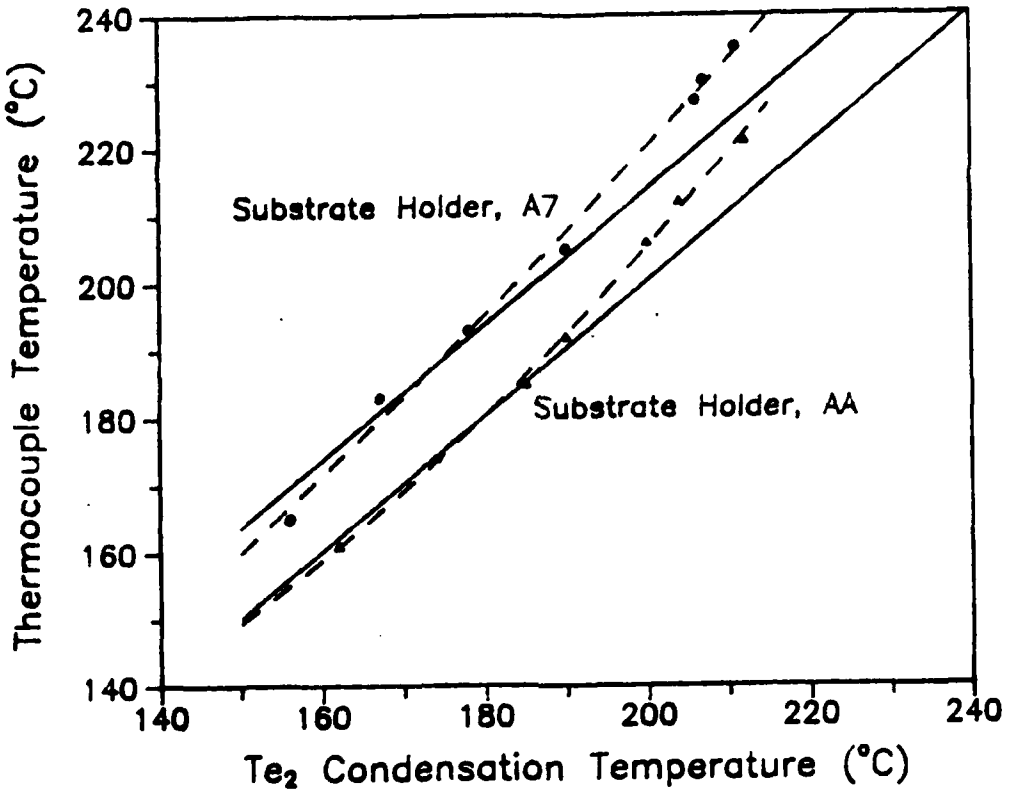

Fig. 1. Substrate thermocouple temperature plotted versus the Te_2 condensation temperature on (001) CdTe surfaces for substrate holders AA and A7. The Te_2 condensation temperature was calculated from the equilibrium vapor pressure versus temperature relationship for tellurium. The dashed lines represent quadratic fits to the experimental data. The solid lines follow from the equilibrium condensation theory and have a slope equal to one. The theory and the experimental data are in good agreement for substrate temperatures between 150-200°C.

The Growth of High Quality CdTe on GaAs by Molecular Beam Epitaxy

J. L. Reno and P. L. Gourley
Sandia National Laboratories

HgCdTe is considered one of the leading semiconductor materials for the production of focal plane arrays for infrared imaging. Advances in this field have been hampered by the lack of high quality material in large enough areas that could be used as a substrate/buffer layer system for the growth of the device structures. CdTe or related II-VI alloys are the standard substrate material but they are typically available in areas of only a few square centimeters. The quality of the CdTe bulk material has been improving but at present is still not as good as needed. The best bulk material presently available has dislocation densities ~ $5 \times 10^4/cm^2$. These substrates have the addition liability of being very fragile.

Because of the problems with CdTe substrates, the growth of CdTe buffer layers on GaAs substrates has been investigated. This growth has been previously demonstrated by many investigators. Since GaAs is available in large areas and is stronger and cheaper than CdTe, it was thought that this would be a solution to the problems with CdTe substrates. The difficulty with this solution is that CdTe and GaAs have very different lattice parameters (~14% mismatch). This causes the quality of the CdTe buffer layers to be quite poor (dislocation densities ~$10^8/cm^2$).

We have studied the use of strained layer superlattices, graded or step buffer layers, and misoriented substrates to improve the quality of CdTe grown on GaAs by MBE. The quality of the CdTe layers has been evaluated by photoluminescence microscopy (PLM). This nondestructive technique provides an image of defects in the layers. Thus information concerning the number, type and location (both across and through the wafer) of the defects can be obtained.

By use of strained layer superlattices, graded or step buffer layers, and misoriented substrates, we have been able to suppress the formation twins in CdTe(111). Also we have been able to grow both CdTe(100) and (111) on GaAs with dislocation densities $\leq 1 \times 10^6/cm^2$. This is a significant improvement of about two orders of magnitude over previously available CdTe on GaAs. The material can dissipate large amounts of power and is therefore quite stable. It can be easily produced in large areas.

Twin-free (111)B Oriented HgCdTe Grown by Photo-Assisted MBE

K.A. Harris, T.H. Myers, R.W. Yanka, and L.M. Mohnkern
Electronics Laboratory, General Electric Company
Syracuse, NY 13221

R.W. Green
Corporate Research and Development Center
General Electric Company
Schenectady, NY 12301

The successful development of second generation HgCdTe IR devices strongly depends on achieving low-noise LWIR diode detectors. LWIR diodes typically exhibit low break down voltages and large dark currents due to excess leakage currents within the space-charge region. The noise associated with these effects adds to the intrinsic resistance noise limits and reduces the R_oA product rapidly as the bandgap of HgCdTe is reduced. Subgrain boundaries, extended dislocations, and planar twinning are contributing sources to these effects. A significant reduction of these microstructural defects will increase the R_oA and, as a result, significantly improve diode performance.

The reduction of microstructural defects is a non-trivial problem for HgCdTe. In particular, the (111)B orientation is plagued by its propensity for planar twinning arising from stacking faults during growth. Growth by conventional MBE produces (111)B films exhibiting extensive planar twinning[1-4]. The technique of Photoassisted Molecular Beam Epitaxy (PAMBE) has already been shown to improve the crystalline properties of HgCdTe.[5] Recently, using the PAMBE technique, we have made significant improvements in the microstructure of (111)B HgCdTe. In particular, we have determined growth conditions which suppress planar twinning and give a reasonable yield of twin free layers with reduced EPD counts for this orientation. This is a significant result because the (111)B orientation is more well-behaved in its electrical properties as compared with the (211)B orientation, and does not suffer from twin formations in the form of pyramidical hillocks as observed for (100) growth. Several films have been grown exhibiting an absence of twinning and average EPD counts as low as $\sim 8 \times 10^4 cm^{-3}$ which is comparable to that obtained from excellent LPE. These results were determined from defect etching and double crystal x-ray diffraction measurements.

[1]R. De Wames, DARPA IR Focal Plane Array Materials and Processing Review, McLean VA (April 5-6, 1988).
[2]J.P. Faurie, DARPA IR Focal Plane Array Materials and Processing Review, McLean VA (April 5-6, 1988).
[3]R.D. Feldman, DARPA IR Focal Plane Array Materials and Processing Review, McLean VA (April 5-6, 1988).
[4]J.M. Arias, S.H. Shin, J.G. Pasko, and E.R. Gertner, Appl. Phys. Lett. 52, 39(1988).
[5]T.H. Myers, R.W. Yanka, K.A. Harris, A.R. Reisinger, J. Han, S. Hwang, Z. Yang, N.C. Giles, J.W. Cook, Jr., J.F. Schetzina, R.W. Green, and S. McDevitt, in the Proceedings of the 1988 Workshop on the Physics and Chemistry of Mercury Cadmium Telluride, Orlando, FL. October 11-13, 1988, to be published in the Journal of Vacuum Science and Technology.

GROWTH OF CdTe, HgTe, AND HgCdTe ALLOYS BY GAS SOURCE MOLECULAR BEAM EPITAXY

R. G. Benz II, B. K. Wagner, and C. J. Summers

Microelectronics Research Center
Georgia Tech Resarch Institute
Atlanta, Georgia 30332

We report the first growth of CdTe, HgTe, and $Hg_{1-x}Cd_xTe$ alloys by gas source molecular beam epitaxy (GSMBE). The layers were grown in a Varian GEN II MBE equipped with a Hg pressure controlled vapor source[1] and direct injection metalorganic Te and Cd gas sources. A special pumping system was designed to meet the handling requirements of the Hg vapor and toxic gas sources. This system includes an 1800 l/s turbomolecular pump and a toxic gas handling unit. The source gasses, diisopropyltellurium (DipTe) and diethylcadmium (DeCd), are precracked in a Varian high temperature injector thus removing the cracking dependence on the growth temperature. Results of the cracking efficiencies of the gas sources as determined by quadrapole mass spectrometry (QMS) will be presented.

Growth of CdTe at substrate temperatures of 180-300 ^{o}C and HgTe and $Hg_{1-x}Cd_xTe$ ($x < 0.3$) at substrate temperatures between 120 and 185 ^{o}C has been achieved on CdTe and GaAs substrates with growth rates of 0.1 - 1.0 um/hr. Figure 1 shows the dependence of CdTe growth rate, as determined by reflection high energy electron diffraction (RHEED) intensity oscillations, on DipTe flow rate for a fixed Cd flux.

Investigations of the different nucleation kinetics and layer properties resulting from conventional and gas source MBE of CdTe and HgTe are presently being conducted with particular reference to the growth enhancement possible by the use of monomer Te as opposed to diatomic Te.[2] Full details of these results will be presented at the conference.

[1]B. K. Wagner, R. G. Benz II, and C. J. Summers, J. Vac. Sci. Technol. A7, 295 (1989)

[2]J. T. Cheung, Appl. Phys. Lett. 51, 1940 (1987)

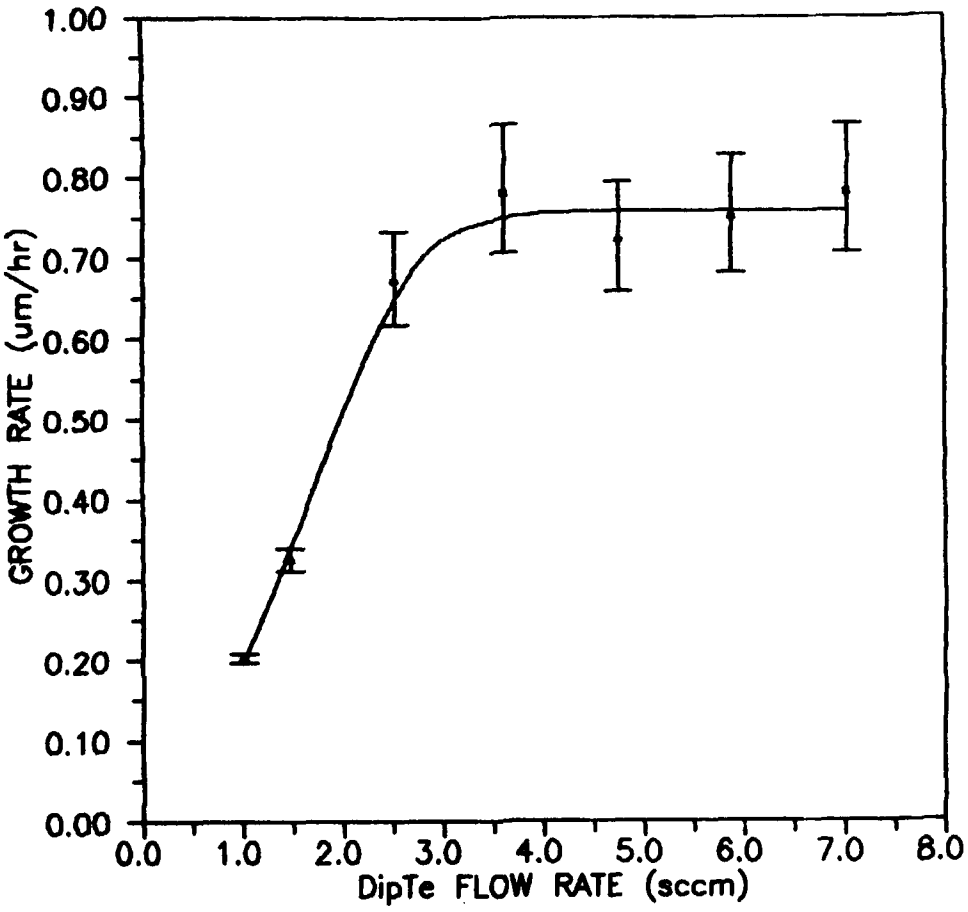

Figure 1. CdTe growth rate, as determined by RHEED intensity oscillations, versus DipTe flow rate at a substrate temperature of 250 ^{o}C and a constant Cd flux

Role of the crystallographic orientation on the incorporation and diffusion of Indium in HgCdTe epilayers grown by Molecular Beam Epitaxy

I.K. Sou, M. Boukerche and J.P. Faurie

Dept. of Physics, University of Illinois at Chicago, Chicago,IL 60680

The incorporation mechanisms of foreign dopant during Molecular Beam Epitaxy (MBE) growth might be strongly dependent upon the orientation of the substrates due to the difference in surface atomic density and stoichiometry. Hall and Secondary Ion Mass Spectroscopy (SIMS) have been used to study HgCdTe epilayers doped with Indium during MBE growth. In a previous paper[1], we have reported the doping behavior of Indium for HgCdTe grown in the (111)B orientation. The data were consistent with a model assuming that most of the Indium atoms were singly ionized in substitutional position on the metal sites, a small fraction of them being incorporated in In_2Te_3 neutral complexes. More recent measurements confirmed this model except that the background acceptor concentration is currently found at least a decade lower i.e. in the low $10^{16}cm^{-3}$ range, in agreement with a better growth control.

In this study, we were surprised to find that the same careful measurements performed on Indium doped epitaxial HgCdTe layers grown in the (100) direction showed an undeniable evidence for more than two electrons being generated for each In atom being incorporated. We suggest that such a high degree of ionization can only be tentatively explained by an interstitial incorporation mechanism. This hypothesis would be in agreement with the presence of Te atoms in antisite positions blocking substantially the In substitution on the metal site in this orientation.

Post-growth capped annealing studies on In δ-doped epilayers are currently being carried out. We will present the preliminary results showing that there are two different diffusion coefficients (fast and slow) for Indium in both the (111)B and (100) epilayers. However, the diffusion mechanisms were found to be quite different in these two orientations. The overall study indicates that Indium is a suitable n-type dopant for in-situ fabrication of HgCdTe p-n junction devices by MBE and also that the crystallographic orientation plays a very important role in the intrinsic as well as the extrinsic doping of MBE-grown HgCdTe.

References:

(1) M. Boukerche, J. Reno, I.K. Sou, C. Hsu, and J.P. Faurie, Appl. Phys. Lett. 48(25), 1733 (1986).

p -Type Arsenic Doping of CdTe and HgTe/CdTe Superlattices Grown by Photo-Assisted and Conventional Molecular Beam Epitaxy

J.M. Arias, S.H. Shin, D.E. Cooper, M. Zandian, J.G. Pasko,
E.R. Gertner and R.E. DeWames
Rockwell International Science Center

J. Singh
The University of Michigan, Ann Arbor

To fabricate advanced VLWIR photodiode structures based on CdTe/HgTe superlattice structures, in-situ doping with elements that have low diffusion coefficients is needed. ***p*** -type HgTe/CdTe superlattices doped with silver atoms have been recently reported[1]. Silver seems to be a well behaved p-type impurity in HgCdTe, but it has a very high diffusion coefficient which imposes severe limitations for the in-situ fabrication of p/n electrical junctions. ***p*** -type arsenic-doped CdTe and modulation doped $Hg_{1-x}Cd_xTe$ epilayers have also been recently demonstrated[2,3]. Arsenic atoms have a low diffusion coefficient in Hg-based II-VI compounds; therefore, it is well suited for the fabrication of stable p/n junctions. To the best of our knowledge, no previous results of arsenic-doped p-type HgTe/CdTe superlattices have been reported.

We have obtained p-type arsenic doping of CdTe and HgTe/CdTe superlattices by photo-assisted and conventional MBE. ***p***-type arsenic-doped CdTe and HgTe/CdTe superlattice epilayers were grown in (100) CdTe and CdZnTe substrates at low temperatures ($T_S \leq 180$ °C) under cation-stabilized conditions, obtained either with excess Cd, or excess Hg fluxes. As-grown arsenic-doped CdTe layers had a room temperature carrier concentration in the 10^{14}-10^{16} cm^{-3} range, and hole mobilities of about 35-65 cm^2/V s. These arsenic-doped epilayers have better electrical activation than those found in bulk or implanted samples. Low temperature photoluminescence spectra of arsenic-doped CdTe epilayers grown by photo-assisted MBE showed an emission peak at 1.51 eV, which is associated to the As_{Te} acceptor (arsenic occupying a Te site) with a 92 meV ionization energy. CdTe epilayers grown at low temperatures with photo-assisted MBE have superior structural, optical, and electrical properties than those grown by conventional MBE.

The application of this arsenic doping process to the doping of the HgTe/CdTe superlattice structure has resulted the growth of p-type superlattices with 77K hole mobilities in the 10^3 $cm^2/V \cdot s$ range, and carrier concentrations in the 10^{16}-10^{17} cm^{-3} range. Undoped superlattices grown by PAMBE under the same conditions are n-type with 77K electron mobilities as high as $3x10^5$ $cm^2/V \cdot s$ and electron carrier concentrations in the low 10^{15} cm^{-3} range.

These results represent a significant step towards the in-situ fabrication of VLWIR high performance stable diodes and other advanced devices.

References:

1. D.J. Peterman, M.L. Wroge, B.J. Morris, D.J. Leopold and J.G. Broerman, J. Appl. Phys.**65**, 1550 (1989).

2. R.L. Harper,Jr., S. Hwang, N.C. Giles, J.F. Schetzina, D.L. Dreifus and T.H. Myers, Appl. Phys. Lett. **54**, 170 (1989).

3. J.W. Han, S. Hwang, Y. Lansari, R.L. Harper, Z. Yang, N.C. Giles,J.W. Cook,Jr., J.F. Schetzina and S. Sen, J. Vac. Sci. Technol. A, **7**, 305 (1989).

Work supported by the Air Force Wright Research and Development Center, Materials Laboratory under contract No. F33615-87-C5254.

Chemical Doping of HgCdTe by Molecular Beam Epitaxy

Owen K. Wu, and G. Sanjiv Kamath
Hughes Research Laboratory, Malibu, CA 90265
and
W. A. Radford, P.R. Bratt and E. A. Patten
Santa Barbara Research Center, Goleta, CA 93117

EXTENDED ABSTRACT

Chemical doping of HgCdTe is an important issue in II-VI compound semiconductors and has been studied extensively (ref.1-5). In this paper, we will report on the molecular beam epitaxy growth and characterization of n- and p-type $Hg_{1-x}Cd_xTe$. We have grown n- and p-type layers of HgCdTe with indium and arsenic as the dopants using molecular beam epitaxy(MBE) at 170-180°C without photo or ion excitation. The doped layers, which range from 10^{15} cm^{-3} to 10^{18} cm^{-3} have been characterized by a variety of techniques including IR transmission, Hall measurement(see table 1), scanning electron microscopy, minority carrier lifetime, x-ray diffraction and secondary ion mass spectroscopy. The results indicate that n-type alloy layers are easier to form than p-type because of the efficient incorporation of indium in the mercury (or cadmium) sublattice. For instance, the HgCdTe(x=0.32) sample doped with indium source temperature at 600°C gives rise to a carrier concentration of $5x10^{16}/cm^3$ and a Hall mobility of $1.6x10^3$ $cm^2/v.sec$ at 77K. Previously reported memory effects were not observed in our experiments (fig.1). We have also demonstrated that our p-type layers remain p-type after mercury anneal indicating that they are extrinsically doped. The breakthrough in chemical doping of HgCdTe has enabled us to grow several hybrid and all MBE double layer heterojunction

structures. Several diodes have been fabricated and their electrical and optical characteristics will be discussed.

Table 1

77°K Hall Data of In and As Doped $Hg_{1-x}Cd_xTe$ Alloy Layers

Sample #	Carrier Conc. (cm^{-3})	Mobilities ($cm^2.v^{-1}.sec^{-1}$)	Dopant	X value
1.SW549	$1x10^{18}$	$1.5x10^4$	In	0.18
2.SW573	$4x10^{17}$	$8.3x10^3$	In	0.21
3.SW594	$5x10^{16}$	$8.0x10^3$	In	0.23
4.SW720	$5x10^{16}$	$1.6x10^3$	In	0.32
5.SW442	$6x10^{18}$	76	As	0.35
6.SW501	$5x10^{15}$	214	As	0.33
7.SW685	$5x10^{16}$	160	As	0.31
8.SW686	$3x10^{16}$	191	As	0.31

Fig1. SIMS profile of In doped HgCdTe sample indicating the In doping levels at 10^{19}, 10^{18}, 10^{17}, and $10^{15}/cm^3$ ranges.

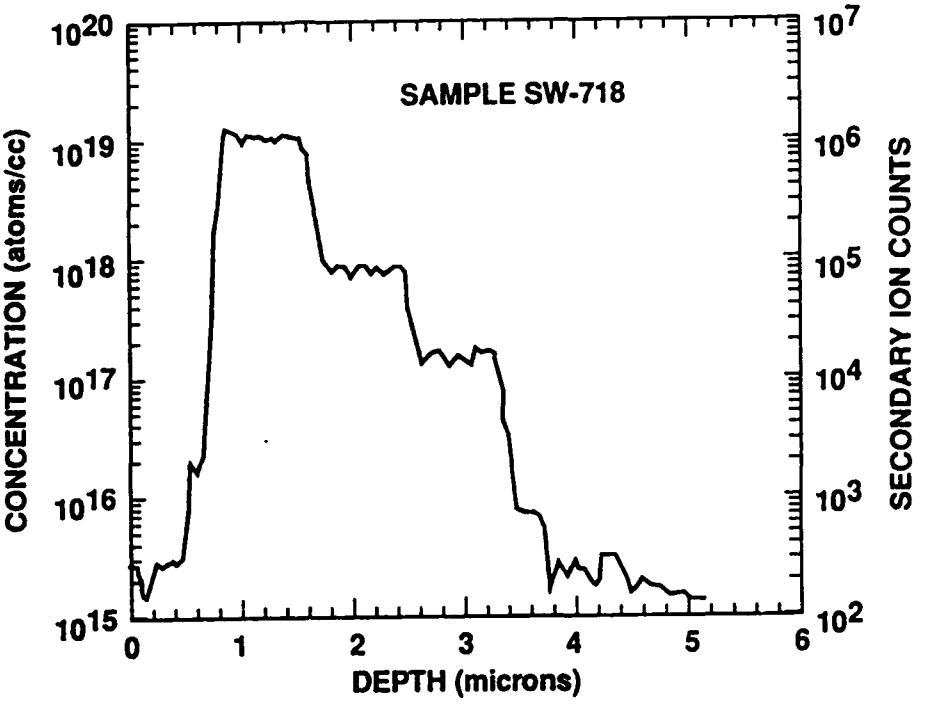

References:

1. M. Boukerche, J. Reno, I.K. Sou, C. Hsu, and J.P. Faurie Appl. Phys. Lett.,48,1733 (1986)

2. R.L. Hrper,Jr., S. Hwang, N.C. Giles, J.F. Schetzina, D.L. Dreifus and T.H. Myers, Appl. Phys. Lett.,54(2), 170 (1989)

3. M. Wroge, D Peterman, B. Feldman, B. Morris, D. Leopold and J. Broerman, J. Vac. Sci. Technol.A7(2),435 (1989)

4. M. Boukerche, P. Wijewamasuniya, S. Sivananthan, I. Sou, Y. Kim and J. Faurie, J. Vac. Sci. Technol. A6,2830 (1988)

5. J. Han, S. Hwang, Y. Lansari, R. Harper, Z. Yang, N. Giles J. Cook and J. Schetzina, J. Vac. Sci. Technol.A7(2), 305 (1989)

The Influence of Crystallographic Orientation on Gallium Incorporation in HgCdTe Grown by MOCVD

R. Korenstein, P. Hallock and B. MacLeod

Raytheon Company, Research Division, Lexington, MA 02173

GaAs is currently being pursued as an alternative substrate to CdTe for HgCdTe epitaxy. Although HgCdTe can be grown on both the (100) and (111) orientations by Metalorganic Chemical Vapor Deposition (MOCVD) most of the work to date has concentrated on the (100) GaAs orientation. We have grown HgCdTe on (111)CdTe//(100)GaAs by MOCVD and find significant incorporation of gallium in the layers. Since this result is not consistent with what has been reported for growth on the (100) orientation[1], we undertook the present study to investigate the effect of crystallographic orientation on gallium incorporation.

HgCdTe was grown simultaneously on both GaAs and CdTe substrates placed side by side by MOCVD at 360°C using diisopropyltelluride, dimethylcadmium and elemental mercury in an atmospheric pressure reactor. For GaAs substrates, a CdTe buffer layer was first grown by hot wall epitaxy prior to HgCdTe growth. The quantity of gallium in the layers was inferred from Hall effect measurements and confirmed by SIMS analysis. The amount of doping was found to be similar for HgCdTe grown simultaneously on GaAs and CdTe substrates.

Hall measurements indicate that HgCdTe grown on the (111)B (Te face) orientation is highly doped n-type with typical carrier concentraions of $1x10^{17}/cm^3$ at 77K for x ~ 0.25. SIMS analysis shows gallium levels in the high 10^{17} atoms/cm^3 and no appreciable arsenic above background. Since gallium is a known n-type donor in HgCdTe, it seems clear that the gallium from the GaAs substrate is responsible for the doping. In addition, the gallium must originate from the backside of the GaAs substrate since the gallium level in the CdTe buffer layers is below 10^{15} atoms /cm^3 and HgCdTe

grown on CdTe substrate is doped at the same level as HgCdTe grown on GaAs. On the other hand, considerably less doping is found in HgCdTe grown on (100) substrates. For x ~ 0.25 material, carrier concentrations are on the order of $5x10^{15}/cm^3$ at 77K and SIMS analysis finds gallium levels on the order of $5-8x10^{15}$ atoms/cm^3 for either GaAs or CdTe substrates. This is approximately an order of magnitude less gallium incorporation than what is found for the (111)B orientation.

The strong orientation dependence of gallium incorporation may be related to the nature of the chemical bonding found in each orientation. Growth on the (111)A (Cd face) should result in a different amount of gallium incorporation. We have grown HgCdTe on the (111)A orientation simultaneously with GaAs substrates and find a considerable reduction in the gallium level. Hall measurements indicate that HgCdTe of x ~ 0.25 is low p-type (carrier concentration < $10^{15}/cm^3$) at 77K and SIMS indicates a gallium level in the low $10^{15}/cm^3$. This is almost another order of magnitude decrease in gallium incorporation compared to (100) growth. The amount of gallium found in the layers grown in this study in decreasing order is as follows: (111)B > (100) > (111)A. A chemical bonding model will be presented to explain these results. This study illustrates the importance of crystallographic orientation in determining the electrical properties of HgCdTe grown on GaAs and may help to reconcile differences in gallium doping found in the literature.

References

1. V. Natarajan, N. R. Taskar, I.B. Bhat, and S.K. Ghandi, J. Elect. Mat., 17(6), 479 (1988).

MATERIAL CHARACTERISTICS OF MOCVD $Hg_{1-x}Cd_xTe$/GaAs/Si

D.D Edwall, L.O. Bubulac, J. Bajaj, R. Zucca and E.R. Gertner

Rockwell International Science Center
1049 Camino Dos Rios
Thousand Oaks, CA 91360

The demonstration of a MWIR photovoltaic focal plane array in MOCVD $Hg_{1-x}Cd_xTe$ grown on bulk GaAs and high performance LWIR detectors have warranted an extension to GaAs/Si substrates. The advantage of GaAs/Si substrates for HgCdTe focal plane technology are the size and ruggedness of Si and the ease of nucleation on GaAs. GaAs/Si substrates are currently the most direct path toward very large hybrid focal plane arrays (overcoming thermal mismatch of substrate and Si multiplexer) and the monolithic integration of IR detectors and readout electronics. We report the results of a MOCVD HgCdTe/Si development effort proceeding in parallel with similar development in material grown on bulk (100) GaAs.

MOCVD HgCdTe layers reported here were grown by the interdiffused process in an atmospheric pressure, horizontal reactor. Similar layers grown by the conventional alloy process had poorer structural characteristics (morphology and crystallinity). A variety of characterization methods were utilized to evaluate the structural, electrical, and optical properties of the epilayers, including optical microscopy, double crystal x-ray diffraction, chemical defect etching, IR transmission, Hall effect, minority carrier lifetime, and laser beam induced current (LBIC). Three-inch dia. (100) GaAs/Si substrates were purchased from the Kopin Corporation.

Table I lists characteristics of layers grown on GaAs/Si substrates compared with similar layers grown on bulk (100) GaAs. Typical surface morphologies are sufficiently smooth for large area focal plane fabrication with macrodefect densities from 325 to 1800 cm^{-2}. Etch pit densities (EPD), measured using a chemical defect etch, range from 5×10^6 to 2×10^7 cm^{-2}, significantly higher than the $(2\text{-}3) \times 10^6$ cm^{-2} values measured for layers on bulk GaAs substrates. Many layers on both types of substrates were p-type as

grown and could be converted to n-type with high mobilites after a 250°C anneal under Hg vapor. With the exception of In-doped layer 598, all layers were p-type after a 250°C anneal under Te vapor. Although the Hall effect results in Table 1 show significant scatter, no obvious general differences have yet been observed for layers grown on GaAs/Si vs bulk GaAs substrates.

Data will be presented for a 3 in. dia. HgCdTe/GaAs/Si layer (x = 0.26) with uniformity figures of merit (expressed as maximum variation divided by the mean) of 6% (x) and 35% (layer thickness, d) for the full wafer, and 0.6% (x) and 21% (d) for the interior 2 in. dia. area.

Although early in its development, MOCVD HgCdTe/GaAs/Si has shown sufficient promise to warrant continued development toward a low cost, high performance HgCdTe focal plane technology.

Table 1

Material Characteristics of MOCVD HgCdTe/CdTe/GaAs/Si Layers Compared with Similar Layers Grown on (100) Bulk GaAs. Ranges of Composition x and Layer Thickness d are Over 2 in. Dia. Areas. Layer 598 was Intentionally Doped with In During Growth; Other Layers are Not Intentionally Doped.

Layer No.	Substrate	x	d, μm	Macrodefect Density, cm^{-2}	DCRC Halfwidth Δθ, arc-min	EPD, cm^{-2}	77K Hall Effect As-Grown c.c., cm^{-3}	As-Grown μ, $cm^2/V\text{-}s$	p-Anneal c.c., cm^{-3}	p-Anneal μ, $cm^2/V\text{-}s$	n-Anneal c.c., cm^{-3}	n-Anneal μ, $cm^2/V\text{-}s$
579	GaAs/Si	0.24-0.25	11-13	1050	1.6	2×10^7	2.9×10^{16}	417			2.6×10^{15}	43,331
580	GaAs/Si	0.24-0.25	11-13	325	1.4	2×10^7	4.4×10^{16}	417	3.1×10^{16}	431	3.8×10^{16}	180
607	GaAs/Si	0.31-0.32	10-12	1800	3.2	5×10^6	9.7×10^{15}	75	6.5×10^{15}	145	2.7×10^{15}	16,506
598(In)	GaAs/Si	0.28-0.31	10-11	1500	2.5	7×10^6	1.7×10^{16}	31,113	5.7×10^{15}	3,951	1.6×10^{16}	23,656
578	GaAs	0.24-0.25	10-12	125	1.2	3×10^6	5.3×10^{14}	26,195	1.7×10^{16}	360	1.4×10^{15}	12,059
581	GaAs	0.24-0.25	11-13	225	1.2	3×10^6	3.7×10^{16}	433	2.9×10^{16}	284	5.1×10^{15}	627
606	GaAs	0.22-0.23	13-14	500	1.8	2×10^6	1.5×10^{17}	214	1.9×10^{16}	636	5.1×10^{15}	60,521

A COMPARISON OF HgCdTe MOCVD FILMS ON LATTICE MATCHED CdZnTe AND CdTeSe SUBSTRATES

M. J. Bevan, N. J. Doyle and J. Greggi, Westinghouse Science & Technology Center, Pittsburgh, PA 15235

D. Snyder, Department of Chemical Engineering, Carnegie Mellon University, Pittsburgh, PA 15213

The quality and uniformity of HgCdTe detector arrays based on epitaxial material are limited by structural defects, generated from structural imperfections in the substrate or from lattice mismatch stress. Anomolous Hall effect behaviour for LPE material has been correlated with these defects[1]. Even the small mismatch between HgCdTe (0.4>x>0.1) and CdTe substrates, which ranges from 0.19 and 0.28%, is sufficient to cause significant interface dislocation densities in the epilayers which can be relieved by using a lattice matched substrate CdZnTe (Zn=4%) or CdTeSe (Se=4%). Detailed structural assessment of HgCdTe films grown by metal organic chemical vapour deposition (MOCVD) on these substrate materials has been performed.

The interdiffused multilayer process(IMP) with growth rates in excess of 10μm/h was used with the diethyl and diisopropyl tellurium precursors over the deposition range 350-420^{o}C for compositions ranging from 0.19 to 0.38 for $Hg_{1-x}Cd_xTe$. The lateral compositional variation in x over a 6cm^2 substrate typically ranged from 0.241 to 0.221. The CdZnTe and CdTeSe substrates were primarily oriented 2^{o} off (100) towards the nearest [110]. The epilayers had a pyramidal defect density in the range 10 to 10^4cm^{-2}. X-ray oscillation photographs and RHEED patterns indicated no signs of twinning in these MOCVD

films even in areas of high defect densities. Alternative orientations have been sought and, although (111)B epilayers are free of growth facets, they have a rotational twinned structure. Specular films free of twinning and pyramidal defects have been grown by MOCVD on (211)B substrates and had double crystal half widths(FWHM) comparable to the substrate batch(40arcsec).

Using diethyltelluride, growth was optimised at 420°C resulting in films with double crystal half widths as low as 25arcsec, comparable to that of the CdZnTe substrate(21arcsec). Cross-sectional transmission electron microscopy showed no defects through the thickness of the film(Fig.1 XTEM montage) correlating with FWHM. Epitaxial films grown at 350°C using diisopropyltelluride had rocking curve widths in the range 60-110arcsec, the spread partly arising from the varying Zn or Se content of the substrates. Their electrical properties at 77K were consistent with an anticipated mercury vacancy concentration of $7x10^{16}cm^{-3}$ with compositional dependency. Improved crystal quality was achieved by using higher deposition temperatures, resulting in HgCdTe comparable in quality to that of the substrate and FWHM's represent the lowest values reported for MOCVD films. Although lattice matching is a key parameter for the improvement in crystal quality, the deposition temperature proved to be equally important. The pyramidal defect density associated with CdTeSe was higher than with CdZnTe and reflects the less mature CdTeSe substrate development. MOCVD can produce HgCdTe epilayers that replicate the crystal quality of the substrate and further development is severely limited by the non-uniformity of the large area CdZnTe and CdTeSe wafers.

[1] B. Pelliciari et al, J. Vac. Sci. Technol. A7(1989)314.

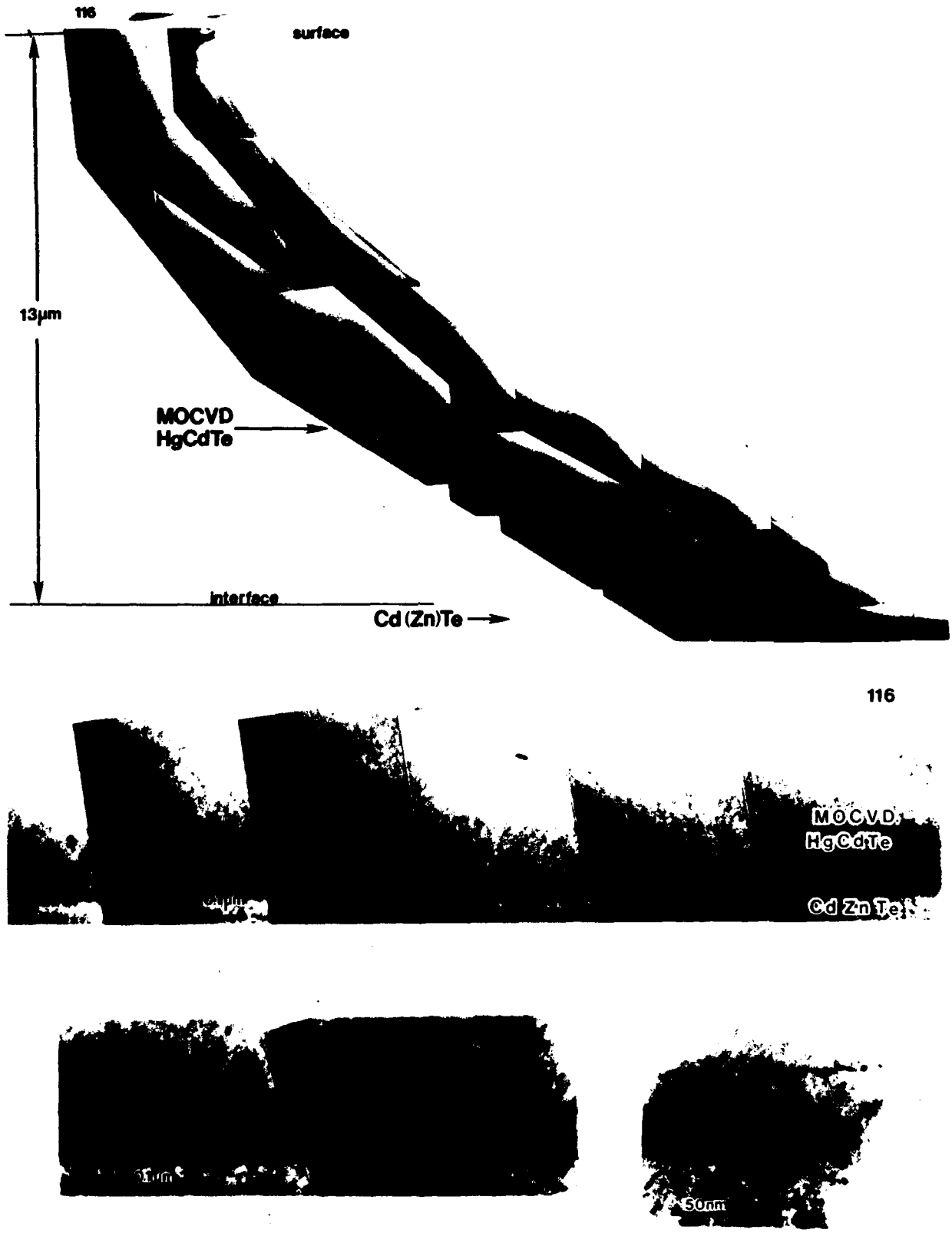

Fig.1 Cross-section TEM through a MOCVD HgCdTe/CdZnTe structure, showing the bulk epilayer and interface regions.

LOW TEMPERATURE GROWTH OF HgTe AND HgCdTe USING METHYLALLYLTELLURIDE

I.B. Bhat, H. Ehsani, S.K. Ghandhi

Electrical, Computer and Systems Engineering Department

Rensselaer Polytechnic Institute

Troy, New York 12180

ABSTRACT

The growth of HgCdTe at reduced temperature has many advantages. In addition to reducing the interdiffusion distance between the epilayer and the substrate, substantial reduction in the native defects is also possible. Low temperature growth may also allow the fabrication of p-n junctions and heterostructures in situ, without using post-growth annealing. In this talk, we will report on the low temperature growth and characterization of HgTe and HgCdTe layers, using methylallyltelluride. Although a number of low temperature Te-precursors have been used in earlier studies, few results are available on the properties of HgTe or HgCdTe layers grown with them.

HgTe and HgCdTe layers have been grown by organometallic vapor phase epitaxy using methylallyltelluride (MATe), dimethylcadmium (DMCd) and elemental mercury. Use of MATe enabled us to grow layers in the 250-320°C range, which is 50°C lower than the growth temperature for diisopropyltelluride (DIPTe), for comparable growth rates. The epitaxial growth of HgTe and HgCdTe was carried out at low pressure (380 Torr) in a vertical reactor. The substrates were (100) CdTe and (100) CdZnTe, 2 degrees misoriented towards (110). Growth was performed with a MATe partial pressure of 1.1 $\times 10^{-3}$ atm and an Hg partial pressure of 0.03 atm. Growth was studied in the temperature range of 240°C to 350°C. Beyond 350°, the growth rate was found to saturate. Growth rates as high as 9 μm/hr at 320° and 1 μm/hr at 240°C were obtained for

HgTe, using this Te-source.

Grown layers of HgTe and HgCdTe were mirror smooth, without the step features usually obtained with growth at higher temperatures. Electrical measurements on HgTe layers indicate that they are of high quality, with 80K mobility of 7×10^4 cm^2/Vs.

The structural quality of the layers was assessed using double crystal x-ray diffraction. For 1.7 μm thick layers grown on CdZnTe substrates, a full width half maximum (FWHM) of 27 arc. sec. was obtained for the (400) reflection (see Fig. 1). For this layer, the substrate FWHM was 23 arc. sec. This is one of the lowest values obtained for HgTe grown by OMCVD. Layers grown on CdTe were misoriented with respect to the substrate by about 60 to 150 arc. sec. This tilt is evidence of a sharp interface between the epilayer and the substrate, and has not been observed for HgCdTe grown with DIPTe. Here, the lattice parameter, in the (100) direction, approached the pseudomorphic limit for thin layers (6.45 $\AA$) and the relaxed limit (a_{HgTe}) for thick layers as shown in Fig. 2. As expected, tilt was not observed when lattice matched CdZnTe substrates were used.

HgCdTe layers were grown using this new Te source, by introducing dimethylcadmium. These layers, grown at 320°C, showed sharp interference fringes even for thin layers, indicating the presence of a sharp interface. A typical FTIR transmission curve is shown in Fig. 3. As grown HgCdTe layers were n-type, with an 80K mobility of 4×10^4 cm^2/Vs and carrier concentration of 2×10^{15} cm^{-3}. The growth conditions will be outlined for HgCdTe and HgTe, and both electrical and structural results will be presented in this talk.

REFERENCES

1. J.D. Parsons and L.S. Lichtmann, J. Crys. Growth, 86, 222 (1988).
2. W.E. Hoke, P.J. Lemonias and R. Korenstein, J. Mater. Res., 3, 329 (1988).
3. S.K. Ghandhi, I.B. Bhat and H. Ehsani, Appl. Phys. Lett., 55, 137 (1989).

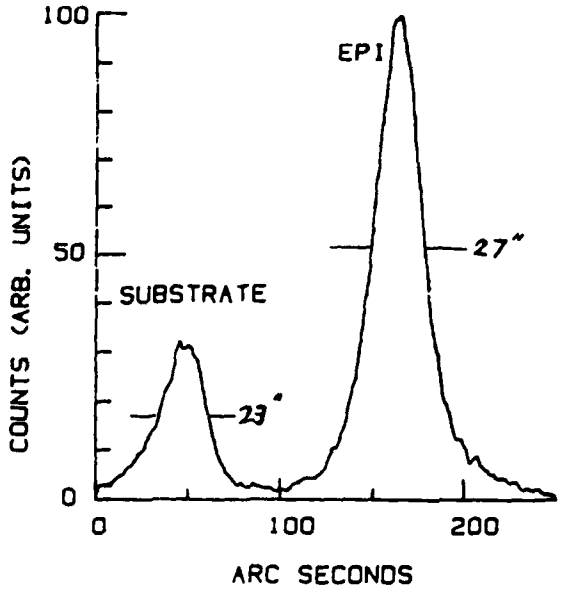

Fig. 1 DCR curve of a 1.7 μm thick HgTe on CdZnTe grown at 320°.

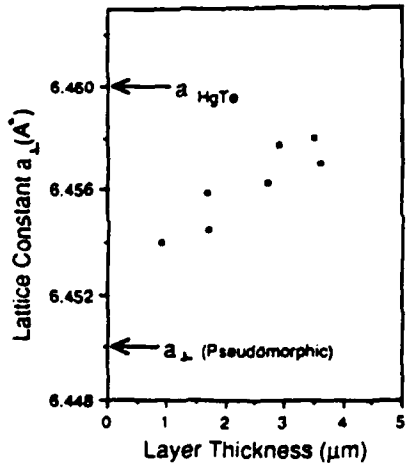

Fig. 2 Lattice constant of HgTe in the growth direction, $a_\perp$ as a function of layer thickness.

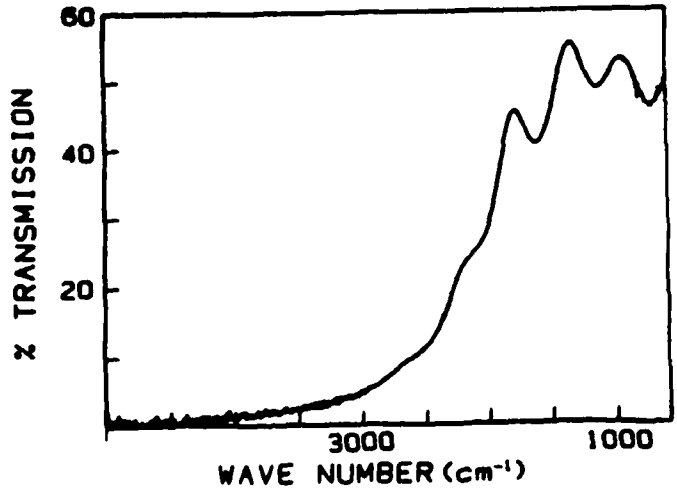

Fig. 3 FTIR spectrum of a 3.3 μm thick HgCdTe layer on CdTe. $x = 0.25$.

Laser-induced Selected Area Epitaxy of CdTe and HgTe

S J C Irvine, H Hill, J E Hails, J B Mullin, S J Barnett, G W Blackmore and O D Dosser
Royal Signals & Radar Establishment, St Andrews Road, Malvern, Worcs WR14 3PS, UK

Photo-induced Metal Organic Vapour Phase Epitaxy (MOVPE) has been used to reduce epitaxial growth temperatures below that at which the precursors would normally pyrolyse with any practical efficiency. Recently, a further advantage for photo-induced MOVPE has been demonstrated, that of selected area epitaxy where growth occurs only on the regions of the substrate illuminated by ultraviolet photons. Growth rate must be low or negligible in the 'dark' which requires a low pyrolytic reaction rate. This will influence the choice of precursors, favouring the more stable organometallics. 'Switching on' the reaction can be achieved using a frequency doubled argon ion laser illuminating the surface. The absorption cross sections of the precursors at the laser wavelength of 257nm must be greater than $\sim 10^{-18} cm^2$ in order to bring about useful photo-dissociation. The results of measurements of absorption cross-section for a number of alternative tellurium precursors will be presented.

Detailed experimental results will be presented for photo-induced epitaxy of CdTe onto GaAs substrates at temperatures in the range 250 to 300°C. The ratio of photo-induced to pyrolytic growth rates (photo-enhancement factor) have been determined for a range of deposition conditions such as UV intensity, substrate temperature and alternative tellurium precursors (dimethyl ditelluride, dimethyl telluride and diethyl telluride). The crystalline quality of these films has been assessed using x-ray texture patterns which shows single crystal epitaxial growth (100)//(100) provided that the correct nucleation conditions are used. *In situ* monitoring of the growth rate and surface morphology has been achieved by measuring the intensity of a HeNe laser beam specularly reflected from the growing film. These results have helped to illucidate the growth mechanisms.

Projected bar and mesa patterns have been replicated by the growing layer with enhanced growth rate in the illuminated regions. A very small proportion of the growth can be attributed simply to diffusion of Cd and Te from the vapour, the very good feature definition is consistent with a surface reaction enhancing the growth rate. The mesa patterns have been analysed using a secondary ion mass spectrometer (SIMS) with imaging facility. Spatial distributions of matrix elements have been determined together with the distributions of impurities. Possible mechanisms for the selected area growth will be discussed. Preliminary results will be presented for HgTe and an assessment made of the potential for projection patterning of epitaxial MCT for focal plane array fabrication.

LARGE-AREA HgTe-CdTe SUPERLATTICES AND $Hg_{1-x}Cd_xTe$ MULTILAYERS ON GaAs AND SAPPHIRE GROWN BY LOW TEMPERATURE METAL ORGANIC CHEMICAL VAPOUR DEPOSITION

G.N. Pain, N. Bharatula, T.J. Elms, P. Gwynn,
M. H. Kibel, M.S. Kwietniak, P. Leech, N. Petkovic, C. Sandford,
J. Thompson and T. Warminski
Telecom Australia Research Laboratories, Clayton, Victoria, Australia

D. Gao, S.R. Glanvill, C.J. Rossouw, A.W. Stevenson and S.W. Wilkins
CSIRO Division of Material Science and Technology,
Clayton, Victoria, Australia

L. Wielunski, CSIRO Division of Applied Physics,
Sutherland, N.S.W. Australia

Specular HgTe-CdTe superlattice epilayers have been obtained on two 2-inch diameter GaAs or sapphire wafers per growth run using a horizontal MOCVD reactor in which pyrolysis of the organometallics is induced by a cracking susceptor suspended above the substrates. Growth below 300°C is achieved using the standard precursors Me_2Cd, Et_2Te and Hg without high temperature pregrowth anneals of the substrates. Annealing the superlattices converts them to homogeneous $Hg_{1-x}Cd_xTe$. Compositional profiling of the $100cm^2$ deposition zone has been achieved by wavelength dispersive analysis of X-rays and inductively coupled plasma atomic emission spectrometry. Depth profiles and interdiffusion data were obtained by e-beam analysis of ultramicrotomed thin cross-sections[1-3] (Figs.1 and 2), sputter Auger depth profiling[4] (Figs.3 and 4) and Rutherford back-scattering (RBS) (Fig.5). Structural quality was studied by HRTEM, RBS and X-ray techniques (Fig.6). Double-crystal rocking curves (400) gave FWHM of ~600 arc seconds for the epilayer shown in Fig.1. Room temperature electron mobilities up to 27,500 cm^2/Vs have been measured for the HgTe layers, and these have been used to improve

contacts. High resistivity (>10^4 ohm cm) epilayers of CdTe have been investigated as passivation and dielectric by C-V and I-V techniques. Arrays of photoconductive detectors with room temperature peak responsivity between 1.3 and 1.6μm have been prepared from incompletely interdiffused material grown directly on semiinsulating GaAs without thick buffer layers. Operating frequency is limited to about 1MHz by high carrier lifetimes of microseconds, however bandwith can be improved, with some loss of sensitivity, by energetic beam damage. MESFETS with 4μm gates have been fabricated as the first step towards integrated circuits.

Growth at even lower temperatures should be possible by suitable choice of organometallics[5], opening the possibility of large area growth with more abrupt interfaces. Conductive CdTe:In has been obtained using Me_3In without photoassistance and use of designer organometallics is encouraging for low temperature p doping[6].

The permission of the Executive General Manager, Telecom Australia Research Laboratories to publish this paper is acknowledged. This work received partial support under the Generic Technology component of the Industry Research and Development Act, 1986, Grant No.15019.

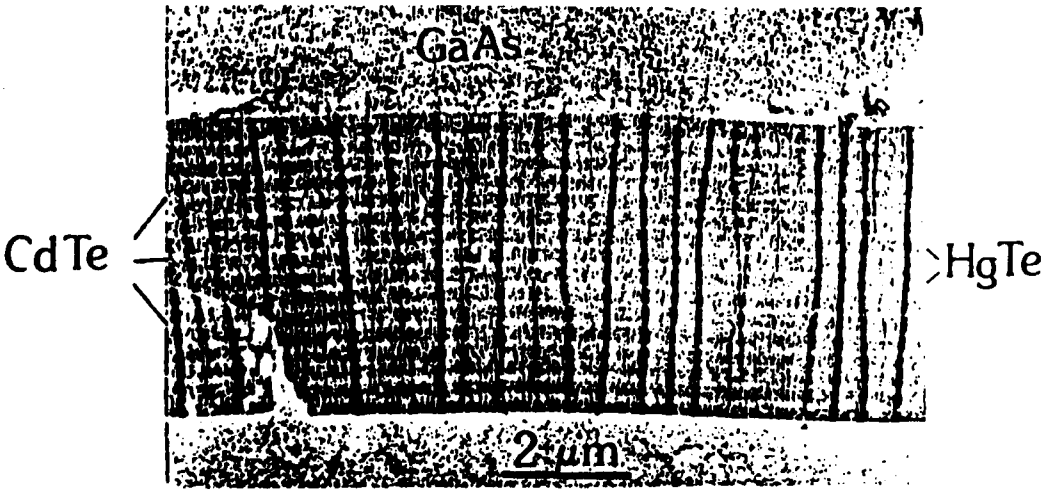

Fig. 1 Low magnification image of ultramicrotomed sample of a 16 period superlattice showing the 5 micron epilayer from the interface to the surface in cross-section.

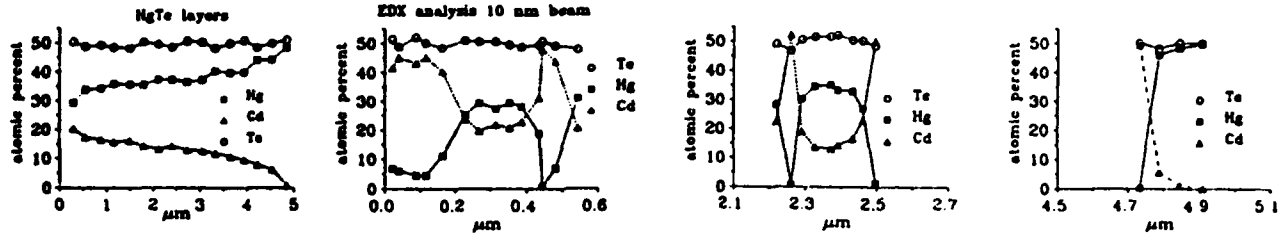

Fig. 2 Atomic concentration profiles as functions of distance from the interface derived from EDX analysis of the epilayer shown in Fig. 1

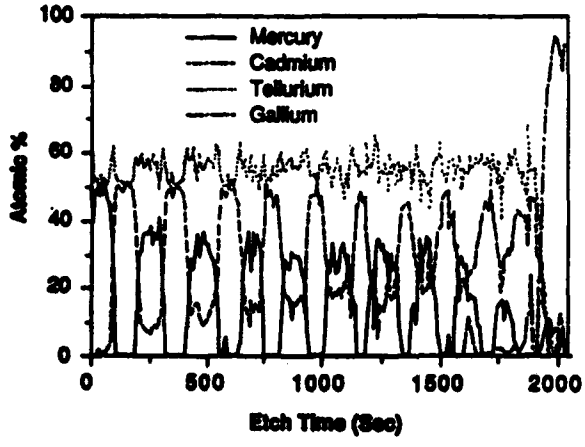

Fig. 3 Sputter depth profile of a 10 period superlattice.

Fig. 4 Back-scattered electron image of the etch crater after obtaining the profile shown in Fig. 3

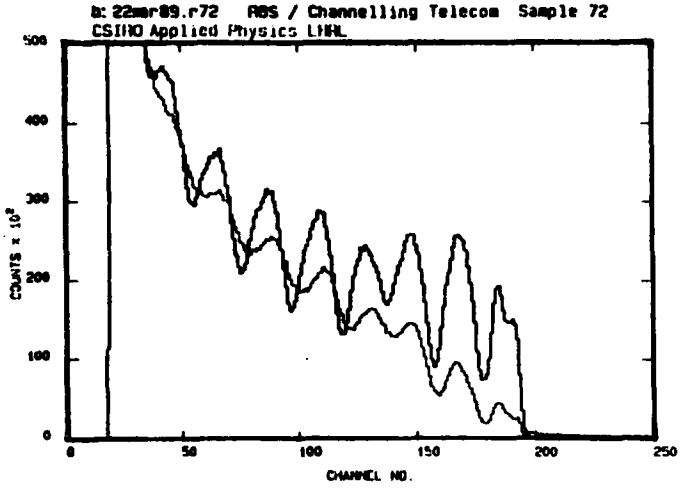

Fig. 5 Rutherford back-scattering and channeling for the epilayer shown in Fig. 1

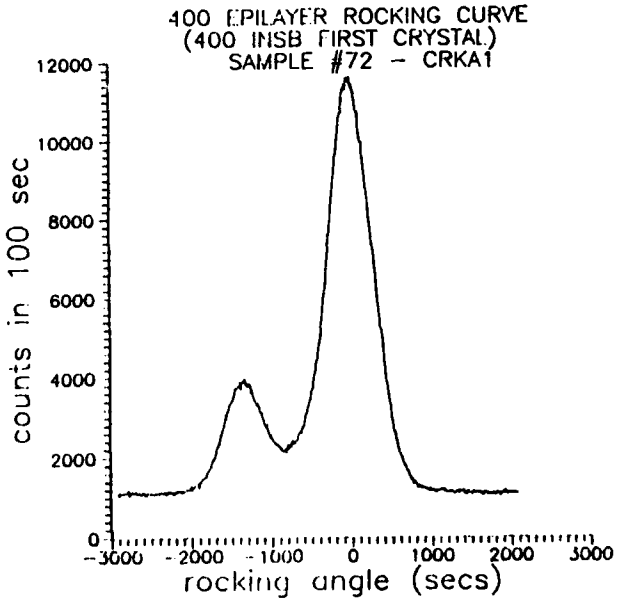

Fig. 6 Double-crystal rocking curve of the epilayer shown in Fig. 1

REFERENCES

1. S.B. Glenville, M.S. Kwietniak, G.H. Pain, C.J. Rossouw, T. Warminski, L.S.Wielunski and I.J. Wilson, Phil.Mag.Lett.1989, 59, 17.

2. C.J. Rossouw, S.B. Glenville, M.S. Kwietniak, G.H. Pain, T. Warminski and I.J. Wilson, J. Crystal Growth, 1988, 91, 937.

3. C.J. Rossouw, S.B. Glenville and G.H. Pain, Proceedings of the Oxford Conference on Microscopy of Semiconductors, in press.

4. M.H. Kibel, to be published.

5. G.H. Pain, R.S. Dickson, G.I. Christiansen, G.B. Rossouw, B.O. West, K. McGregor and R.S. Rowe, Polyhedron, in press.

6. G.H. Pain and R.S. Rowe, patent pending.

Extrinsic P-Type Doping of HgCdTe With Diethylarsenic Hydride Grown by Metalorganic Chemical Vapor Deposition (MOCVD)

V. G. Kreismanis, J. Elliott,
R. J. Olson, Jr., and P. J. Lemonias
Raytheon Co. Research Division
Lexington, MA 02173

ABSTRACT

Extrinsic impurity doping is critical to the fabrication of HgCdTe infrared detector structures. Recent work has shown the ability to extrinsically dope MOCVD grown HgCdTe using both metalorganic and gaseous sources [1,2]. In this work, in-situ, extrinsic p-type doping of mercury cadmium telluride (HgCdTe) grown by conventional atmospheric pressure metalorganic chemical vapor deposition has been achieved with diethylarsenic hydride (DEAsH). All of the films were grown at 360°C with diisopropyltelluride (DIPTe), dimethylcadmium (DMCd), and elemental mercury, as the tellurium, cadmium, and mercury sources, respectively. Both <100>4°---<110> and <111>B CdTe substrates were used. The epitaxial layers were evaluated by Hall, EDAX, and SIMS measurements. Doping levels in the low $10^{15}/cm^3$ to $10^{17}/cm^3$ range were obtained. The effect of pre-cracking the DEAsH prior to it reaching the growth zone and Hg/Te mole fraction ratios were investigated. The effect of pre-cracking was to give higher doping levels for identical source mole fractions, and a high Hg/Te ratio (48) gave a higher doping

level than a low Hg/Te ratio (2.8). Samples were annealed for 15 hours at 220°C, and this was found not to significantly alter the 77K Hall data indicating extrinsic p-type doping. Also, SIMS data showed the presence of As in the films at levels equal to the Hall carrier concentration with a definite step in the As level between the substrate and the film. Linkage between the doping level and the amount of Cd incorporation was observed and results in decreased Cd incorporation as the doping level is increased. However, this can be compensated for by simply increasing the Cd mole fraction. Preliminary performance data for p on n diodes grown by an all MOCVD process will also be presented.

REFERENCES:

1. J. S. Whiteley, P. Koppel, V. L. Conger, and K. E. Owens, J. Vac. Sci. Technol. A 6(4), 2804 (1988).

2. S. K. Ghandi, N. R. Tasker, K. K. Parat, D. Terry, and I. B. Bhat, Appl. Phys. Lett. 53(17), 1641 (1988).

THE GROWTH OF CdHgTe ON GaAs AND FABRICATION OF HIGH QUALITY PHOTODIODES

L M Smith, C F Byrne, D Patel, P Knowles and J Thompson*
GEC Sensors, Hirst Infrared Division, GEC Hirst Research Centre, East Lane, Wembley, Middlesex, UK
* Now at Plessey Research (Caswell) Ltd, Caswell, Towcester, Northants, UK

G T Jenkin
GEC Hirst Research Centre, East Lane, Wembley, Middlesex, UK

T Nguyen Duy, A Durand and M Bourdillot
Societe Anonyme de Telecommunications, 41 Rue Cantagrel, 75013, Paris, France

The use of MOVPE for the growth of device quality CdHgTe on GaAs has been extensively studied. We wish to report, for the first time, the fabrication of MWIR photodiodes from the MOVPE grown material.

The initial growth studies of CdTe/HgTe on (100) and (111) GaAs were performed to determine the most appropriate buffer structures with the aim of reducing defect densities as well as containing any Ga out-diffusion. (100) CdTe/(100) GaAs samples exhibited very sharp, well defined PL spectra and X-ray rocking curve FWHM peaks of <90 arc secs were found for layers of 6-10 μm thick. Furthermore, by choosing an appropriate nucleation temperature (100)/(100) could be grown over the Cd:Te ratio 0.3-3:1 whilst maintaining a pre-growth bake. Generally (111) CdTe/(111) GaAs layers were dominated by twins. However we will report the growth and characterisation of untwinned (111)CdTe and (111)CMT.

Choosing the correct combination of CdTe/HgTe buffer structure, highly crystalline, low defect density CMT was grown on GaAs in a single growth run. Hall characterisation showed that the CMT was p-type with similar carrier concentrations and mobilities to that obtained on CdTe substrates.

Linear diode arrays have been fabricated by mercury diffusion and results will be presented. 77K R_0A values of 3×10^3 Ωcm^2 have been measured for 7.5 μm cut-off wavelengths with yields of 90%. The detectivity was typically 1.5×10^{11} $cmHz^{\frac{1}{2}}W^{-1}$ for 5.5 μm cut-off diodes at 77K, and 1.3×10^{10} $cmHz^{\frac{1}{2}}W^{-1}$ at 193K. These results are comparable to performance obtained in THM and LPE produced material.

PARTIAL PRESSURES OF Hg AND Te_2 OVER $(Hg_{1-x}Zn_x)_{1-y}Te_y$ SOLID SOLUTIONS

Robert F. Brebrick, Kuo-Tong Chen, and Yi-Gao Sha

Materials Science and Metallurgy Program, College of Engineering

Marquette University, Milwaukee, WI 53233

The partial pressures of mercury, P_{Hg}, and of Te_2, P_2, over $(Hg_{1-x}Zn_x)_{1-y}Te_y(c)$ have been determined by measuring the optical density of the coexisting vapor phase between 250 and 750 nm. Portions of the Te-saturated and metal-saturated legs of the three-phase curve have thereby been established for x = 0.10, 0.20, 0.30, 0.50, and 0.70. HgTe and ZnTe were synthesized by reaction of the spectroscopically pure elements within evacuated, fused-silica ampoules. The solid solutions were generally prepared by heating weighed amounts of the binary compounds, ground to pass a 120 μm sieve and then mixed, plus a weighed amount of extra Hg within an evacuated, fused-silica, T-shaped optical cell for 7 dys at 650 – 700° C. After measurements these samples were reused by first driving off the extra Hg, grinding to 120μm, weighing, and loading into a new optical cell with another weighed amount of Hg. The samples were then heated again at 650 – 700°C for 7 dys before measurement. This was done twice for some x-values with the amount of extra Hg increased with each reuse. A schematic of the optical cell within a T-shaped furnace showing the placement of six $Pt - 10\%Rh/Pt$ thermocouples about the optical cell proper (the top line of the T) and seven around the sidearm, and a discussion of the measurement technique has been given elsewhere[1]. The sample is located at the end of the sidearm (the vertical line of the T) furthest from the cell proper. During a set of measurements, the temperature of the optical cell proper was kept at either 755 or 800°C while the sample temperature was held at one of a set of lower temperatures. The latter included values of 200°C or lower, insufficient to provide enough vapor for a detectable absorption, in order to establish a zero for the optical density. It is known that at 800°C and below that Hg absorbs between 240 and 340 nm, but not beyond, for P_{Hg} as high as 35 atm. On the other hand, Te_2 absorbs weakly between 240 and 340 nm but strongly in the visible. There is a

maximum in the vibronic spectrum near 415.0 nm. Thus P_2 was obtained as the average of values obtained from a set of vibronic maxima using

$$P_2(atm) = \alpha_\lambda D_\lambda / L \tag{1}$$

where D_λ is the optical density of the vapor at a vibronic maximum at wavelength λ, L is the optical path length through the vapor phase in cm, and α_λ is a Bee's law constant that depends upon the optical cell temperature as well as upon λ. Fifty-two vibronic maxima between 400.1 and 496.8 nm were used. The Beer's law constants established by measurements with a pure Te sample have been tabulated[2]. For a 700° C cell the constant is 0.0211 at 416.3nm and is between this value and 0.023 for 16 maxima beytween 400.1 and 428.9 nm. It is 0.112 for the maximum at 496.8 nm. Finally the values of P_2 obtained with Eq.(1) that fell in the range between 2.5×10^{-4} to 1.78×10^{-2} atm were corrected by an amount that ranged from -15% at the lower end to zero at the upper end. This correction is necessary because of a small downward shift in the vapor pressure of Te(l) made in a recent third law analysis of the liquid-vapor equilibrium for tellurium[3]. Having obtained P_2, the Te_2 contribution to the vapor optical density in the 254.4 – 340.4 nm range was calculated assuming that the Te_2 spectrum is essentially unchanged by the presence of Hg. This contribution was then subtracted from the observed vapor optical density in this wavelength range, but was never more than 1% of the observed value. Then P_{Hg} was calculated as the average of the values obtained from 4 – 8 wavelengths with

$$P_{Hg}(atm) = r_\lambda (D_\lambda / L)^{1/2} \tag{2}$$

where r_λ is a constant dependent upon λ and the optical cell temperature which has been obtained from measurements with a pure Hg sample and tabulated[4]. For $0.0 \leq x \leq 0.70$, mercury is the predominant vapor species, even for the Te-saturated solid solutions. Consequently, as a sample is heated to progressively higher temperatures the preferential loss of Hg to the vapor phase causes the sample to leave the metal-saturated state, cross the

homogeneity range at a nearly constant value of P_{Hg}, and become Te-saturated. The changes in x and y were calculated knowing the temperature-volume distribution along the cell and sidearm. For the metal-saturated state the results are:

At 315° C, $P_{Hg} = 0.5$ atm for all the x-values. At 589, $P_{Hg} = 17.5$ atm for $x = 0.30$ and, within about 5% is the same for the higher x-values. For $x = 0.50$ the maximum in the P_{Hg} three phase curve was observed and is at 34 atm and 727° C while the solidus point is at 28 atm and 758° C.

For the Te-saturated state the results are:

For the various x-values $\log P_{Hg}$ vs $10^3/T$ is a straight line between about 560 and 727° C and P_{Hg} is higher the smaller x is. For $x = 0.70$, $P_{Hg} = 5$ atm at 727° C and 1.5atm at 644° C. At 636° C, $P_{Hg} = 1.2$ atm for $x = 0.70$, 1.7 atm for $x = 0.50$, 2.2 atm for $x = 0.30$, 2.6 atm for $x = 0.20$, and 3.0 atm for $x = 0.10$.

Between 560 and 636° C, P_2 for the Te-saturated state falls roughly between 1.5 and 8.0×10^{-3} atm. For all the x-values except 0.70, $\log P_2$ vs $1000/T$ falls on straight lines that are higher the larger x is and that are converging near 560° C. At 636° C the values in units of 10^{-3} atm are 7.0, 6.2, 4.6, and 4.0 for $x = 0.50$, 0.30, 0.20, and 0.10, respectively. At 560° C, P_2 falls between 1.6 and 1.8×10^{-3} atm for all these x-values. For $x = 0.70$, $P_2 = 7.5 \times 10^{-3}$ atm at 636° C and 1.3×10^{-3} atm at 560, the values crossing those for the lower x-values.

This work was supported by NSF under Grant DMR-87001160.

REFERENCES

1. Yu Huang and R.F. Brebrick, J.Electrochem. Soc. 135 486 (1988)

2. Yi-Gao Sha, Ph.D. Thesis, submitted to the Graduate School, Marquette University, Milwaukee, WI 53233, Nov. 1988

3. R.F. Brebrick. accepted May 1989 for publication in High Temp. Science.

4. J.P. Schwartz, Tse Tung, and R.F. Brebrick, J. Electrochem. Soc. 128 438 (1981)

Ariel Sher and Alex Tsigelman
Solid State Physics Department,
Soreq Nuclear Research Center,
Yavne, 70600, Israel

Eliezer Weiss and Nilly Mainzer
SCD-Semiconductor Devices,
DN Misgav 20179, Israel

The solid solution of $Hg_{1-x}Zn_xTe$ has been considered for the last few years as an alternative to $Hg_{1-x}Cd_xTe$ for PV detectors, mainly in the LWIR range (1-4).

In this presentation, the interrelation between the LPE growth conditions, post growth Hg annealing conditions and the material properties are discussed. Systematic study of the growth and annealing conditions, followed by optimization of the processes, led to epilayers with the desired properties for the realization of n on p diodes.

The epitaxial layers are currently grown from Te solution, using the semiclosed, horizontal, slider boat method (5,6). On closely lattice matched substrates, the rate of growth was found to be limited by the diffusion of the solutes in the liquid. The experimental results of the epilayers growth rate vs the time-temperature profile of the growth process, were found to fit theoretical curves in both the limited and unlimited growth solutions (7). Under the appropriate growth conditions, the thickness and the composition of the epilayers are well

controlled. The morphology as well as the crystallinity are strongly dependent on the substrate orientation and the degree of lattice mismatch between the epilayer and the substrate (8).

Post growth Hg annealing experiments were performed in order to decrease the hole concentration in the as grown p-type layers. Under the annealing temperatures of 340-360·C, the typical results of the hole concentration in the LWIR annealed samples, at 77K, were $1\text{-}2\times10^{16}cm^{-3}$. Hole mobilities varied between 300 and 600 $cm^2/V.sec$ and the minority carrier life time was found to be 20-40ns. The results of the annealing experiments under lower temperatures (200-220·C) were dependent on the Zn concentration in the epilayers. With relatively high Zn concentration, $x>0.20$, the epilayers remained p-type with hole concentration of $3\text{-}5\times10^{15}cm^{-3}$. The epilayers with low Zn concentration which were annealed under low temperatures were converted to n-type, with electron concentration of $3\text{-}10\times10^{14}cm^{-3}$. The electron mobilities in the n-type epilayers were dependent on x. The highest measured electron mobility was $700000cm^2/V.sec$, for $x=0.13$.

Experiments of fabrication of n on p junctions were performed on some of the annealed samples. The results of which will be presented and correlated with the material properties.

1. Arden Sher, An-Ban Chen, W.E. Spicer and C-K Shih, J. Vac. Sci. Technol. A (3), 105, (1985).

2. Ariel Sher, D. Eger and A. Zemel, Appl. Phys. Letters, 46, 59, (1985).

3. T. Tung, M.H. Kalisher, S. Sen, B.F. Zuck, E.J. Smith and W.H. Konkel, extended abstracts of the 1985 U.S. Workshop on the Physics and Chemistry of Mercury Cadmium Telluride, p. 53.

4. R. Triboulet, J. Crystal Growth, 86, 79, (1988).

5. Ariel Sher, D. Eger, A. Zemel, H. Feldstein and A. Raizman, J. Vac. Sci. Technol. A4, 2024, (1986).

6. Ariel Sher, SPIE Vol. 1038, 13, (1988).

7. R.L. Moon, J. Crystal Growth, 27, 62, (1974).

8. Ariel Sher, D. Eger and A. Raizman, J. Crystal Growth 87, 507, (1987).

Improved LPE Growth of HgZnTe on CdZnTe and CdTe Substrates*

M.H. Kalisher, E.A. Patten and S. Sen
Santa Barbara Research Center
75 Coromar Drive, Goleta,CA 93117

Results of studies on the properties of HgZnTe alloys grown by liquid phase epitaxy (LPE) from Te-rich melts have previously been reported (1,2,3). Among the potential advantages of this material as compared with HgCdTe are increased hardness, improved stability against defect formation, and reduced Hg diffusion. These and other advantages have motivated continued investigation of HgZnTe at Santa Barbara Research Center. We report here recent results on the electrical, optical, and structural properties of these alloys grown by LPE under various conditions on CdTe and CdZnTe substrates with several different Zn fractions. In general, crystal quality of recent layers is significantly improved over that of layers reported earlier. In addition we report the somewhat unexpected results of superior growth of HgZnTe on lattice mismatched substrates (lower Zn composition) versus on matched substrates.

$Hg_{1-x}Zn_xTe$ layers with compositions ranging from x=0.11 to x=0.16 have been grown on $Cd_{1-y}Zn_yTe$ substrates with $0 \leq y \leq 20$. Growths were performed using Zn-saturated Te-rich melts in a horizontal slider-boat furnace system at atmospheric pressure. The layer morphology was better for layers grown on CdTe and on CdZnTe substrates with about 4% Zn than for layers grown on substrates containing greater Zn fractions (≈ 20%) and which are therefore more closely lattice matched to HgZnTe. The improved morphology was in part due to the reduced melt retention and ease of decanting the melt at the end of the growths performed on lower Zn composition substrates. For one particular growth, a CdZnTe substrate was used that had a Zn composition gradient across its surface. For this case, the smoother part of the layer occurred on the lower Zn portion of the substrate.

X-ray double-crystal rocking curves (using 1 x 8 mm beam) on these layers had full width at half-maximum (FWHM) values typically of ~150 arc-seconds. The best result was 72 arc-seconds for a $Hg_{0.87}Zn_{0.13}Te$ layer grown on a $Cd_{0.96}Zn_{0.04}Te$ mismatched substrate. Hall-effect measurements at 77 K on long-wavelength (x=0.13) layers after annealing show mobilities greater than 10^5 $cm^2/V\text{-}sec$ and carrier concentrations of 10^{15} cm-3 or less.

Our current HgZnTe growth conditions have been modified as compared with those used for our previously reported work. These new growth modifications result in higher quality layers on lattice mismatched substrates as compared with those grown on both matched and mismatched substrates in the past. Under current growth conditions, however, melt retention on the layer is much worse when growing on substrates with higher Zn content (which are also more closely lattice matched to the layer). It is believed

that residual oxygen in the growth system is more detrimental to layer quality when growing on substrates with higher Zn content. In order to fully realize the benefits of growing HgZnTe on lattice matched substrates, we are addressing these issues and will report the results of these analyses.

1. E.J. Smith, et al.,"Epitaxial Growth, Characterization, and Phase Diagram of HgZnTe",Proceedings of the 1986 U.S. Workshop on the Physics and Chemistry of Mercury Cadmium Telluride, pg. 3043-3047.

2. Ariel Sher, et al., "Mercury Zinc Telluride, A New Narrow Gap Semiconductor", Appl.Phys.Lett.46(1),1 January 1985,pg.59-61.

3. S. Sen, et al.,"Crystal Growth and Properties of Bulk HgZnTe: A New Alternative",Extended Abstracts of the 1986 U.S.Workshop on the Physics and Chemistry of Mercury Cadmium Telluride.

*Work supported by NASA/LRC through Contract No. NAS 1-8232, W.E.Miller, contract monitor.

HgCdTe Grown by Low-Temperature LPE

J.S. Chen, S.L. Johnston
Rockwell International Science Center
Thousand Oaks, CA

Liquid Phase Epitaxy (LPE) is the most mature epitaxial growth technique for HgCdTe (MCT). LPE offers a simple method of obtaining a range of MCT composition suitable for IR detectors in thermal detection and imaging systems.

The solidification temperatures of the melts used for the LPE growth of HgCdTe layers are dependent of the composition of the LPE melts. In the case of LPE growth from Te-rich melts, solidification temperatures between 400°C and 550°C are suitable for growth of HgCdTe LPE layers.

Traditionally, most LPE growth from Te-rich liquids has occurred in the 480-520°C range. The selection of this temperature range was the result of tradeoffs in Hg vapor pressure, Hg loss, Cd solubility and compositional interdiffusion. At Rockwell, a large data base exists for HgCdTe LPE layers grown from Te-rich melts at temperatures between 490 and 510°C. The electrical conductivity of the as-grown layers is p-type with carrier concentrations in the low 10^{17} cm^{-3} range. The full width at half maximum (FWHM) of (333) reflection measured by the double crystal rocking curve technique is typically 45 arc seconds. The dislocation densities of most of the layers is in the low 10^{5} cm^{-2} range. On a CdTe substrate, misfit dislocations are generated at the HgCdTe/CdTe interface. As shown by dislocation revealing on (110) cleavage plane, most of the misfit dislocations are confined in the interdiffused region between the epilayer and substrate. The thickness of this region varies from 5 to 10 um depending on growth temperature and time. It is agreed with a value predicted using diffusion constants obtained by Tang and Stevenson.[1]

We are evaluating low temperature growth (400-420°C) as a means for reducing the misfit dislocation region on CdTe substrates. CdTe substrates do not suffer the compositional non-uniformities and large Te precipitates found for CdZnTe and the purity issues of CdSeTe. In addition, low temperature LPE growth benefits from lower outdiffusion of substrate impurities and less Te precipitation.

The preliminary results are promising. Both the interdiffused and misfit dislocation regions are reduced to a 1 um width. As estimated, using Tang and Stevenson's diffusion constants, the crystallinity of the low-temperature grown layers has improved over 500°C grown layers. It indicates that to limit misfit dislocations at interface region one may use CdTe instead of CdZnTe or CdTeSe substrates when a low temperature growth technique is utilized. The FWHM of the (333) reflection ranges from 20 to 30 arc seconds. Low temperature growth also gives smoother morphologies compared to 500°C growth as well as spatial compositional uniformity at current LPE standards, $^{x}/_{x} < 2\%$ Initial electrical measurements indicate suitability for the fabrication of IR detectors.

[1]M-F S Tang and D.A. Stevenson, J. Vac Sci. Technol A7(2), 544 (1989)

GROWTH AND CHARACTERIZATION OF ISOVPE MERCURY CADMIUM TELLURIDE

S. B. Lee*, L. K. Magel, M. F. S. Tang and D. A. Stevenson
Department of Materials Science and Engineering, Stanford University
Stanford, CA 94305

J. H. Tregilgas, M. W. Goodwin and R. L. Strong
Texas Instruments Incorporated
Dallas, TX 75265

The Isothermal Vapor Phase Epitaxial method (ISOVPE) has a number of attractive aspects for the growth of Mercury Cadmium Telluride (MCT). It is easy to implement, it is close to equilibrium growth, surface morphology is excellent, and purification may be implemented by the transport step of the growth process.[1,2] Very little detail and characterization of the material, however, is reported. We describe a study of ISOVPE growth of MCT with the objective of evaluating the material quality and its suitability for devices.

The surface composition is controlled during growth using a Te-rich ternary two phase source, as shown in Fig. 1, and a CdTe or $Cd_{0.95}Zn_{0.05}Te$ substrate. The growth is limited initially by gas phase transport and limited later by interdiffusion; the transition point for these growth regimes is about 3 to 5 hours of growth at 550°C (Fig.2). The as-grown layers are p-type at liquid nitrogen temperature and are converted to n-type by low temperature annealing in a Hg ambient.

Dislocation etch pit density is measured at the surface of the film and at the interface between film and substrate with two different etchants. Etch pit density at the surface of the film grown by ISOVPE technique is in the range of $5 \times 10^4/cm^2$ to $5 \times 10^5/cm^2$ and we observe etch pits on both A and B face of (111) orientation. The crystal perfection is also evaluated using electron beam electroreflectance, electrolyte electroreflectance, Rutherford back scattering, and

x-ray methods. The crystal quality of HgCdTe film grown by ISOVPE technique is comparable to the best of LPE grown HgCdTe (Fig. 3). Surface concentrations and concentration profiles are determined by FTIR and electron probe microanalysis and values measured by the two techniques agrees well within 5%. A typical graded profile of ISOVPE grown HgCdTe is shown in Fig. 4. Carrier densities and mobilities are measured by Van der Pauw Hall measurement. Typical carrier densities and mobilities at liquid nitrogen temperature for the n-type layers are in the low $10^{15}/cm^3$ and 30,000 $cm^2/V\text{-}s$, respectively, for the materials with a cut-off of about 5.5 μm at 77°K.

The MCT layers grown by ISOVPE technique are also characterized for their MIS properties. The compositional uniformity as measured by spectral response measurements of MIS photocapacitors is very good; the cutoff wavelength varies from 10.3 to 11.2 μm on the film. The carrier concentration is also uniform and low (ranging from $1 \times 10^{15}/cm^3$ to $2 \times 10^{15}/cm^3$ generally). The storage times and RA products are within a factor of two of standard SSR material of comparable cutoff wavelength ($10.5\ \mu m \leq \lambda_c \leq 11.2\ \mu m$) indicating that the dark currents are within a factor of two. These results indicate that ISOVPE grown MCT films show great promise for infrared devices.

ACKNOWLEDGEMENT

Portions of this work were supported by DARPA under NRL contract No. N00014-86-C-2379.

REFERENCES

1. G. Cohen-Solal, Y. Marfaing, F. Bailly and M. Robot, C. R. Acad. Sci. Paris. 261, 931 (1965)
2. J. G. Fleming and D. A. Stevenson, J. Cryst. Growth 82, 621 (1987)

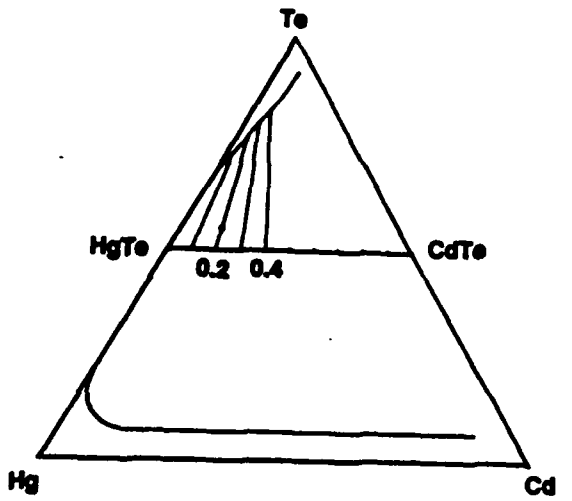

Fig. 1. Ternary phase diagram of Hg-Cd-Te system at 550°C (Dot indicates Te rich source for X=0.2 solidus line)

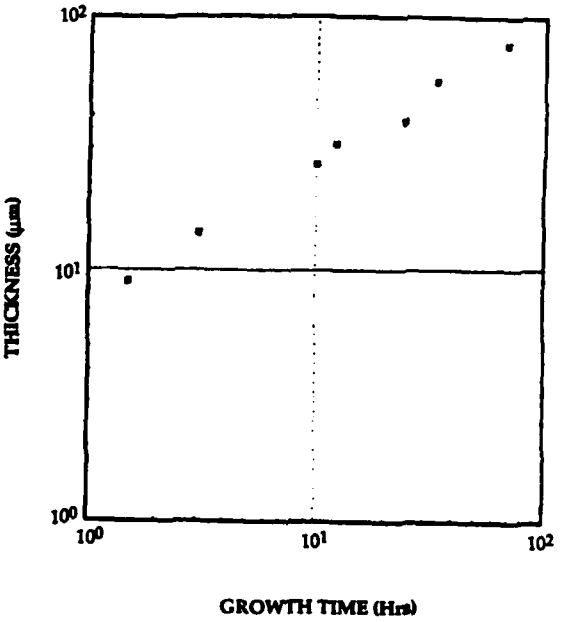

Fig. 2. A plot of thickness vs. growth time for samples grown at 550°C from a Te-rich source

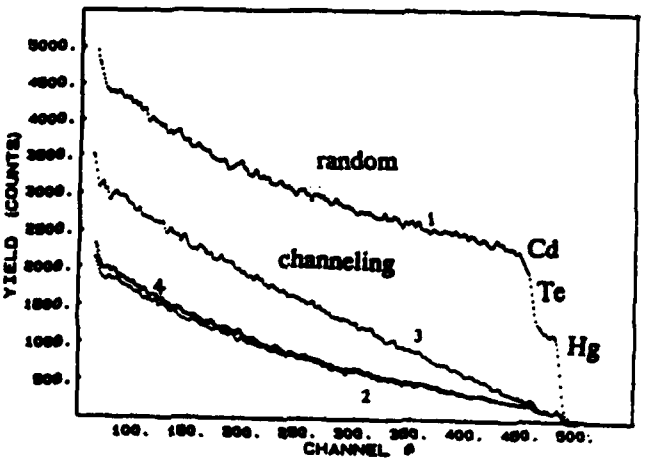

Fig. 3. RBS channeling measurement on as-grown LPE and ISOVPE films;(1)random(for concentration analysis),(2)best LPE, (3)LPE(worse than average),(4)ISOVPE

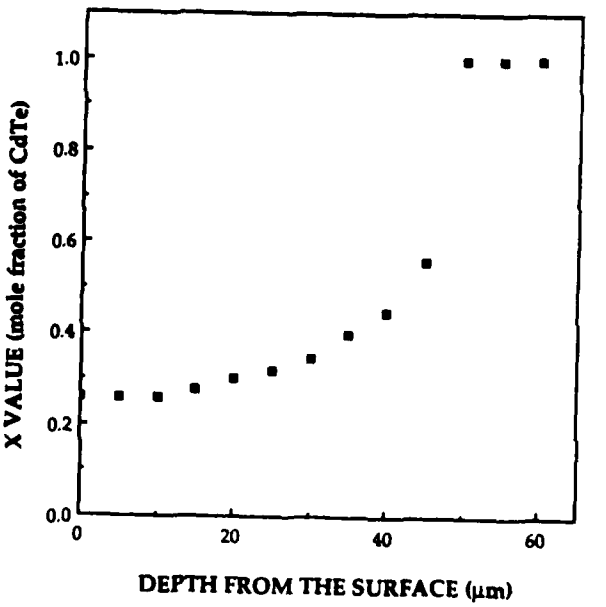

Fig. 4. Typical concentration profile of ISOVPE film measured by EPMA

RECENT ACTIVITIES ON HgCdTe AT FUJITSU

H. Takigawa

Infrared Devices Laboratory, Fujitsu Laboratories Ltd.
Morinosato-Wakamiya, Atsugi 243-01, Japan

This paper reports on HgCdTe growth activities at Fujitsu. We have been studying the growth of HgCdTe using LPE and MOCVD, and the growth of CdTe using MOCVD and hot-wall epitaxy.

Closed-tube tipping LPE using Te rich growth solutions were developed[1]. If the closed-tube apparatus is in an isothermal condition, it yields LPE wafers with a uniform alloy composition. The compositional uniformity in a typical 1-inch-square HgCdTe wafer is less than 0.08% of the CdTe mole fraction. High-purity epilayers with net impurity concentration, N_D-N_A, of about 5 X 10^{13} cm^{-3} can be obtained reproducibly by complete deoxidization of the growth solution[2].

The misfit dislocations and the origin of threading dislocations in the LPE wafer were investigated using etch pitting. In a HgCdTe/CdTe heterojunction, misfit dislocations are distributed in areas where the composition changes. The lattice mismatch at any position in the compositional transient region is accommodated by the misfit dislocation lying near the position[3]. During epilayer growth, misfit dislocations generated in the original abrupt heterojunction move in the direction of growth together with interdiffusion[4]. In a HgCdTe/CdZnTe heterojunction, misfit dislocations were found only at the original surface of the CdZnTe substrate[5]. The etch pit density distinct from the interface is almost the same as that for the substrate, and is independent of the amount of lattice match[6,7] (Figure 1). We therefore concluded that, in both heterojunctions, the threading dislocations through the LPE layers originated not from misfit dislocations in the interface, but from dislocations in the substrate. We also found that lattice match influenced the surface morphology of the epilayer, especially in the growth pattern of thin layers[8] (Figure 2).

CdTe grown by MOCVD on sapphire substrates were investigated. CdTe (111) layers grown on precise (0001)-oriented sapphire substrates exhibited a twinned structure[9]. We showed that single-domain CdTe layers can be grown on an offset-angle substrate, and also proposed a model based on surface metal organic reactions to explain single-domain formation on vicinal surfaces[10]. Spherical-surface substrates with a <0001> axis in their center were used to examine the offset-angle of domain formation. Figure 3 shows the etched surface and schematic domain structure of CdTe grown on a spherical-surface substrate. Etching revealed six domain structure regions divided by three boundary lines passing through the center of the wafer. A single-domain structure was observed in these six regions, away from the wafer edge. This indicates that the offset-angles for the single-domain CdTe layers are between 0.1° and 7°.

The dislocations in HgCdTe layers grown by MOCVD on (0001)-oriented sapphire substrate were studied. The HgCdTe layers were grown continuously after the growth of the CdTe buffer layer. Dislocation etch pit density gradually decreases from the HgCdTe/CdTe interface to the surface[11], as in heterojunctions grown by LPE. A large mismatch in the CdTe/sapphire interface causes an increase in dislocations threading through the HgCdTe layers, however.

CdTe layers were also grown by hot-wall epitaxy. Hot-wall epitaxy is growth under quasi-equilibrium. We used a (111)B GaAs substrate, holding it at 300°C during growth. Good crystallinity can be expected, even at a low temperature. An etch pit density of single-domain layers grown on offset substrates is in the range of 10^6 cm^{-2}, similarly to CdTe layers grown by MOCVD on sapphire substrates. Lamellar multilayered structures were observed by TEM up to about 0.3 μm from the hetero-interface[12].

Fujitsu has been developing IRCCDs using the crystal growth techniques we have reported here.

References

1. M. Yoshikawa, S. Ueda, and H. Takigawa, Fujitsu Sci. Technical J. 21, 494 (1985).
2. M. Yoshikawa, S. Ueda, K. Maruyama, and H. Takigawa, J. Vac. Sci. Technol. A 3, 153(1985).
3. H. Takigawa, M. Yoshikawa, M. Ito, and K. Maruyama, Mater. Res. Soc. Symp. Proc. 37, 97 (1985).
4. H. Takigawa, M. Yoshikawa, and T. Maekawa, J. Cryst. Growth 86, 446 (1988).
5. T. Maekawa, T. Saito, M. Yoshikawa, and H. Takigawa, Mater. Res. Soc. Symp. Proc. 56, 109 (1986).
6. M. Yoshikawa, K. Maruyama, T. Saito, T. Maekawa, and H. Takigawa, J. Vac. Sci. Technol. A 5, 3052 (1987).
7. M. Yoshikawa, J. Appl. Phys. 63, 1533 (1988).
8. K. Yamamoto, T. Maekawa, and H. Takigawa, Mater. Res. Soc. Symp. Proc. 130, 315 (1989).
9. K. Maruyama, M. Yoshikawa, and H. Takigawa, *ibid.* 94, 275 (1987).
10. K. Maruyama, M. Yoshikawa, and H. Takigawa, J. Cryst. Growth 93, 761 (1988).
11. K. Maruyama and K. Shinohara, J. Vac. Sci. Technol. A 7, 291 (1989).
12. K. Shinohara, Y. Nishijima, H. Ebe, and O. Ueda, Proc. of SPIE 944, 97 (1988).

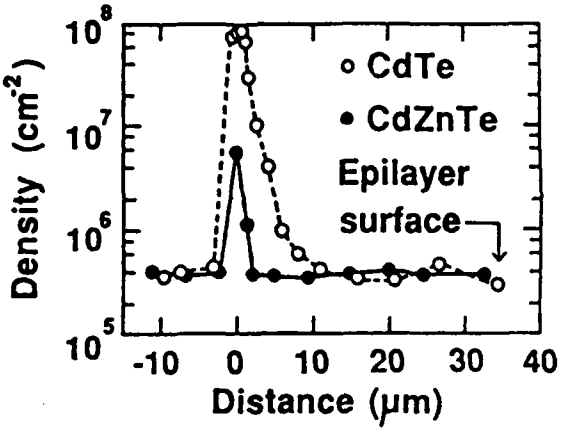

Fig. 1 Etch pit density in the direction of growth in LPE.

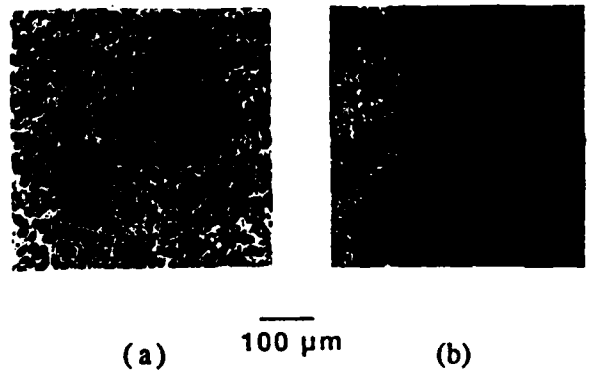

Fig. 2 Photomicrographs of the surface pattern of 3-μm-thick HgCdTe LPE layers on substrates with the following lattice mismatch: (a) CdTe ($\Delta a/a$=0.2%), (b) $Cd_{0.97}Zn_{0.03}Te$ ($\Delta a/a$=0.05%).

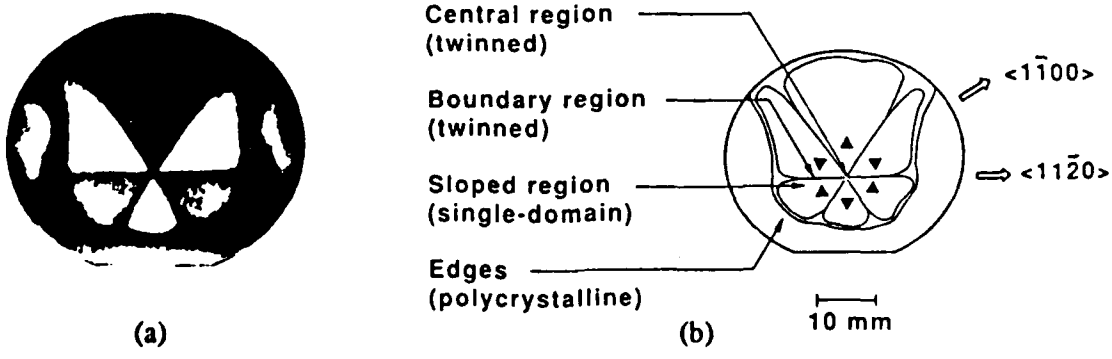

Fig. 3 CdTe layer grown on a spherical sapphire substrate: (a) etched surface, (b) schematic domain structure.

DEFECTS IN HgCdTe AND HgZnTe

M.A. Berding, M. van Schilfgaarde, A. Sher
SRI International

Controlled doping of HgCdTe and HgZnTe during bulk and epitaxial growth is of primary importance for device fabrication from these materials. A first step towards controlling the doping in these narrow gap alloys is understanding the thermodynamics of the various native point defects and impurities, based on a knowledge of the defect formation energies and impurity substitution energies in these materials.

In this paper we will discuss the results of our recent calculations of the defect formation and impurity substitution of energies in ZnTe, CdTe and HgTe. Total energy were calculated using the LMTO (Linear Muffin Tin Orbitals) method in the local-density and atomic spheres approximations. Preliminary results indicate indium substitutes on the cation site most easily in HgTe, followed by CdTe and ZnTe, with Es = +0.9, -0.8, and -2.1 eV respectively, where the reference state is the free atom state. Results for Cu, Ag, and Au acceptor- and B, Al, Ga, In donor- impurities on the cation sublattice, and P, As and Sb acceptor impurities on the anion sublattice will be presented and discussed in light of current experimental results on bulk growth and epitaxial growth of these materials. Estimates of the effect of the alloy environment on the above defect and impurity substitution energies, expected to be largest for defects substituting on the anion sublattice, will be presented. From the results on the theory and current experimental results on HgCdTe, recommendations will be made as to which dopants may work best in HgZnTe.

The antisite defect formation energies have also been calculated and preliminary results are summarized below.

COMPOUND	Te antisite energy (eV)	cation antisite energy (eV)
ZnTe	5.4	4.3
CdTe	2.5	3.7
HgTe	0.7	2.9

As expected, based on simple bond strength arguments, the antisites defect energy is largest in ZnTe and smallest in HgTe. From the above energies and the vacancy formation energies, thermodynamic reactions for the defect interactions will be calculated and discussed.

POINT DEFECTS WITH LATTICE DISTORTION IN CdTe AND HgCdTe*

J.T. Schick and C.G. Morgan-Pond
Department of Physics and Astronomy, Wayne State University
Detroit, MI 48202 USA

Results of self-consistent supercell calculations, including the effects of lattice distortion, are reported for interstitials and vacancies in CdTe and HgCdTe. We have used the tight-binding model of Majewski and Vogl, which predicts semiquantitatively the lattice constants, bulk moduli, and stable structures of perfect semiconductor crystals.[1] For interstitials in tetrahedral positions and for vacancies, a simple breathing mode relaxation of the nearest neighbors outward was considered, and the total energy was minimized to find the preferred amount of lattice distortion around the defect. For hexagonal interstitials, both relaxation outward and a possible increased puckering of the ring of neighbors surrounding the interstitial were included.

Experimental studies using different overpressures of Hg have led Vydyanath to suggest that the midgap tunneling centers in Hg-rich HgCdTe may be due to Hg interstitials.[2] Using the less accurate small-basis method,[3] we have previously found that the tetrahedral Hg interstitial between anions in Hg-rich HgCdTe has a deep defect level or resonance of A_1 symmetry in the gap region. This level holds the last two electrons for the neutral interstitial, and appears to be located close to the conduction band edge. In this work, we find that the Te nearest neighbors of this interstitial relax outward by about 3% of the unrelaxed nearest-neighbor distance. This allows the A_1 defect level occupied by the last two electrons of the neutral interstitial to become more localized on the interstitial itself, and to move lower in the gap.

Both Hg and Cd interstitials appear to play an important role in

diffusion in $Hg_{.8}Cd_{.2}Te$[4] and interdiffusion in HgTe/CdTe superlattices.[5] Experimental evidence[4] and theoretical calculations[6] indicate that Hg interstitials may diffuse through the lattice along the open channel between tetrahedral sites, while Cd interstitial diffusion requires a more complicated process, involving interchanges with atoms on lattice sites. Ultimately, calculation of total energies for complex defects involving substantial lattice distortion will be required, in order to estimate diffusion barriers and identify likely paths for diffusion of Cd interstitials. In this work, we find that the nearest neighbors of the tetrahedral Cd interstitial in CdTe are displaced away from the interstitial by 3% of the unrelaxed nearest-neighbor distance, if they are anions, and by 6%, if they are cations. For a Cd interstitial placed at the hexagonal site, we find a breathing mode relaxation of 6%, with an additional 5% increase in puckering of the ring of nearest neighbors, measured by the fractional change in the distance between the planes containing the nearest neighbors. Results for vacancies, dopant interstitials, and other self-interstitials will also be discussed.

References

* Work supported by the NVEOC and the ARO under ARO contracts DAAL03-87-K-0061 and DAAL29-85-K-0119, and by the Institute for Manufacturing Research.

1. A. Majewski and P. Vogl, Phys. Rev. B 35, 9666 (1987).
2. H. R. Vydyanath, private communication.
3. S. Goettig and C. G. Morgan-Pond, J. Vac. Sci. Technol. A 6, 2670 (1988), and to be published.
4. M.-F. Sung Tang and D.A. Stevenson, J. Vac. Sci. Technol. A 7, 544 (1989), and additional references listed here.
5. M.-F. Sung Tang and D.A. Stevenson, Appl. Phys. Lett. 50, 1272 (1987).
6. C. G. Morgan-Pond, J. T. Schick, and S. Goettig, J. Vac. Sci. Technol. A 7, 354 (1989).

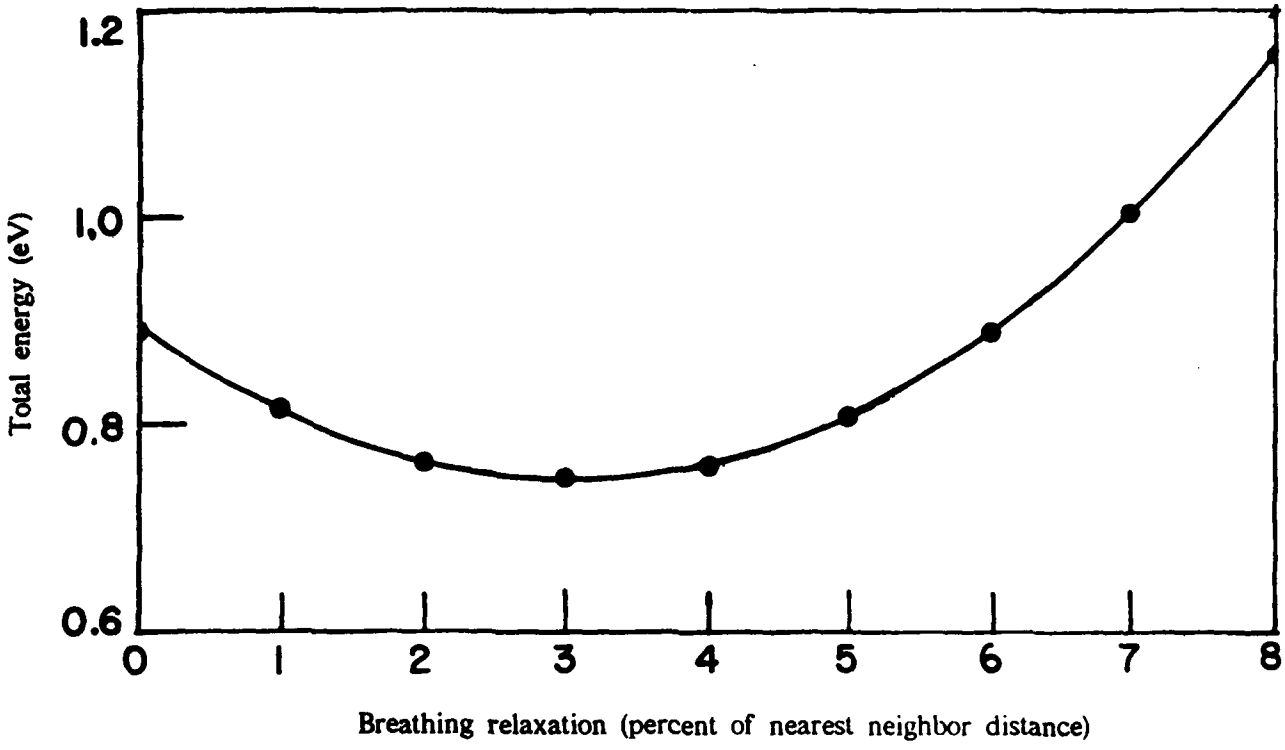

Total energy vs. breathing mode of relaxation for Hg tetrahedral interstitial between anions in HgTe.

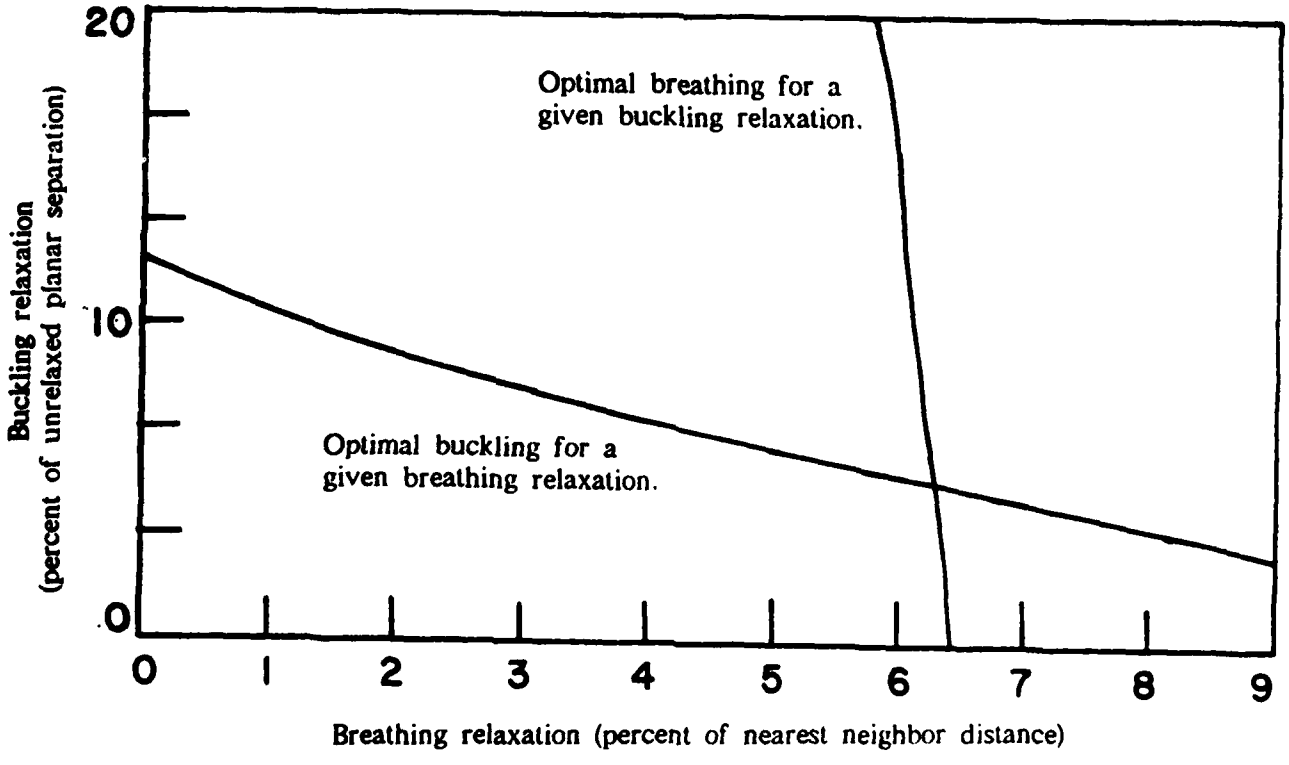

Breathing and buckling modes of relaxation for a Cd hexagonal interstitial in CdTe. The intersection of the two curves is the predicted most favorable relaxation.

POSSIBLE NEGATIVE-U PROPERTIES OF THE CATION VACANCY IN MCT

Donald E. Cooper
Rockwell International Science Center

Walter A. Harrison
Stanford University

The cation vacancy in MCT is often used to produce p-type electrical behavior, but the ionization energies of the two acceptor levels of this defect are not known. Previous workers have attributed an acceptor observed by DLTS at 15 meV above the valence band [1] to the second acceptor level (--/-) of the vacancy, and assumed that the first acceptor level (-/0) is located below the top of the valence band and is always ionized [2]. The lack of experimental evidence (DLTS and temperature-dependent Hall measurements) for the second acceptor level can also be explained if the vacancy is a negative-U center [3], for which the ionization energy of the first acceptor level is greater than that of the second acceptor level. This would make a pair of singly ionized vacancies unstable relative to a neutral and a doubly charged center. Holes would be released in pairs with an apparent ionization energy midway between the two acceptor energies.

Negative-U behavior occurs when the Jahn-Teller stabilization associated with the binding of an electron at a defect center is greater than the repulsive coulombic potential U. The vacancy in Si is one of the best characterized examples of a negative-U center [3], and we will compare the properties that determine the ordering of the defect levels in Si and MCT. The soft lattice and high dielectric constant of MCT make negative-U behavior of the vacancy very likely. Various experiments to confirm this model will be proposed. We will also discuss the implications of this model for minority carrier lifetimes in vacancy-doped MCT.

[1] C.E. Jones, K. James, J. Merz, R. Braunstein, M. Burd, M. Eetemadi, S. Hutton and J. Drumheller, J. Vac. Sci. Technol. A3, 131 (1985).

[2] C.G. Morgan-Pond, R. Raghovan, Phys. Rev. B. 31, 6616 (1985).

[3] George D. Watkins, Festkorperprobleme XXIV, 163 (1984).

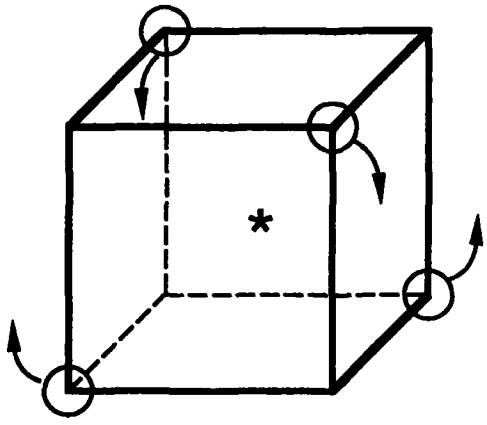

DISTORTION OF MCT LATTICE AT TETRAHEDRAL SITES SURROUNDING VACANCY.

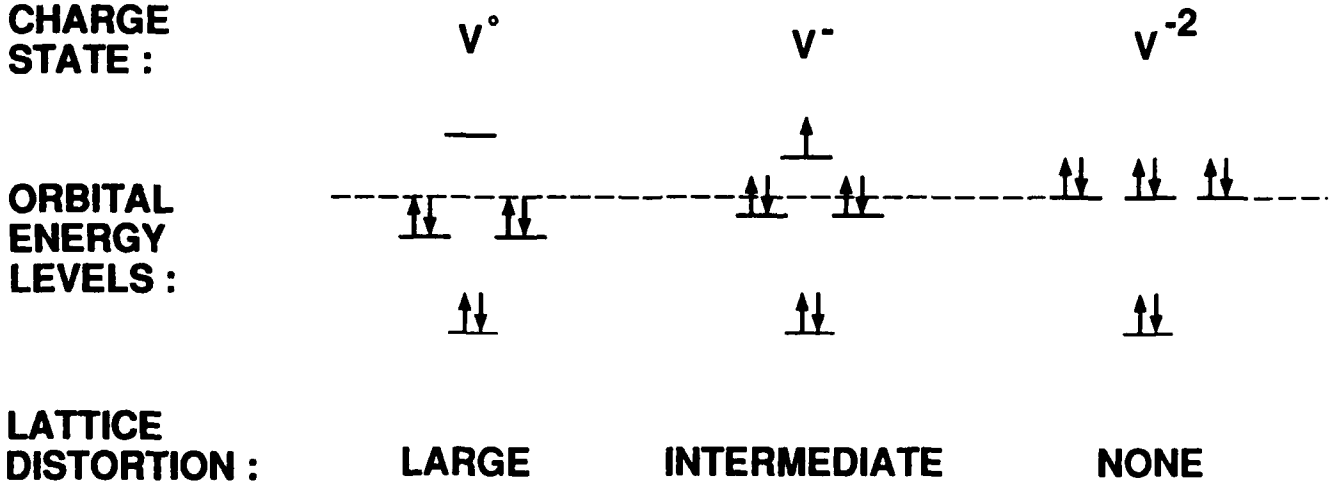

SHIFT OF VACANCY ENERGY LEVELS PRODUCED BY TETRAGONAL JAHN-TELLER DISTORTION. THE SMALLER SPLITTING OF THE V^- STATE MAKES IT UNSTABLE

LOW TEMPERATURE INTERDIFFUSION IN THE HgCdTe/CdTe SYSTEM, STUDIED AT NEAR ATOMIC RESOLUTION

Y. KIM, A. OURMAZD, and R.D. FELDMAN
AT&T Bell Labs, Holmdel, NJ 07733

We combine chemical lattice imaging and vector pattern recognition[1,2] to determine, as a function of annealing temperature, the composition of individual atomic planes across each HgCdTe/CdTe interface of a multi-quantum well stack. The resultant composition profiles, which directly reveal the chemical change across each interface at near atomic resolution, are analyzed in terms of linear and non-linear diffusion theory, to deduce the interdiffusion coefficient and its activation energy.

50 periods of HgCdTe/CdTe were grown at 180 C on GaAs (100) substrates with ZnTe buffer layers. Samples were annealed in the temperature range 200 C to 265 C for half an hour in an Ar-filled furnace. Figure 1 shows a chemical lattice image of a quantum well interface, while figure 2 shows the composition profile of the same interface before and after annealing. Such composition profiles are obtained from chemical lattice images by pattern recognition. Starting from the measured initial profile, we solve the linear diffusion equation to fit the annealed profile, using the diffusion coefficient as the fitting parameter.

Figure 3 shows an Arrhenius plot of the diffusion coefficients thus obtained for interfaces at three different distances from the surface, together with a representative selection of published data from the literature. The results show interdiffusion to be a sensitive function of the interface depth beneath the surface; the interdiffusion coefficient increases by two orders of magnitude as the quantum well depth is reduced from 7000 to 100 Å. Analysis in terms of linear diffusion theory results in a depth dependent activation energy, which decreases by nearly a factor of two from 0.83 to 0.47 eV, as the quantum well depth is changed from 7000 to 100 Å. This implies a dramatic change of up to 10^5x in the room temperature stability of a quantum well as its depth beneath the surface is varied[2].

For high temperature anneals, analysis in terms of non-linear diffusion theory gives more satisfactory fits to the composition profiles. We have numerically solved the non-linear diffusion equation by assuming a linear variation of the defect formation energy with composion[3]:

$$D(C,T)=D_o(T)exp(\alpha(T)C_{Hg}),$$

where $\alpha(T)=(\Delta F_{Cd}-\Delta F_{Hg})/kT$, $\Delta F_{material}$ the free energies of formation of vacancies and C_{Hg} is the Hg concentration. Plots of $\ln D_o$, and α vs 1/kT shown in figure 4 show that the enthalpies and entropies for diffusion are depth independent, but the pre-exponent factor varies with depth. This indicates the depth dependence of the interdiffusion to arise from an inhomogeneous, depth dependent distribution of the point defects involved in the diffusion process.

References

1. A. Ourmazd, D.W. Taylor, J. Cunningham and C.W. Tu, Phys. Rev. Lett., 62 933 (1989).

2. Y. Kim, A. Ourmazd, R.D. Feldman, J.A. Rentschler, D.W. Taylor and R.F. Austin, Proc. MRS Fall Meeting, Boston (1988), in press.

3. Y. Kim, A. Ourmazd, M. Bode and R.D. Feldmann, Phys. Rev. Lett., 63 636 (1989).

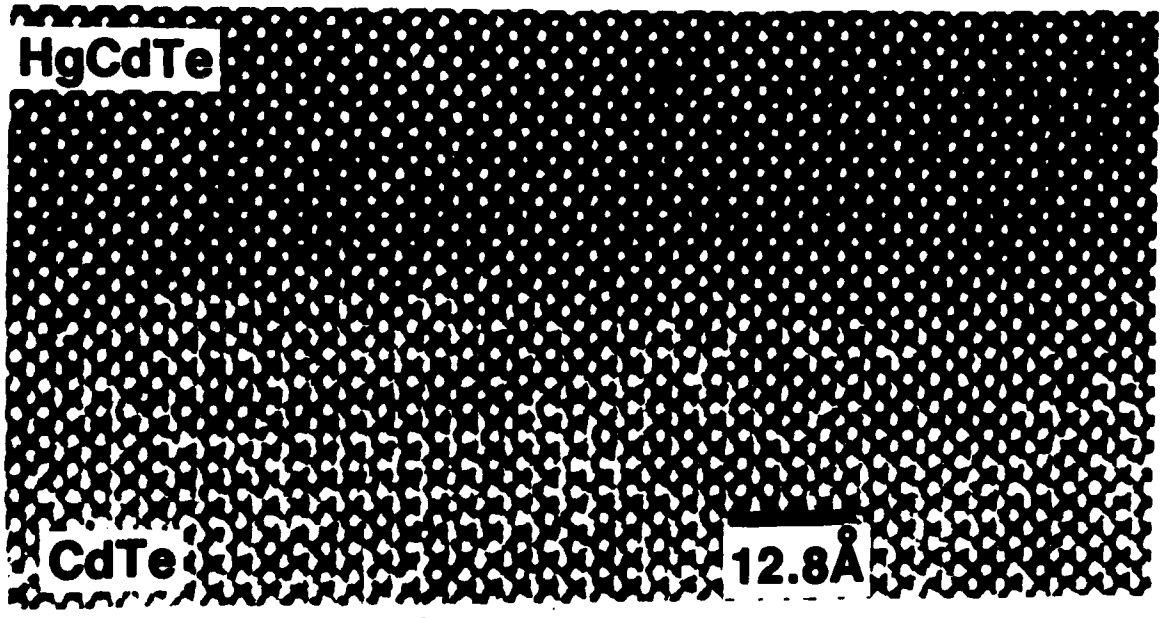

Figure 1. Chemical lattice image of HgCdTe/CdTe showing bottom interface of 27th quantum well, as-grown.

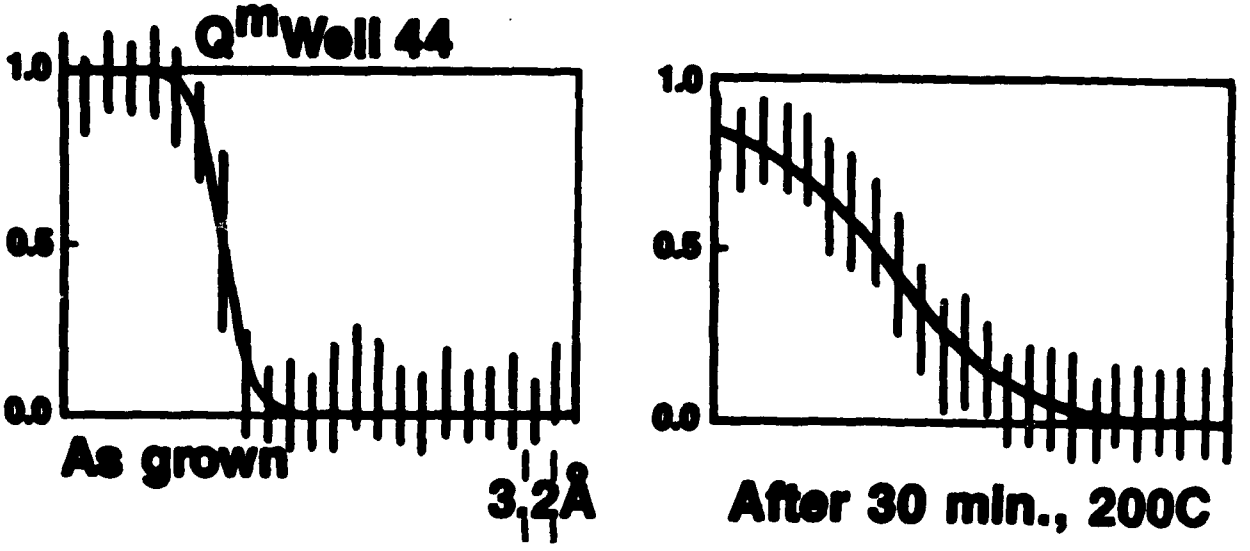

Figure 2. Composition profile at the bottom interface of the 44th quantum well, as-grown and after a 200 C, 1/2 hr. anneal. The vertical bars represent ± one standard deviation around the average value. One interval between bars is an atomic layer (3.2 Å).

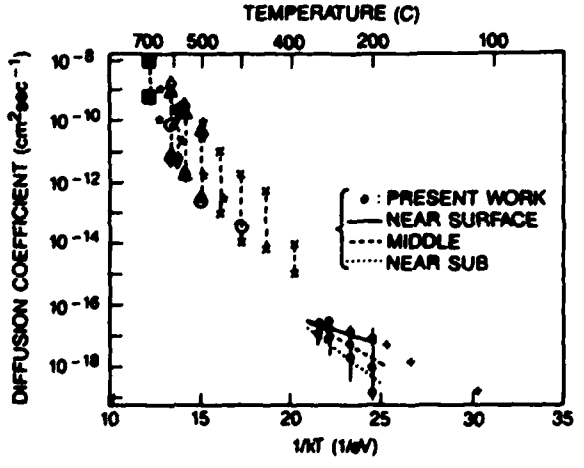

Figure 3. Arrhenius plot of interdiffusion coefficients deduced from linear diffusion theory. A selection of data from the literature is also shown. Dotted vertical lines show variation of diffusivity with Hg content or ambient conditions.

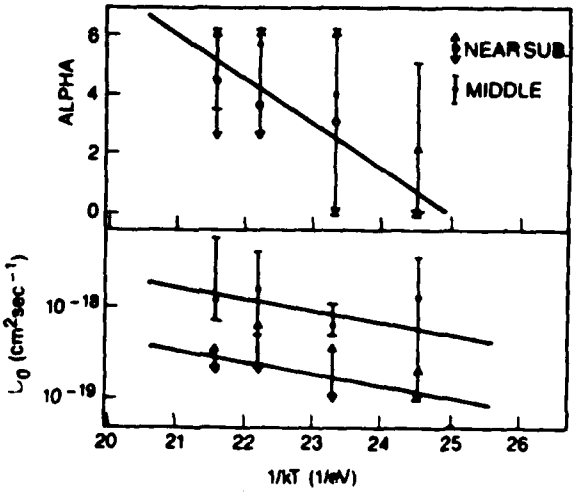

Figure 4. PLots of the exponent α and $lnD_o vs\, 1/kT$. Note that only the pre-exponential factor (given by the intercept of D_0 at large T) changes with depth.

DIFFUSION AND HARDNESS STUDIES IN MERCURY ZINC TELLURIDE

S. Fang, L. J. Farthing, M. F. S. Tang, and D. A. Stevenson
Department of Materials Science and Engineering
Stanford University, CA 94305

The ternary compound $Hg_{1-x}Zn_xTe$ (MZT) has been proposed as a superior infrared detector material, based on predictions that it is more stable than $Hg_{1-x}Cd_xTe$ (MCT)[1]. A lower diffusion rate[2] and superior mechanical properties[3,4] could moderate processing difficulties and improve device performance. We report studies of self-diffusion, interdiffusion, and hardness measurements in MZT in order to compare relative properties of MCT and MZT.

Tracer self-diffusion (D*) studies are made in x = 0.1 MZT using Hg^{203} and Zn^{65} tracers and mechanical sectioning techniques. The diffusion profiles for Hg are complex and can be represented by two branches corresponding to a slow (s) and fast (f) process. In contrast, there is only one branch consistently observed for Zn. The diffusion mechanism is elucidated by studying the dependence of the diffusion quantities on the Hg partial pressure (P_{Hg}). Figure 1 shows a diffusion isotherm ($\log D^*_{Hg}(f)$ vs $\log P_{Hg}$) with the slope changing from -1 to +1 as the stoichiometry varies from Te rich to Hg rich, while the values of $D^*_{Hg}(s)$ and D^*_{Zn} are independent of P_{Hg}. The self-diffusion behavior of MZT is similar to that of MCT[5]. The self-diffusion coefficient of Hg in x = 0.1 MZT is faster than that in x = 0.2 MCT, and the diffusion rate of Zn is comparable to that of Cd (s) in the respective compounds.

Interdiffusion measurements are made using HgTe/ZnTe diffusion couples with the Boltzmann-Matano analysis and also by analysis of isothermal vapor phase epitaxial (ISOVPE) growth kinetics[6]. Figure 2 shows interdiffusion coefficients versus composition for MCT and MZT at 500°C and 600°C. Our results are comparable to Pobla et al.[2] within factor of two. Interdiffusion behavior in MZT is similar to that of MCT at low x values and shows a significant decrease with increasing x, but is less x dependent at high x values than in MCT. The self and interdiffusion results in MZT are related with a Nernst-Planck type of equation that is relevant for pseudobinary systems in which one sublattice is relatively immobile[5]. It indicates that the Te sublattice is relatively immobile and the slower diffusing metal species (Zn) is the rate limiting species in the interdiffusion process. The interdiffusion quantities in MZT are only marginally lower than in MCT for the conditions studied.

Compound semiconductor alloys are very difficult to grow in single crystal bulk form and are usually prepared in thin film form only. Because of this, hardness measurements are the only practical method for evaluating the mechanical properties. Hardness values are determined as a function of composition in MCT and MZT using a Vickers indenter, a Knoop indenter, and a Nanoindenter. Thick films (50-100 μm) of MCT and MZT grown by ISOVPE have graded

compositions, so hardness can be measured in a few films for a wide range of compositions. Figure 3 shows hardness, as measured by either a Vickers indenter or a Knoop indenter, as a function of x for both MCT and MZT. Our hardness values for MZT agree with those of Triboulet et al.[4] and Schenk and Fissel[7]. Our MZT samples are thick films while Triboulet et al. and Schenk and Fissel used bulk MZT samples grown by the travelling heater method (THM). Our hardness values for MCT agree with those of Triboulet et al.[4] and Cole et al.[8]. Our MCT samples are thick films while Triboulet et al. and Cole et al. studied bulk THM and Bridgman MCT samples, respectively. Our data for both MCT and MZT show excellent agreement with published hardness values, despite the differences in types of samples. Bowing is more pronounced in the MZT system due to solid solution hardening arising from the strains induced in the matrix by the significant difference in the bond lengths of HgTe and ZnTe (5.5%). There is little difference in the bond lengths of HgTe and CdTe; thus, the bowing in hardness is thought to be due either to the elastic and electrical interactions of solute atoms with dislocations[8] or to bond length changes in MCT during alloying[9].

In summary, MZT seems to have significant advantages over MCT with regard to improved hardness, but only marginal difference in diffusion behavior.

This research was sponsored by DARPA through ONR N00014-84-K-0423 and the AFOSR 86-01588. We thank Dr. A. Sher and Dr. M. Berding of SRI International and Dr. M. Sen of the Santa Barbara Research Center for their many helpful discussions.

References:

1. A. Sher, A.-B. Chen, W. E. Spicer, and C. K. Shih, J. Vac. Sci. Technol. A3, 105 (1985)
2. C. Pobla, R. Granger, S. Rolland, and R. Triboulet, J. Crystal Growth 79, 515 (1986)
3. E. J. Smith, S. Shen, M.T. Smith, C. R. Curtis, L. J. Farthing, T. Weihs, M. F. S. Tang and D. A. Stevenson, paper presented in IRIS meeting 1987.
4. R. Triboulet, A. Lasbley, B. Toulouze and R. Granger, J. Crystal Growth 79, 695 (1986).
5. M. F. S. Tang and D. A. Stevenson, submitted for publication.
6. J. G. Fleming and D. A. Stevenson, J. Crystal Growth 82, 621 (1987).
7. M. Schenk and A. Fissel, J. Crystal Growth 86, 502 (1988).
8. S. Cole, M. Brown, and A. F. W. Wiloughby, J. Materials Science 17, 2061 (1982).
9. A. Sher, A.-B. Chen, and W. E. Spicer, Appl. Phys. Lett. 46, 54 (1985).

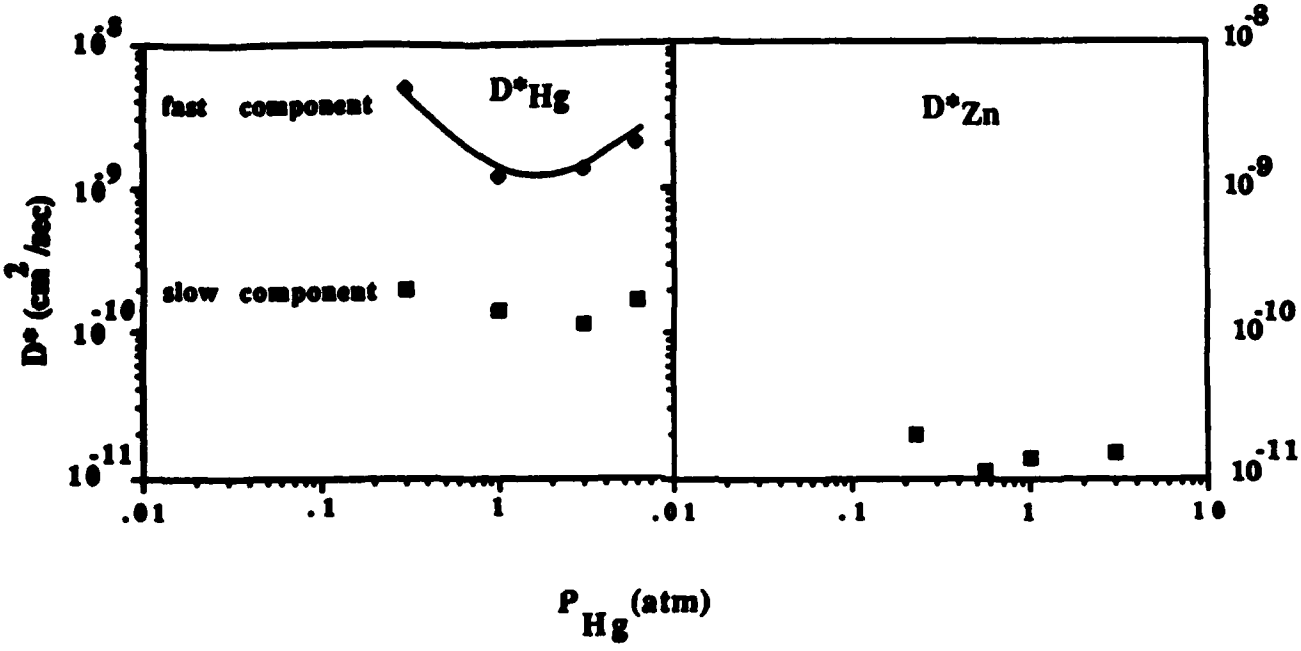

Fig. 1. D^*_{Hg} and D^*_{Zn} diffusion isotherms at 500°C

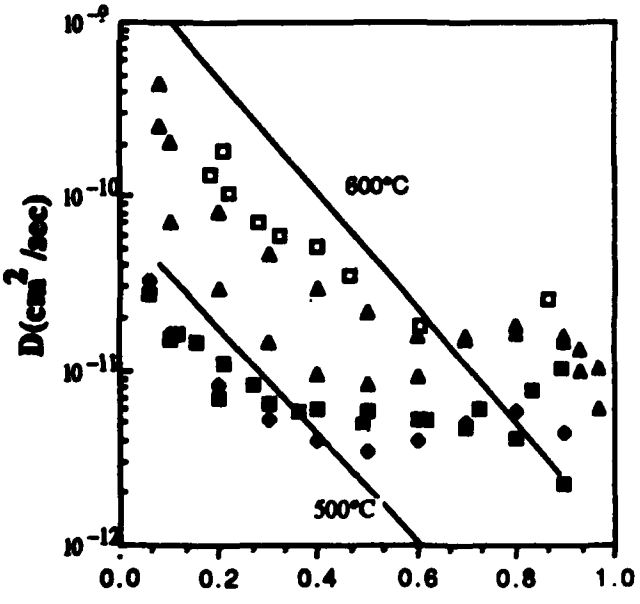

MZT { ■ ▲ - diffusion couple, our data
■ □ - ISOVPE, our data
◆ ▲ - Pobla et al.
—— - MCT

Fig. 2. Interdiffusion coefficients of MZT and MCT

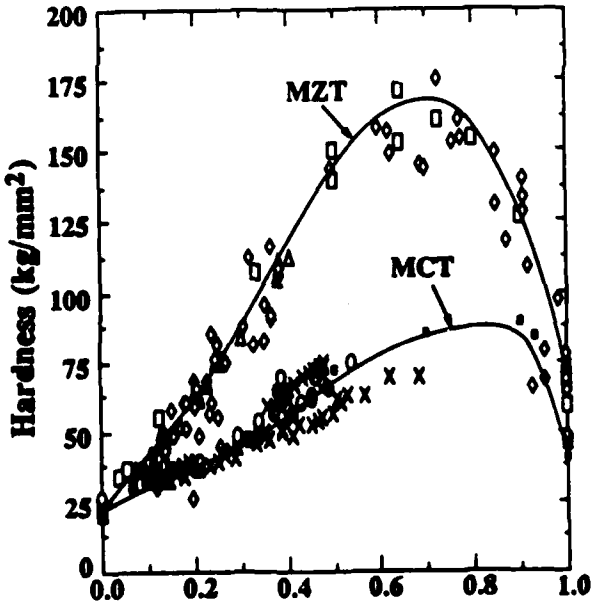

□ • Triboulet et al. ▲ Schenk and Fissel
○ Cole et al. ● × Our data

Fig. 3. Hardness of MZT and MCT as a function of composition

Simple Interpretation Techniques for Laser Beam Induced Current Measurements in HgCdTe

John Hennessy,
Waterloo Scientific Inc., 419 Phillip St., #9, Waterloo, Ontario, Canada. N2L 3X2

Paul McDonald,
Honeywell Electro-Optics Division, 2 Forbes Rd., Lexington Massachusetts, USA.

Laser Beam Induced Current imaging is a powerful method for investigation of the distribution of electric fields in HgCdTe materials and devices. Bajaj et.al (1987), in the first publication on the topic, illustrated its application to the mapping of focal plane arrays at a fairly advanced stage in processing and to mid-wave and long-wave epilayer material. In the case of arrays they were able to show a correlation between LBIC and the physical structure of the samples, but could not identify features in the epilayer samples. We present results from LBIC examination of epilayer materials with interpretations based on well established modeling methods used in self-potential geophysical surveying. (Babu & Atchuta Rao (1988), Grant & West (1965)).

By considering the electric field surrounding a variety of simple charged bodies buried in an otherwise homogeneous medium, we can calculate the induced current profile that would be observed when scanning over them. The shape of the profiles contains information about the shape and orientation of the anomalous regions; analysis of complex patterns is possible by superposition of a number of these simple curves.

The validity of this modeling process is checked by reference to data recorded from samples with recognizable physical defects. As the bulk material characteristics and dimensions are well known in semiconductors when compared with the regime of geophysical modeling, this technique offers the possibility of a reliable semi-quantitative method for modeling the three dimensional electric properties of materials such as HgCdTe.

References:

Babu, H.V. and Atchuta Rao, D. A rapid graphical method for the interpreta on of the self-potential anomaly over a two-dimensional inclined sheet of finite depth extent. Geophysics Vol 43 (8), p1126-1128. 1988

Bajaj, J., Bubulac, L.O., Newman, P.R., Tennant, W.E. and Raccah, P.M.. Spatial mapping of electrically active defects in HgCdTe using laser beam-induced current. J. Vac. Sci. Technol. A5(5), p3186-3189. 1987.

Grant, F.S. and West, G.F. Interpretation Theory in Applied Geophysics. McGraw-Hill Book Company. 583pp. 1965.

Magneto-Optical Investigation of Impurity and Defect Levels in HgCdTe Alloys

C. L. Littler and M. R. Loloee
Department of Physics
University of North Texas
Denton, Texas 76203

D. G. Seiler
Semiconductor Electronics Division
National Institute of Standards and Technology
Gaithersburg, Maryland 20899

Alloys of mercury cadmium telluride ($Hg_{1-x}Cd_xTe$) constitute one of the most important detector materials for infrared applications in both the 3-5 and 8-14 μm spectral regions. The performance of this material is primarily related to the number of impurities, defects, and trap levels that are present in the alloy. Hence, detection and identification of these impurities or defects is needed both for guiding material advances and improving the theoretical modelling of detector performance.

To characterize impurities and defects present in a semiconductor material, one prefers a technique that is sensitive, rapid, and straightforward to analyze. In the past two decades, different techniques - deep level transient spectroscopy (DLTS), thermally stimulated current (TSC), optical modulation absorption (OMA) diode pulse recovery, etc. have been used for this type of characterization. In contrast to these methods, we have used magneto-optical spectroscopy to directly measure the impurity/defect activation energies in a number of $Hg_{1-x}Cd_xTe$ alloys.

Recently, two-photon magneto-optical (TPMO) techniques were used to accurately determine the energy gap (E_g) of a number of HgCdTe samples from $x \simeq 0.24$ to 0.30.[1] In addition to TPMO, initial observations of magneto-optical transitions of electrons from both near midgap and shallow acceptor levels to the conduction band Landau levels were reported. Here, we present extensive new magneto-optical results on impurity and defect levels in ten samples of HgCdTe. The samples were grown by solid state recrystallization and the traveling heater method (THM). The output of a grating tunable CO_2 laser was focussed onto samples placed in a 12 T superconducting magnet/variable temperature dewar. The impurity magneto-optical spectra were recorded by monitoring the photoconductive response of each sample using boxcar averaging techniques. Light polarization and variable temperature data were taken to verify the origin of the observed magneto-optical resonances. The activation energies of these levels appear to fall into three catagories: (1) 10-12 meV above the valence band edge (VBE), independent of E_g, (2) $\simeq 0.25\ E_g$ above VBE, and (3) two closely spaced levels at $\simeq 0.5\ E_g$.

[1] D. G. Seiler, C. L. Littler, M. R. Loloee, and S. A. Milazzo, J. Vac. Sci. Technol. A7, 370 (1989) and D. G. Seiler, M. R. Loloee, S. A. Milazzo, A. J. Durkin, and C. L. Littler, Solid State Commun. 69, 757 (1989).

Work supported by the U. S. Army Center for Night Vision and Electro-Optics, Contract No. DAAB07-87-C-FO94 and a grant from Texas Instruments, Inc.

RAPID ELECTRICAL CHARACTERIZATION OF PROCESS INDUCED DAMAGE IN MERCURY CADMIUM TELLURIDE

J. L. Elkind and M. C. Chen
Texas Instruments Incorporated
Dallas, Texas 75265

Despite HgCdTe's widespread importance as a material for the detection of infrared radiation, its processing is still not well understood. Ion milling is one example of a standard semiconductor processing technique, whose effect on the electrical properties of HgCdTe is not completely understood. Building actual devices to evaluate process induced effects is not only time consuming, but may also superimpose other effects onto the results of the experiment. Here we report how two rapid techniques may be utilized to replace device fabrication as a first pass evaluation.

Microwave Reflectance Measurements of Minority Carrier Lifetime:[1]

A 10 GHz, 50 mW microwave beam is directed through a horn antenna toward the surface of a HgCdTe bar. When the sample is illuminated by an infrared light pulse its conductivity increases temporarily and a microwave detector senses the transient change in the reflected microwave power.

Shown in Fig. 1 is a typical lifetime trace for bulk SSR n-type HgCdTe. The lifetime is approximately 1.0 us. Table I contains data derived from another sample, that same sample after having 5 microns ion milled from the surface, and that same sample after having several microns removed from the ion milled surface by a wet etch. The signal magnitude is down dramatically after ion milling, and to a lesser extent following the wet etch. It is

interesting that the lifetime is not reduced after the ion mill.

MIS C-V studies indicate that the original surface is of high quality material, the ion milled surface has an extremely elevated net donor concentration, and the ion milled surface after removal of several microns by wet etch is intermediate between the two. This qualitative result was "predicted" by the microwave reflectance measurements in which the relected signal is dependent on the sample's conductivity.

Eddy Current Conductivity Measurements:[2]

A probe consists of two sets of rf coils, with a driving coil and a sensing coil in each set. The driving coil, using an rf current, induces an eddy current in the sample. This eddy current, whose magnitude is proportional to the sample's conductivity and thickness, is then detected using a phase sensitive technique. The coils typically have a diameter of 1 mm.

Table II shows the conductivity, measured by the eddy current technique, of a bar of n-type HgCdTe grown by SSR, that after having 5 microns ion milled from the surface, and that after several microns have been removed from the ion milled surface. Clearly, the ion mill treatment has raised the conductivity of the HgCdTe bar. Even after removing several microns from the ion milled surface, the conductivity is elevated relative to the original value.

Clearly, both microwave reflectance measurements of minority carrier lifetime and eddy current measurements of conductivity may be used to probe process induced damage. Additionally, these

techniques may be combined with a chemical polish to provide detailed damage depth information, or coupled with Hall measurements to separate changes in conductivity into changes in mobility and in carrier concentration.

References:

1. M. C. Chen, J. Appl. Phy. 64, 945 (1988).
2. M. C. Chen, Rev. Sci. Instrum. 60, 1116 (1989).

FIGURE I:

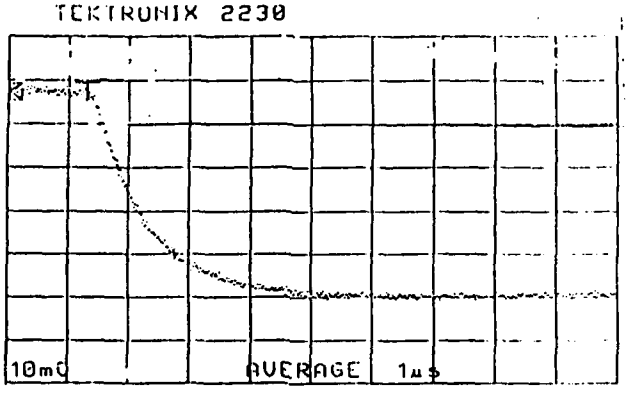

TABLE I:

Microwave Reflectance Data:

Sample Description	Signal Magnitude (mV)	Lifetime (us)
Before Ion Milling	35	1.7
After Ion Milling	3.5	1.4
After Wet Etch	9	1.8

TABLE II:

Eddy Current Conductivity Data:

Sample Description	Conductivity (1/ohm*cm)
Before Ion Milling	4.7
After Ion Milling	23.2
After Wet Etch	16.9

ION IMPLANTATION INTO MCT THROUGH DIELCTRIC ENCAPSULANTS[1]

by

N.F. Deutscher R.J. Roedel

Center for Solid State Electronics Research, Arizona State University, Tempe, AZ, 85287

L. McIntyre J. Leavitt

Department of Physics, University of Arizona, Tucson, AZ, 87520

Ion implantation through dielectric caps is a common method used in GaAs processing. The encapsulant acts as a passivation layer to prevent any unwanted changes to the underlying semiconductor that might occur during the implantation or heat treatments. This technique has not been applied to implantation in MCT, as most implants have been performed on bare surfaces. The purpose of this work has been to find an effective encapsulant that will passivate the surface preventing Hg loss or any other untoward changes during implantation or heat treatments. To this end implantations and subsequent anneals were carried out on samples protected by differing thicknesses of silicon dioxide and indium tin oxide (ITO).Implantations were also performed on uncapped samples for comparison.

Epitaxial MCT material was provided by Litton Industries, grown on <111> oriented (Cd,Zn)Te. The mercury telluride fraction was approximately 70%. The dielectric caps were deposited by radio frequency (RF) sputtering, and the samples were implanted with aluminum ions at an energy of 200keV and a dose of 1e14 ions/cm^2. After implantation some samples were annealed in a conventional furnace at 300°C for 1 hour in a nitrogen atmosphere with no Hg overpressure. The implants were then characterized by Rutherford backscattering(RBS) and Hall measurements.

Hall measurements on the implanted and annealed samples indicate that the samples were converted n-type by the implantation and remained n-type after annealing. The channeling RBS experiments indicate that the implantation damage was removed and the ITO capped samples were returned to the original crystallinity. Figure 1 shows RBS spectra for an implanted

[1] This research was supported by Litton Industries

sample, LPE-465.2, and an implanted and annealed sample, LPE-133.2, that had caps of 650Å of ITO. Random RBS experiments show that the implanted and annealed sample did not suffer Hg loss during the heat treatment, Fig. 2. Sample LPE-133.4 is an as grown sample and shown for comparison. Figure 3 shows the random RBS spectrum for a sample that was implanted and annealed with a SiO_2 cap of about 600Å, LPE-457.3, and an as grown sample, LPE-457.4. The RBS results show that Hg has been lost during the heat treatment. These results indicate that ITO may be a good encapsulant to preserve the stoichiometry of MCT during heat treatments.

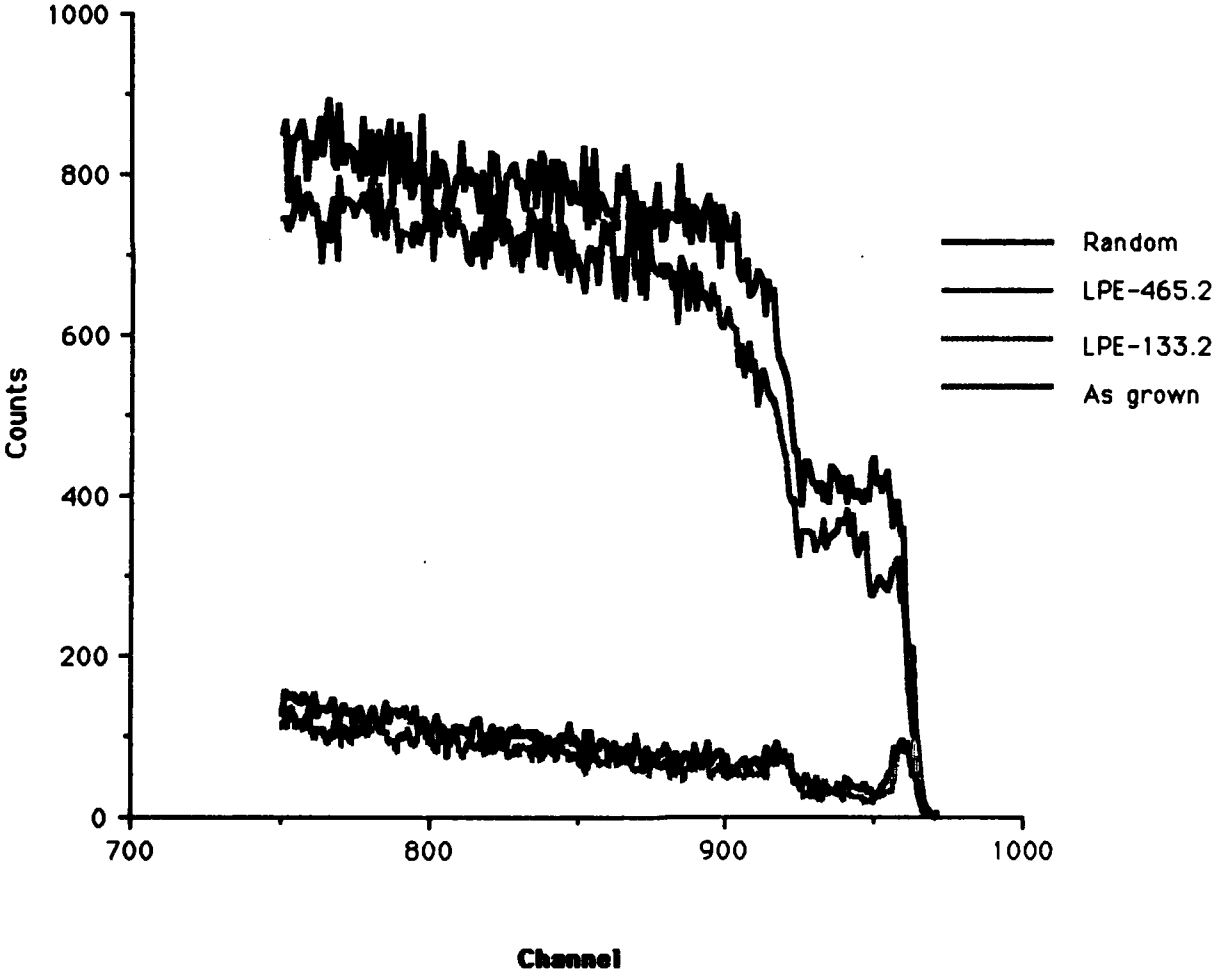

Figure 1. Channeling RBS spectra for implanted (LPE-465.2) and implanted and annealed (LPE-133.2) samples capped with 650Å of ITO

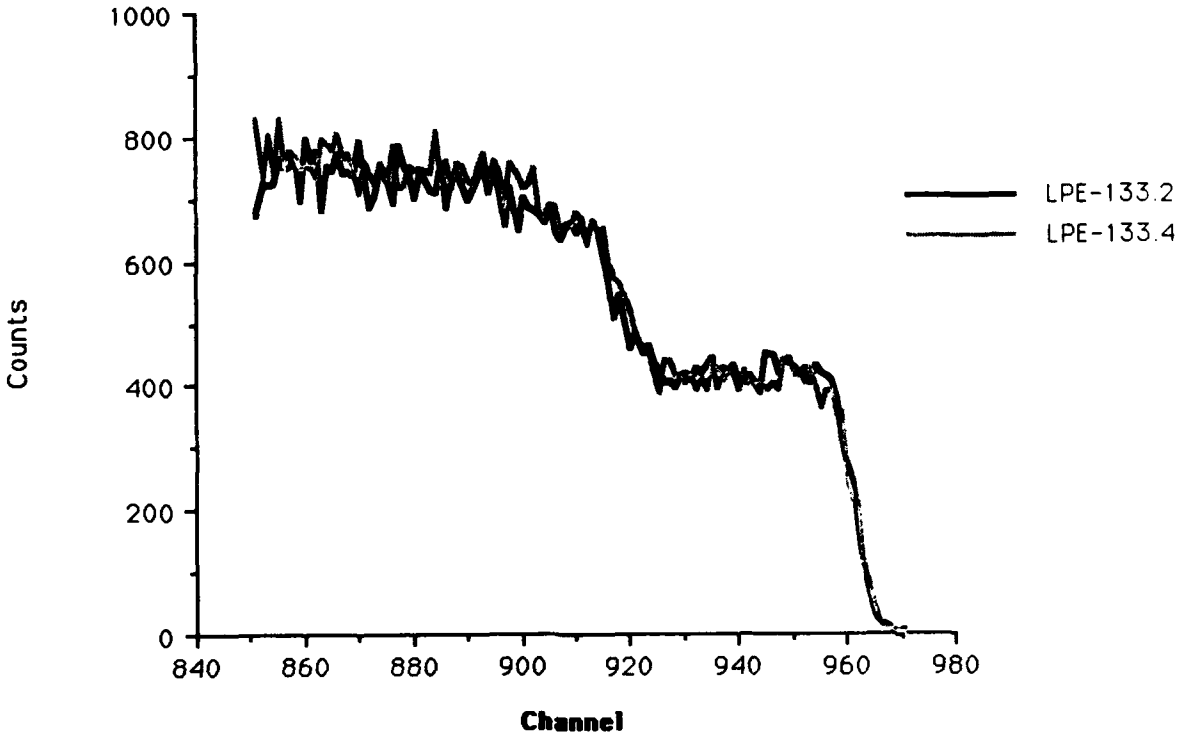

Figure 2. Random RBS spectrum of implanted and annealed sample capped with 650Å of ITO

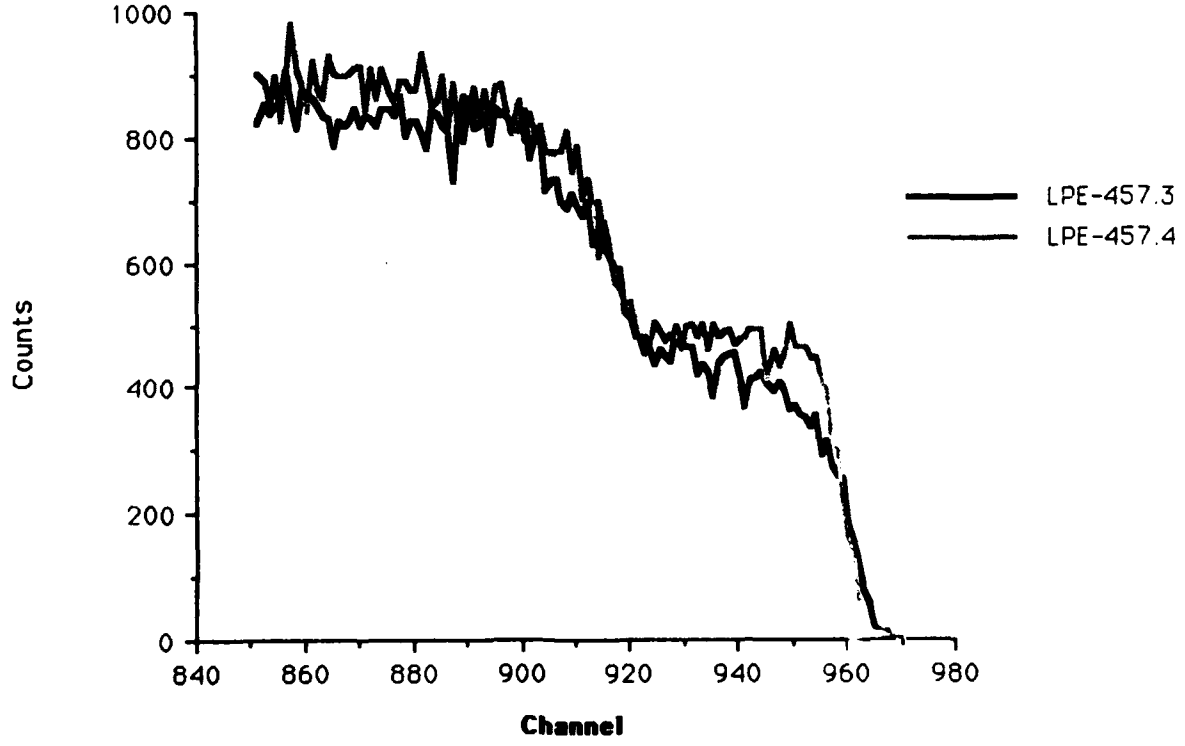

Figure 3. Random RBS spectrum of implanted and annealed sample capped with 600Å of SiO2

Effect of Twinning in (111)B $Hg_{1-x}Cd_xTe$ Grown by MBE

S. Sivananthan, S.S.Yoo, M. Boukerche, R. Sporken, G. Monfroy,
P.S. Wijewarnasuriya, M.Lange and J.P. Faurie

Dept. of Physics, University of Illinois at Chicago,
Chicago, IL 60680

The potential electrical and optical performance capabilities of $Hg_{1-x}Cd_xTe$ (MCT) are not reached due to its structural imperfections. The major problem is the occurrence of twinning faults in this compound. Twins are predominant for epitaxial growth in the (111) orientation. In (111)B MCT grown by MBE, a columnar type and a laminar type of twinning is observed. The presence of twinning is evidenced by double crystal x-ray rocking curves recorded on the (422) reflection, chemical etch pits and scanning electron micrographs. Here we will present the study of different types of twins, and their relation to the transport properties of (111)B MCT layers, as well as, to the performance of photodiodes fabricated in them.

Neither drastic degradation nor enhancement in the transport properties and diode performances is observed when the columnar type twins are present. On the other hand, laminar twins in MCT totally degrade diode performance and minority carrier life-time. However, enhancements in the hole hole concentration and hole mobility are often observed with the presence of laminar twins. This increase in hole concentration is attributed to an out diffusion of Hg, which is evidenced by X-ray photoelectron spectroscopy. The enhancement of the hole mobility is probably due to a type III interface, related to the presence of laminar twins.

These observations were confirmed by the detailed investigation of an MCT layer in which laminar twins are present only in the uppermost 3 microns, and in which the remaining 8 microns are twin-free. The results which will be discussed include the differential Hall measurement of this layer and characteristics of the diodes fabricated on a wedge-shape etched section of it. The differential Hall measurement at 80K gave a carrier concentration (N_A-N_D) of 5.2×10^{14} cm^{-3} for the twin-free portion of the layer and $1.2\times10^{15}cm^{-3}$ for the uppermost portion in which laminar twins are present. The zero-bias resistance-area product (R_0A) at 80K was 2×10^{1} ohm-cm^2 for the area with laminar twins, which was distinctly lower than the value of 2×10^{4} ohm-cm^2 for the twin-free part of the layer.

STUDIES OF Au "OHMIC" CONTACTS TO P-TYPE $Hg_{1-x}Cd_xTe$

V.Krishnamurthy [a], A. Simmons [b], and C.R. Helms [a]

[a] Dept. of Electrical Engineering, Stanford University, Stanford, Ca. 94305

[b] Texas Instruments Inc., Dallas, Texas 75265

Ohmic contacts to p-type $Hg_{1-x}Cd_xTe$ are instrumental to the development of advanced monolithic $Hg_{1-x}Cd_xTe$ IR / CCD technologies [1,2]. At present, Au is the primary metal used for ohmic contacts. We investigated the electrical and morphological properites of electroless Au contacts and Au contacts with and without a thin plasma oxide layer . The electroless Au contacts are formed by immersing $Hg_{1-x}Cd_xTe$ in a .5% $AuCl_3$ solution . The plasma oxide is formed by exposing the $Hg_{1-x}Cd_xTe$ to an oxygen plasma in an RF chamber. In this paper, we show that Au contacts with interfacial oxide layers and electroless Au contacts exhibit relatively low barrier heights and contact resistances. In comparison, Au contacts without interfacial layers are rectifying with barrier heights at or above the bandgap.

I-V data on as-deposited unoxidized contacts indicated a high contact resistance. The annealed unoxidized contacts also exhibited this behavior. These contacts were rectifying with a high barrier height giving contact resistances greater than $7 \times 10^{1}\ \Omega\text{-cm}^2$. Fitting the I-V data, we obtained an approximate barrier height on the order of the bandgap (.25eV at 77 °K). Auger sputter profiles of Au (200Å) / p-type $Hg_{.7}Cd_{.3}Te$ contacts (as-deposited and annealed at 100°C) are shown in Fig. 1(a) and Fig. 1(b). We observe that the Au has reacted with the substrate in both cases. Correlating the electrical data with the Auger sputter profiles, we infer that the Au reaction with the substrate is responsible for the rectifying behavior. The Au reaction may have produced a large number of interface states pinning the Fermi level near the conduction band minimum (CBM). Also, Au probably does not provide heavy substrate doping because the solid solubility of Au in $Hg_{1-x}Cd_xTe$ (x=.2, .3) is only 10^{16} / cm^3 [3]. For the plasma oxidized contacts , the as-deposited devices were rectifying with an approximate barrier height of .1eV and contact resistances ranging from $8 \times 10^{-1}\ \Omega\text{-cm}^2$ to $6\ \Omega\text{-cm}^2$. An Auger sputter profile of as-deposited

Au (200Å) / plasma oxidized Hg.7Cd.3Te is shown in Fig. 1(c). We observe that the plasma oxide has inhibited any reaction between the Au and the substrate. Therefore, the relatively low barrier height is possibly a result of the low interface state density at the plasma oxide / $Hg_{.7}Cd_{.3}Te$ interface. This is substantiated by Y. Nemirovsky *et al* [4] work on plasma oxides in which they reported that the plasma oxide / $Hg_{1-x}Cd_xTe$ interface possesses a low interface density. Following the 100ºC anneal, most of these contacts became ohmic and the contact resistances varied from 3×10^{-1} Ω-cm^2 to 1 Ω-cm^2. An Auger sputter profile of annealed Au (200Å) / plasma oxidized $Hg_{.7}Cd_{.3}Te$ is shown in Fig. 1(d). The plasma oxide layer is thermally stable and as a result, no reaction between the Au and the substrate is observed. This indicates that the ohmic behavior can possibly be attributed to a further reduction in the interface state density. Electrical measurements performed on the as-deposited electroless contacts to $Hg_{.7}Cd_{.3}Te$ indicated ohmic behavior with contact resistances varying form 2×10^{-1} Ω-cm^2 to 6 Ω-cm^2. For these electroless contacts, an interfacial layer was also found. This is shown in Fig.2, an Auger sputter profile of as-deposited Au (600Å) / $Hg_{.8}Cd_{.2}Te$ in which we observe an the interfacial layer a few hundred angstroms thick and composed of Te, O, and Cl. This interfacial layer may be responsible for the ohmic behavior since this interface may also possess a relatively low interface state density. The annealed electroless contacts, compared to the as-depostied electroless contacts, exhibited even lower contact resistances and this can also be attributed to a further reduction in the interface state density.

This work was supported by DARPA through NRL with subcontract 7482253 to Stanford University from Texas Instruments.

References

[1] M.B. Reine, A.K. Sood, and T.J. Tredwell, in *Semiconductors and Semimetals*, edited by R.K. Willardson and A.C. Beer (Academic Press, New York, NY, 1981), vol. 18, p.304.

[2] M.A. Kinch, R.A Chapman, A. Simmons, D. D. Buss, and S.R. Borrello, Infrared Phys. 20, 1 (1980).

[3] A.I. Andreivskii, A.S. Teodorovich, and A.D. Schneider, Sov. Phys. Semicond 7, 1112 (1974).

[4] Y. Nemirovsky and R. Goshen, Appl. Phys. Lett. 37, 813 (1980).

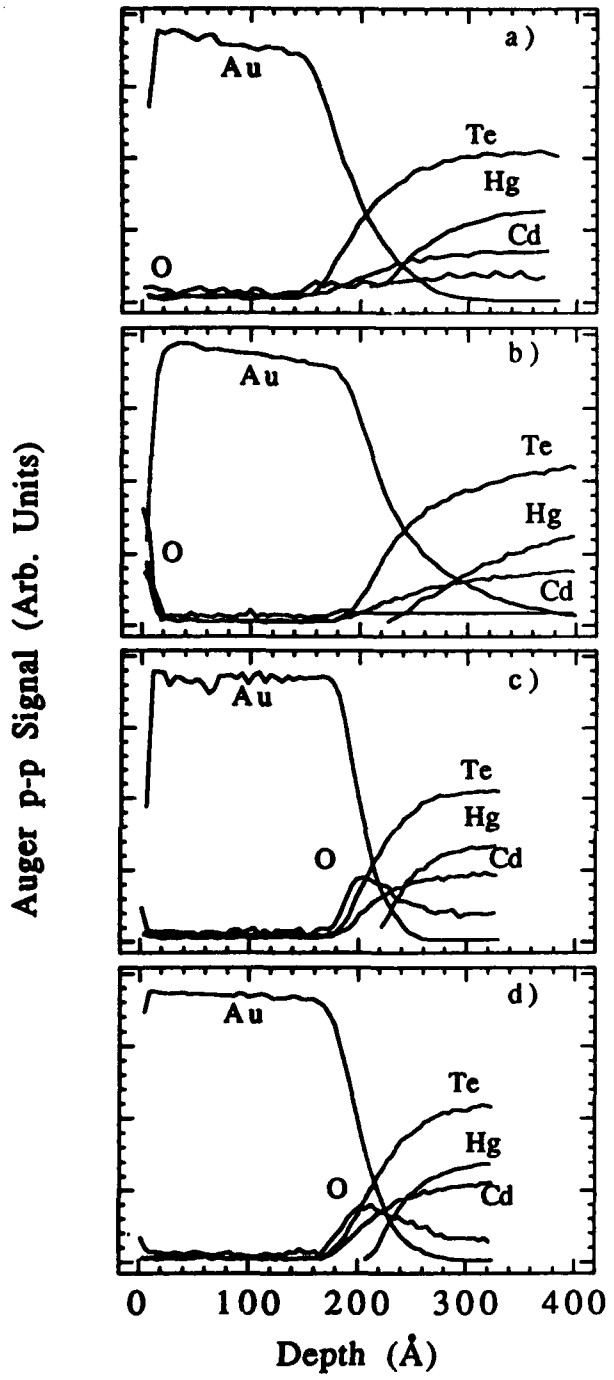

Figure 1. Auger sputter profiles of a) as-deposited Au (200Å) / $Hg_{.7}Cd_{.3}Te$, b) annealed (100°C for 216 hrs.) Au (200Å) / $Hg_{.7}Cd_{.3}Te$, c) as-deposited Au (200Å) / plasma oxidized $Hg_{.7}Cd_{.3}Te$, and d) annealed (100°C for 216 hrs.) Au (200Å) / plasma oxidized $Hg_{.7}Cd_{.3}Te$.

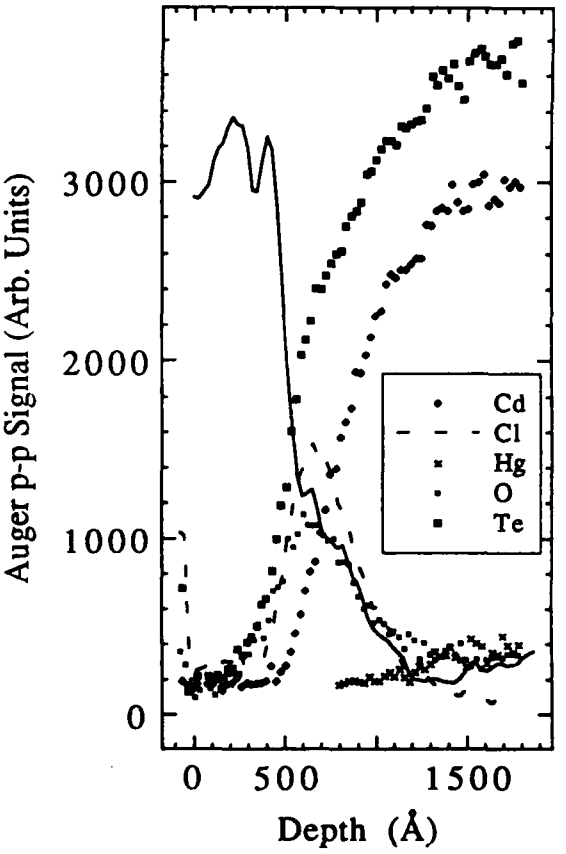

Figure 2. Auger sputter profile of as-deposited electroless Au (600Å) / $Hg_{.8}Cd_{.2}Te$.

THE ELECTRICAL PROPERTIES OF METAL CONTACT Au AND Ti ON p-TYPE HgCdTe

G. Bahir, R. Adar and R. Fastow

Kidron Microelectronics Research Center, Dept. of Electrical Engineering
Technion - Israel Institute of Technology, Haifa 32000, Israel

Introduction

Over the past several years the physical picture of metal-semiconductor interfaces has been modified drastically relative to the traditional models.[1] These changes are primarily due to the application of ultra-high vacuum (UHV) surface science techniques, which have demonstrated that atomic layers of metal can interact strongly with clean semiconductor surfaces. Interfacial reactions between HgCdTe and various metal overlayers have recently begun to be studied.[2-4] Most of these studies are limited to photoelectron spectroscopy (PES) on cleaved surfaces in UHV environment. Cleaved surfaces with atomic layers of metal coverage represent the simplest systems and facilitate the understanding of mechanisms driving reaction at the interfaces. However, since devices are not made on cleaved substrates, it is important to correlate the results obtained on cleaved surfaces with the electrical properties of metal contact on HgCdTe. Au and Ti are common metal contacts to p-type HgCdTe; Au because of its properties as an acceptor dopant, and Ti because of its good adhesion properties. According to the PES studies, the Au and Ti are classified into different classes; Ti is ultrareactive[4] and Au is unreactive[2], depending on the relative heats of formation of HgTe and the overlayer metal Te.

Experimental Results and Discussion

In this work, Schottky barrier diodes have been fabricated on undoped p-type x=0.22 HgCdTe samples, using Au and Ti as barrier metals having carrier concentrations between $6 \cdot 10^{15} cm^{3}$ to $5 \cdot 10^{16} cm^{-3}$. The barrier height is obtained from the forward I-V characteristics or the reverse I-V characteristics as a function of temperature.

It has been found that for low carrier concentration, $6 \cdot 10^{15} cm^{-3}$-$2 \cdot 10^{16} cm^{-3}$, the contacts are rectifying. The effective barrier height for the as deposited metals is a function of the sample carrier concentration, and Au barrier height is lower than that of Ti for all samples. For high carrier concentration, $5 \cdot 10^{17} cm^{-3}$, the contacts are nearly extrinsic ohmic. Low temperature annealing, 75°C, reduces the effective Au Barrier and raises the Ti barrier heights (Fig. 1). Annealing at 110°C for 20 h changes the Au Schottky diodes from rectifying to ohmic characteristics (Fig. 2).

The electrical measurements are correlated with Auger depth profiles of HgCdTe samples deposited with 1000 Å of Au or Ti.

Fig. 3a shows that room temperature deposition of an Au layer exhibits profound intermixing of the semiconductor and Au overlayer. Annealing at 110°C for 24 h causes strong indiffusion of the Au, and creates broad interface (Fig. 3b).

Fig. 4a shows the as deposited Ti layer. The interface formed exhibits an intermixing and non-stoichiometric nature. Even at room temperature the Hg diffuses into the interface and depletes from the near surface area. Annealing at 100°C 24 h (Fig. 4b) extracts more Hg into the interface, and the interface becomes sharper.

Based on these results, a model for the current transport mechanisms will be presented. The transport mechanism of the Au layer is a result of the unreactive nature of Au. The Au atoms diffuse into the semiconductor and act as acceptor, thus the depletion width becomes small enough so that holes can tunnel through it.[5] The Ti layer interacts with the HgCdTe in such a way that it forms a thin layer of Titanium Telluride.[4] Some of the freed Hg diffuses into the near surface region to form a degenerate n^+ layer on top of the p-type substrate, which explains the Ti barrier height enhancement.[4]

References

1. M. Sze, Physics of Semiconductor Devices, 2nd Edn. Chap. 5, Wiley, N.Y. (1981).
2. G.D. Davis, W.A. Beck, M.K. Kelly, N. Tache and G. Margaritondo, J. Appl. Phys. 60, 3157 (1986).
3. A. Wall, A. Raisanen, S. Chang, P. Philip, N. Troullier, A. Franciosi and D.J. Peterman, J. Vac. Sci. Technol. A5, 3193 (1987).
4. G.D. Davis, W.A. Beck, Y.W. Mo, D. Kildag and G. Margaritondo, J. Appl. Phys. 61, 5191 (1987).
5. W.E. Spicer, D.J. Friedman and G.P. Carey, J. Vac. Sci. Technol. A6, 2246 (1988).
6. J.M. Shanon, Solid-State Electron. 19, 537 (1976).

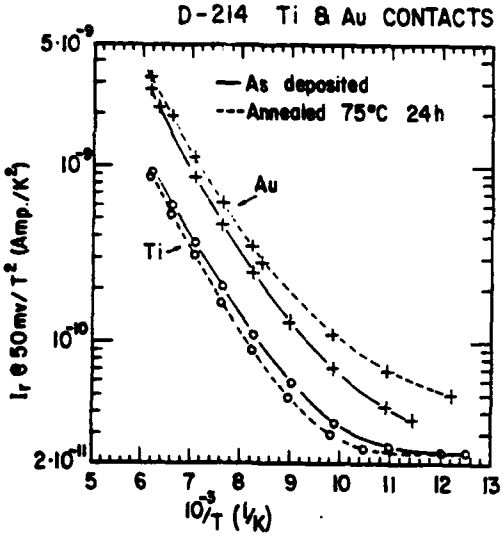

Fig. 1
Inverse current at 50 mV as a function of inverse temperature in Au/MCT abd Ti/MCT Schottky diodes for different annealing temperatures.

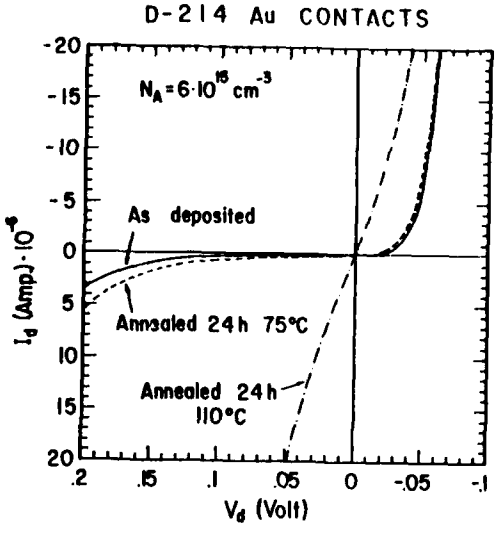

Fig. 2
Current-voltage characteristics of Au/MCT Contacts as a function of temperature.

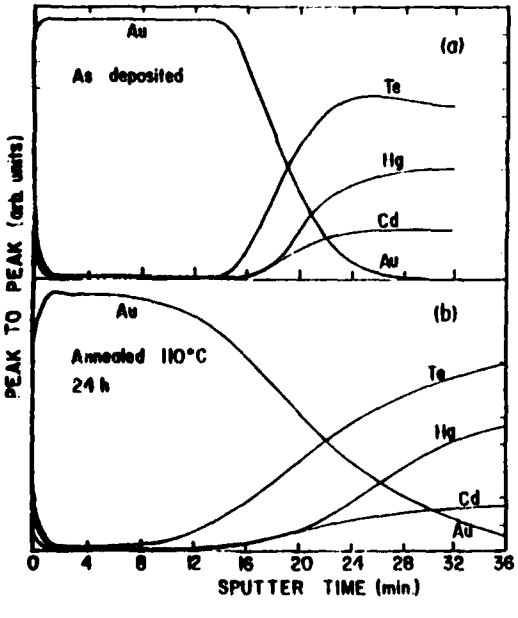

Fig. 3
Auger peak heights vs. sputtering time of Au/MCT interface, as deposited (a) and following 110°C 24 h annealing (b).

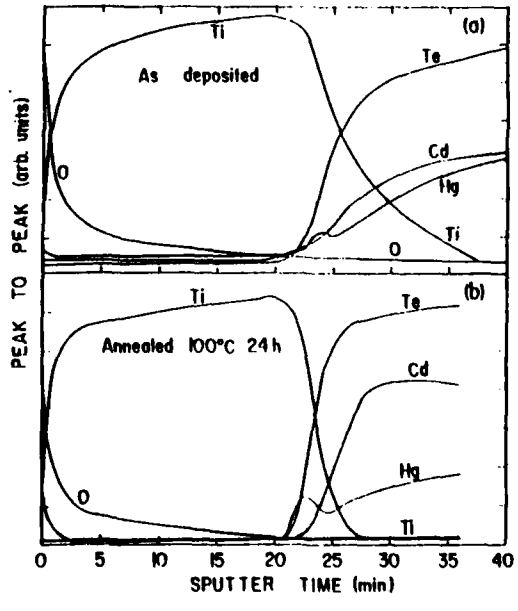

Fig. 4
Auger peak heights vs. sputtering time of Ti/MCT interface, as deposited (a) and following 110°C 24 h annealing (b).

INTERFACIAL CHEMISTRY OF METALS ON CdTe AND ZnTe*

A. K. Wahi, G. P. Carey, T. T. Chiang, K. Miyano, I. Lindau, and W. E. Spicer
Stanford Electronics Laboratoratories, Stanford University, Stanford, CA 94305

Recognizing the importance of interfacial chemistry and morphology to the electrical characteristics of metal contacts to II-VI materials, we have studied interfacial chemistry and morphology for Al, In, Ag, and Pt overlayers on CdTe and ZnTe (110) bulk single crystals cleaved in vacuum. Growth of the overlayer and band bending with metal deposition were monitored using both surface-sensitive (probing the top 5 -7 Å) and bulk-sensitive (the top ~25 Å) photoemission. We reported during last year's proceedings our findings that Al, highly reactive with Te, yields a significantly more extensive reacted region on CdTe than seen on HgCdTe, which suggests that the severe and rapid Hg loss at the Al/HgCdTe interface inhibits further reaction [1]. The Al overlayer thus presents a case where a higher degree of intermixing is possible in absence of Hg. The Al/CdTe interface was also found to be significantly more intermixed than the corresponding Al/ZnTe interface. We report further studies comparing interfacial morphology for In, Pt, and Ag overlayers on CdTe and ZnTe. We find In to be much less reactive than predicted by bulk thermodynamics, with only limited reaction for In on CdTe with initial metal deposition, and no evidence for reaction on ZnTe. We note the same trend, however, in which the metal/ZnTe interface is found to be more abrupt than the corresponding metal/CdTe interface. In contrast, Pt overlayers exhibit high reactivity with the cation, with movement of Cd or Zn into the overlayer and formation of dissociated Te. For Pt, similar interfacial reaction is seen for both CdTe and ZnTe, suggesting that the driving force for reaction at the surface in this case dominates any differences between the CdTe and ZnTe. Band bending behavior for these metal overlayers is examined as a function of metal coverage. Schottky barriers are formed for all metals studied. A mechanism for Fermi level movement due to defects produced at the interface is found to provide a consistent explanation of the narrow range of barrier heights observed. Formation of defects is likely in view of the chemical reactions and intermixing seen, with only In/ZnTe showing no evidence for reaction. The interfaces with In also show slower band bending with metal deposition for both CdTe and ZnTe, consistent with slower defect formation. We also consider the possible role of doping of the substrate by the metal to explain a bowing, or overshoot, behavior of the Fermi level relative to its final position within the bandgap that is seen for Al/CdTe and Ag/ZnTe. There is strong evidence that such doping by the deposited metal occurs also at metal/HgCdTe interfaces [3,4].

* Work supported by NASA and DARPA.

1. A. K. Wahi, G. P. Carey, T. T. Chiang, I. Lindau, and W. E. Spicer, J. Vac. Sci. Technol. A 7, (1989).
2. D. J. Friedman, I. Lindau, W. E. Spicer, Phys. Rev. B 37, 731 (1988).
3. D. J. Friedman, G. P. Carey, I. Lindau, and W. E. Spicer, J. Vac. Sci. Technol. A 5, 3190 (1987).
4. G. P. Carey, A. K. Wahi, D. J. Friedman, C. E. McCants, and W. E. Spicer, J. Vac. Sci. Technol. A 7, 483 (1989).

AN ANOMALOUS DIFFUSION BARRIER CASE: MCT/Yb/Ag JUNCTION

A. Raisanen[a)], D.J. Peterman[b)], G. Haugstad[a)], X. Yu[a)], and A. Franciosi[a)]

a) Department of Chemical Engineering and Materials Science, University of Minnesota, Minneapolis, MN 55455
b) McDonnell Douglas Research Laboratories, St. Louis, MO 63166

Recent experiments have demonstrated that thin rare earth layers can be employed as diffusion barriers at the junction between $Hg_{1-x}Cd_xTe$ (MCT) and reactive metals such as Al, In and Cr. The barrier greatly reduces atomic interdiffusion, overlayer-Te reaction, and the consequent Hg-depletion of the MCT surface and near-surface regions. Calculations of binary thermodynamic parameters following Miedema's model indicate that the diffusion barrier effect derives from the high thermodynamic stability of the MCT/rare earth interface relative to the overlayer-Te reaction enthalpy. The latter is usually the major driving force behind MCT/metal interdiffusion. Ag overlayers represent an important test case since it has been shown that long-range atomic interdiffusion at the MCT/Ag interface is driven by a defect-mediated Ag-indiffusion mechanism, and not by the negligible Ag-Te reaction enthalpy.

We performed synchrotron radiation photoemission studies of MCT/Ag junctions formed *in situ* at room temperature on atomically clean $Hg_{1-x}Cd_xTe(110)$ cleavage surfaces to monitor the effect of Yb barriers of variable thickness. Barriers $\geq$ 5 monolayers (ML)-thick dramatically reduced Ag indiffusion at all Ag coverages explored (1-200Å), with an increase of over one order of magnitude in the Ag 4d emission from the junction relative to the no-interlayer case. The resulting Ag films exhibit a layer-by-layer growth mode, as indicated by the novel technique of *in situ* photoemission-of-adsorbed-Xenon (PAX). The PAX study was conducted by cooling the sample at 50K and chemisorbing a Xe monolayer on the MCT/Yb/Ag junction. The Xe 5p and 4d level binding energies reflecting the <u>local</u> work function of the surface, no Ag-island growth was detected.

3-5 ML-thick barriers trap most of the Ag atoms at low Ag coverages ($<$20Å), but <u>fail</u>, at higher Ag coverages, with the sudden appearance at the surface of Hg atoms displaced from the MCT bulk, and a corresponding drop in the surface Ag concentration. The appearance of Hg is directly related to the onset of Ag indiffusion. Monolayer Yb barriers hinder Ag indiffusion only in part. Such ultra-thin barriers, however, are five times more effective than Sb-barriers of comparable thickness. We propose that in the case of Yb the barrier atoms not only quickly saturate the Hg vacancies which assist Ag indiffusion, but also trap indiffusing Ag due to the surprising large enthalpy of Yb-Ag alloying, that we calculate to be -87.5 KJ/mole.

SURFACE PASSIVATION AND 1/f NOISE PHENOMENA IN HgCdTe PHOTODIODES

Y. Nemirovsky and D. Rosenfeld
Kidron Microelectronics Research Center, Dept. of Electrical Engineering
Technion - Israel Institute of Technology, Haifa 32000, Israel

The emerging Infrared Focal Plane Arrays based on HgCdTe photodiodes coupled to silicon signal processors, have led to increased interest in understanding and controlling 1/f noise in HgCdTe n^+p photodiodes.[1,2] Recent studies have associated 1/f noise in these devices with surface and bulk dark currents.[3-17]

In order to identify the dominant noise mechanism in HgCdTe photodiodes, to illustrate the relationship between the quality of the surface passivation and 1/f noise phenomena, and to further demonstrate the strong correlation between tunneling and 1/f noise, we study the noise current spectral density in the low-frequency range and the dark dc currents in HgCdTe photodiodes as well as in gate-controlled diodes. We characterize the 1/f noise in gate-controlled HgCdTe ion-implanted diodes fabricated on bulk p-type metrial with $x \approx 0.22$, that are passivated with native anodic sulfides and evaporated ZnS.[18] The dc dark current-voltage characteristics and excess 1/f noise currents as a function of gate reverse bias and gate voltage are reported and are empirically correlated.

It is suggested that tunneling is often the dominant mechanism that contributes dark current and 1/f noise in narrow bandgap HgCdTe photodiodes and in gate-controlled diodes. Surface as well as bulk tunneling induce 1/f noise, and band-to-band as well as trap-assisted tunneling play a dominant role in producing the dark and 1/f noise currents.[12-16] The surface potential determines whether surface or bulk tunneling prevails. The material doping properties, the junction formation and profile, and the bias voltage determine whether bulk band-to-band or trap-assisted tunneling dominates.[16]

The low frequency noise current spectral density of a gate-controlled HgCdTe diode as a function of gate bias, is shown in Fig. 1(a). The low frequency noise exhibits an exponential dependence on the gate voltage that is very similar to that observed for the dark current of Fig. 1(b). The

noise current increases exponentially with the gate voltage and is correated to the tunneling currents that dominate either in surface accumulation or in surface inversion. Reduced low-frequency noise currents are observed with optimized gate voltages corresponding to near flat-band conditions. However, excess noise currents with the low-frequency contribution increasing as frequency decreases, are observed even in the gate bias region with optimized dark currents, where trap-assisted tunneling is the dominant mechanism below 50 K, and diffusion current is dominant around 77 K.

The correlation between 1/f noise and tunneling processes in HgCdTe diodes and gate-controlled diodes has been previously suggested.[12-16] The present study emphasizes the role of the surface passivation in the light of these related phenomena: the surface passivation must impose near flat-band conditions to reduce the tunneling of electrons across the field-induced junctions beneath the surface or across the pinched-off junction depletion region adjacent to the surface. The experimental data indicate that tunneling of electrons produces dark dc currents as well as an

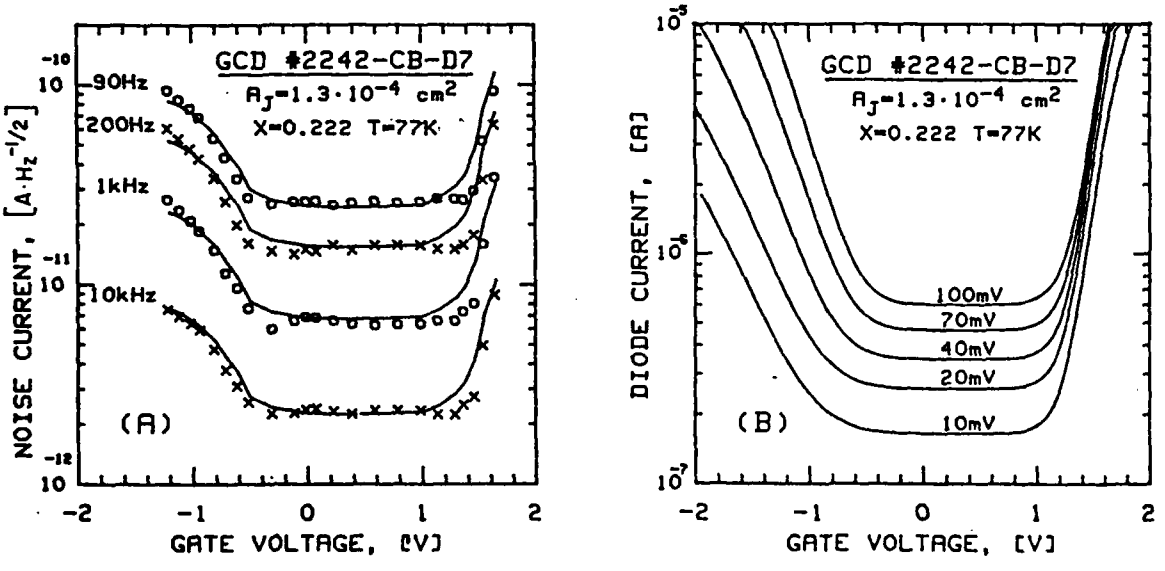

Fig. 1: Noise current spectral density measured at several frequencies vs. gate voltage, for diode reverse bias voltage 60 mV (a) and diode reverse current at 77 K as a function of gate voltage, with junction reverse bias as a parameter (b). The junction area is $1.31 \cdot 10^{-4}$cm², and the gate area is $1.6 \cdot 10^{-3}$cm². The composition x is 0.222. The substrate doping level is $N_A = 10^{16}$cm^{-3}. The gate insulator is composed of a 3000 A ZnS layer and a ≈300 A anodic sulfide layer. The reference shot noise level $(2qI)^{1/2}$ for I=480 nA is $3 \cdot 10^{-13}$ A/Hz$^{1/2}$.

appreciable 1/f noise current that can be empirically correlated with the excess dc tunneling currents. An empirical approach is applied to characterize the effect of surface passivation on 1/f noise phenomena in HgCdTe diodes, based on empirical parameters, in particular the noise factor. In the measured frequency range, at 77K, the noise current is modeled using the expresion:

$$I_n = \alpha \cdot \left[\frac{I_t}{f}\right]^{1/2} \quad (1)$$

where I_n is the noise current, I_t is the measured tunneling current, f is the frequency and $\alpha = 3.25 \cdot 10^{-7}$ $[A^{1/2}]$.

References

1. R. Balcerak, J.F. Gibson, W.A. Gutierrezand, J.H. Pollard, Optical Eng. 191 (1987).
2. M.B. Reine, A.K. Sood, and T.J. Tredwell, in Semiconductors and Semimetals, ed. by R.K. Willardson and A.C. Beer, (Academic, N.Y. 1981) Vol 18, ch.6.
3. S.P. Tobin, S. Iwasa, and T.J. Tredwell, IEEE Trans. Elec. Dev. 27, 43 (1980).
4. A. Radford and C.E. Jones, J. Vac. Sci. Technol. A3, 183 (1985).
5. J. Bajaj, G.B. Williams, M.H. Sheng, M. Hinnrichs, D.T. Cheung, W.P. Rode, and W.E. Tennant, J. Vac. Sci. Technol. A3, 192 (1985).
6. G.M. Kleinpenning, J. Vac. Sci. Technol. A3, 176 (1985).
7. H.K. Chung, M.A. Rosenberg, and P.H. Zimmerman, J. Vac. Sci. Technol. A3, 189 (1985).
8. A. van der Ziel and P.H. Handel, IEEE Trans. Elec. Dev. 32, 1802 (1985)
9. A. van der Ziel, P.H. Handel, X.L. Wu and J.B. Anderson, J. Vac. Sci. Technol. A4(4), 2205 (1986).
10. A. van der Ziel, P. Fang, L. He, X.L. Wu, A.D. van Rheenen, and P.H. Handel, J. Vac. Sci. Technol A7(2), 550 (1989).
11. X. Wu, J.B. Anderson and A. van der Ziel, IEEE Trans. Electron Devices 34, 1971 (1987).
12. W.W. Anderson and J.J. Hoffman, J. Vac. Sci. Technol. A1, 1730 (1983).
13. R.E. DeWames, J.G. Pasko, E.S. Yao, A.H.B. Vanderwyck, and G.M. Williams, J. Vac. Sci. Technol. A6(4), 2655 (1988).
14. R.E. DeWames, G.M. Williams, J.G. Pasko and A.H.B. Vanderwyck, J. Cryst. Grow. 86, 849 (1988).
15. Y. Nemirovsky, R. Adar, A. Kornfeld and I. Kidron, J. Vac. Sci. Technol. A4, 1986 (1986).
16. Y. Nemirovsky, D. Rosenfeld, R. Adar and A. Korfneld, J. Vac. Sci. Technol., A2(2), 528 (1989).
17. D. Rosenfeld and Y. Nemirovsky, The 16th Conference of Electrical and Electronics Engineers in Israel, March 7-9 (1989), 1-3-1.
18. Y. Nemirovsky and I. Bloom, J. Vac. Sci. Technol. A6, 2710 (1988).
19. Y. Nemirovsky and G. Bahir, J. Vac. Sci. Technol. A2(2), 450 (1989).
20. R. Adar, I. Bloom and Y. Nemirovsky, Solid State Electronics, 32, 111 (1989).

CHARACTERIZATION OF (Hg,Cd)Te BY SURFACE RECOMBINATION VELOCITY MEASUREMENTS

V. C. Lopes, W. H. Wright, and A. J. Syllaios
Texas Instruments Inc.
Dallas, Texas 75266

Dark current in Metal-Insulator-Semiconductor (MIS) depletion devices fabricated on (Hg,Cd)Te is determined by material parameters such as composition, carrier concentration, point defects, and by the nature of the (Hg,Cd)Te surface[1]. The technique of photoconductive (PC) decay was used to characterize (Hg,Cd)Te material and the anodic oxide-(Hg,Cd)Te interface by its minority carrier lifetime (τ_p) and surface recombination velocity (S), respectively. τ_p is related to carrier recombination in the bulk, while S is a measure of carrier recombination at the passivant-semiconductor interface.

PC decay measurements were made on n-type (Hg,Cd)Te samples grown by the Solid-State-Recrystallization (SSR) technique[2]. The samples were alloyed for a 77K 10μm cut-off wavelength and had Hall mobilities greater than 10^5 cm^2/V-s. The samples were passivated in a KOH electrolytic solution and fabricated with MIS capacitors. The PC decay apparatus used a mid-IR (mid- infrared) diode laser as the excitation source and was equipped with mapping capabilities which allowed for spatial resolution of S and τ_p.

The finite difference method was used to solve the one dimensional transport equation with the surface recombination velocity as the boundary condition[3]. The numerical model was used to fit PC decay waveforms to extract S and τ_p from the experimental data.

The PC decay waveform in Figures 1a and 1b illustrates the effect of carrier recombination at the surface. The experimentally obtained PC decay waveform exhibits the classical surface

recombination decay characteristics, that is, faster than exponential decay for short times after injection. The solid line in Figure 1a is the simple exponential fit of the waveform. The solid line in Figure 1b is a fit of the waveform using the numerical model with S = 275 cm/s.

S as a function of net carrier concentration (as determined from MIS Capacitance-Voltage analysis) for KOH passivated (Hg,Cd)Te samples is shown in Figure 2. For the samples studied, the determined S is a function of the carrier concentration. A similar relationship between S and carrier concentration was observed previously in Germanium[4]. The solid line is a fit of the data assuming a uniform density of surface states. The fast state density is determined to be approximately 2×10^{11} eV^{-1} cm^{-2}.

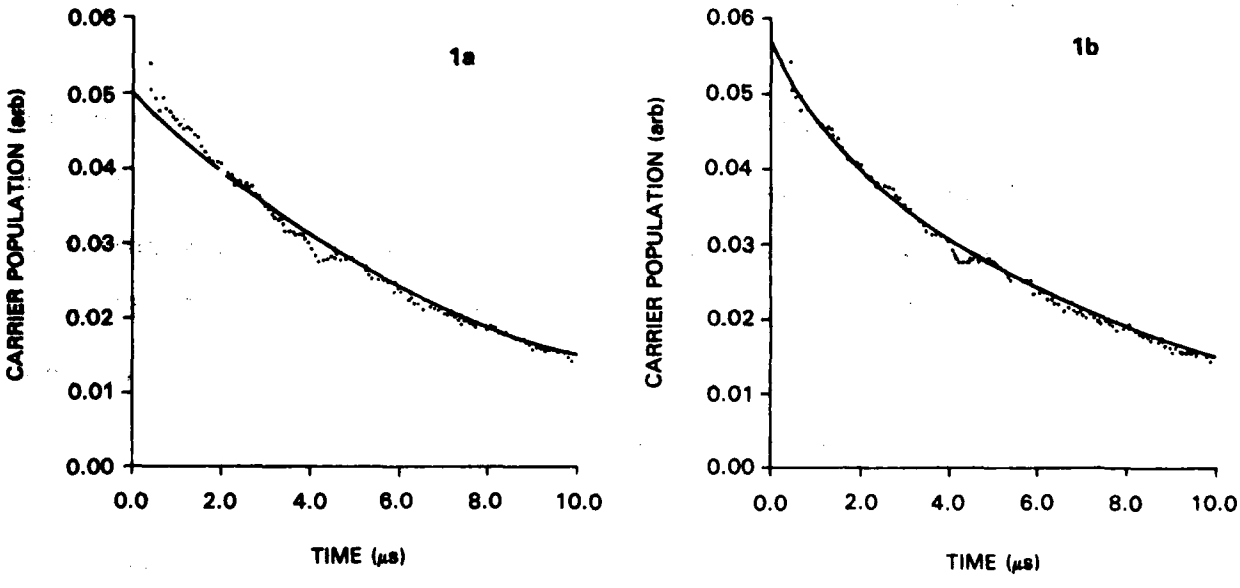

Figure 1. Experimental PC Decay Data (Dots) Measured on a (Hg,Cd)Te Sample Passivated with KOH Anodic Oxide. The solid line in 1a is the simple exponential fit to the data. The solid line in 1b is the fit using the numerical model with S = 275 cm/s.

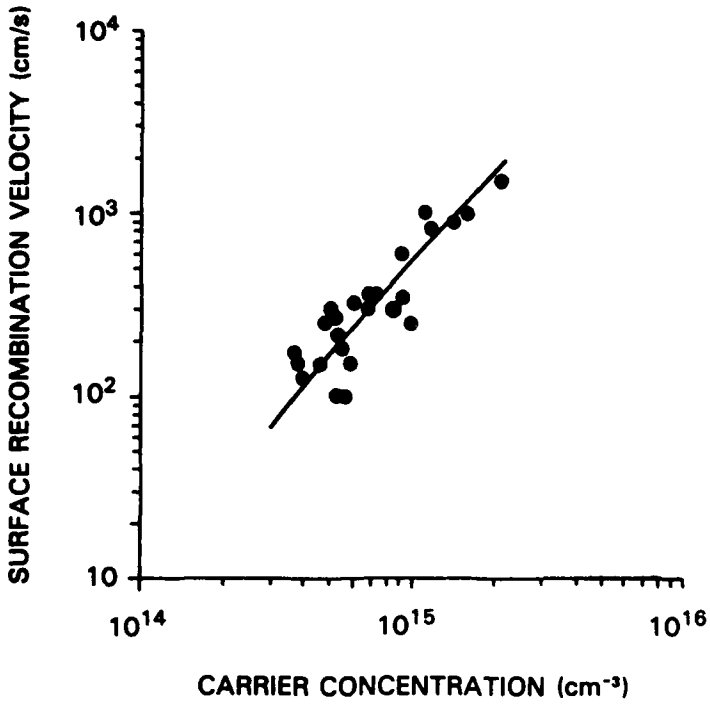

Figure 2. The Surface Recombination Velocity of KOH Passivated (Hg,Cd)Te as a Function of Carrier Concentration.

References

1. M. A. Kinch, Semiconductors and Semimetals, Vol. 18, (ed.) R. K. Willardson and A. C. Beer, Academic Press New York 1981, p 313.
2. M. J. Brau, U.S. Patent No. 3,655,944 (1972).
3. W. H. Wright, V. C. Lopes, and A. J. Syllaios, Proc. of SPIE Conference on Infrared Materials, Orlando FL (1989).
4. B. H. Shultz, Physica 20, 1031 (1954).

Properties of Insulator Interfaces with p-HgCdTe

E. Finkman and S.E. Schacham
Department of Electrical Engineering and Solid State Institute
Technion - Israel Institute of Technology, Haifa 32000, Israel

We have studied the interface properties of p-type HgCdTe using various opto-galvano-magnetic methods to identify the interface trap parameters, and those of the n-type skin inversion layer that is often formed in such structures. Heat treatment of the passivated HgCdTe was found to change the surface charge density, and hence the surface potential. As a consequence, we are able to study the dependence of surface recombination velocity as a function of surface potential (in a limited range, though), without a need for a transparent gate.

Last year we reported the results of preliminary studies on ZnS and anodic sulfide interfaces [1]. Analyzing the temperature dependence of the surface recombination velocity we concluded that the surface traps can be related to lattice defects, most probably vacancies, as can be deduced from the similarity in their activation energies. We suggested that their concentration at the surface should be nearly equal to that in the bulk. The present results indicate that this indeed is the case. Studying sulfidized p-type samples, with carefully prepared thin anodic sulfide, reducing the interface fixed positive charge to a minimum, we were able to measure samples with acceptor concentration as low as $8\times10^{14}cm^{-1}$ which did not show anomalous Hall effect, even at low temperatures [2]. It was found that the surface recombination velocity is lowered when lowering the acceptor concentration, still having the same activation energies as those known for the metal vacancies. This proves that in well prepared interfaces, the recombination at the surface is controlled by vacancies already presented in the bulk, and that anodic sulfide is minimizing the introduction of excessive additional surface traps.

Heat treatment of passivated samples with low acceptor concentration at 70 C, with annealing times of few hours to few days, result in forming an inversion layer at the interface, with surface charge density that increases with anneal time, up to about $5\times10^{11}Cb/cm^2$. The surface recombination velocity decreases with increasing surface charge density, indicating that the change in surface potential drives the Fermi level at the surface away from the trap level. Recombination velocity as low as ~ 350 cm/sec at 77K was measured. The surface carrier mobility at the inverted layer generated by this heat treatment is relatively low, of the order of $10^4cm^2/V\cdot sec$.

Anodic oxide interface of p-HgCdTe is always inverted, with surface charge density of the order of $10^{12}Cb/cm^2$. This n-type skin layer often exhibits good n-type properties, which equal, and even surpass, bulk properties, with electron mobility as high as $1.5\times10^5cm^2/V\cdot sec$. Usually we expect the electrons to have reduced mobilities near the semiconductor surface, due to increased interface scattering. The fact that this is not observed in the case of anodic oxide interface may suggest that the electronic-levels in the space charge region are quantized with respect to their motion normal to the surface, forming a quasi two-dimensional electron gas with modified transport properties.

References

[1] E. Finkman and S.E. Schacham, J. Vac. Sci. Technol. A7, 464 (1989).

[2] M.C. Chen, J. Appl. Phys. 65, 1571 (1989).

SPATIALLY-RESOLVED LIGHT-INDUCED EFFECTS IN HgCdTe PHOTODIODES

J. Bajaj, R. E. DeWames and W. E. Tennant

Rockwell International Science Center
Thousand Oaks, CA 91360

J. C. Pickel

S-Cubed
San Diego, CA

Spatially averaged light-induced effects on flood-illuminated HgCdTe photodiodes were reported[1] last year. The light-induced effects were shown to exhibit similar diode responses as those produced by high energy electrons and gamma-rays.[2] This similarity suggested an alternate way of studying radiation effects, since light studies offer an opportunity to selectively excite different portions of the diode architecture by appropriately selecting the laser wavelength. This wavelength dependence allows separation of effects originating in the passivation layer, HgCdTe/insulator interface and bulk HgCdTe. Using variable wavelength flood illumination, previous work showed[1] unambiguously that the effects occur in the vicinity of the HgCdTe/insulator interface.

Use of light beams allows quick assessment of radiation effects in the laboratory and the ease of focusing laser beams to a very small spot size allows an opportunity to explore spatial effects. In this paper, we report on spatial nonuniformity in light-induced effects within a device. Experiments were carried out using a scanning laser microscope.[3] The microscope provides a focused laser spot of approximately 5 μm in diameter and a spatial scanning resolution of up to 0.5 μm. It can house up to three lasers, any of which can be selected remotely for experiments. A specially designed cold-stage for the microscope allows the sample to be cooled to 77K. The microscope is also equipped with powerful image processing software for image analysis.

The technique is demonstrated using planar ZnS/SiO_2-passivated long wavelength infrared (LWIR) HgCdTe photodiodes fabricated in a 1 × 32 configuration. The diodes

were n^+/p fabricated by boron ion implantation and had a center-to-center spacing of 125 μm. The laser used for the present study is a diode-pumped Nd:YLF at 1.047 μm, which can operate in a cw mode with more than 100 mW at the sample or in a Q-switched mode to give 25 nS pulses with a peak power of up to 20 W at the sample and a maximum repetition rate of 10 KHz. The diodes were front-side illuminated through the passivation layer. The insulating passivation layer is transparent to 1.047 μm laser which gets absorbed in the HgCdTe with a penetration depth of approximately 1 μm. A cold narrow band-pass filter peaked at 1.06 μm was placed in front of the sample to obtain low background (near dark) conditions.

All measurements were made with the sample at 77K. The sample, mounted on a x-y translation stage, was spatially scanned to change the position of the laser beam on the diode. The diode leakage current at 100 mV reverse bias and at 77K was measured as a function of the location of the laser beam on the diode. The measured current at each point is therefore an accumulation of the excess currents induced by damage incurred at all the positions the beam has passed until this point during the scan. The current scan is transformed into a false color (or a gray scale) image, in real time, and displayed on the screen and also stored in the computer. This image is then processed using the imaging software on the microscope to produce another image that represents the derivative of the signal at each point. This produces a spatial image of the radiation-induced sensitivity. The reflected light from the sample was recorded simultaneously into another channel of the microscope to produce an optical image of the diode area.

Pulsed light illumination was used, since it produced significantly more degradation than cw illumination. Light pulses had a 100 Hz repetition rate and energy per pulse of approximately 1 nJ. We show that the regions in the diode architecture that are most susceptible to a light-induced degradation are at the surface of HgCdTe where the electrical junction meets the HgCdTe/passivation interface. The response to radiation also varies significantly within this perimeter. Our speculation is that the radiation

response across the perimeter is nonuniform because the light-induced states at the semiconductor/insulator interface near the junction react differently at each point depending on the variations in junction parameters and/or the distribution of defects in the junction perimeter region. In principle, one should be able to correlate the radiation sensitive regions with nonuniformities in materials properties which can be determined by related scanning laser microscopy.

The scanning laser microscope technique we have described is a convenient way of studying radiation effects minimizing the use of conventional electron and gamma radiation facilities that have limited access. It also offers a convenient way of studying diode/passivation interface nonuniformity and could be checked against changes in the device processing and surface preparation steps. The described technique is equivalent to using a focused electron beam in an SEM, except that the latter alllows only spatial and not depth resolution and requires a high vacuum.

REFERENCES

1. R.E. DeWames, J. Bajaj, E.S. Yao, and G.M. Williams, 1988 U.S. Workshop on the Physics and Chemistry of HgCdTe, Orlando, FL. J. Vac. Sci. Tech. A7(2), 536 (1989).

2. R.S. Stapp, D.G. Feller, L.R. Johnson, C.I. Westmark, J. Bajaj, K. Vural, P.R. Newman, and E.R. Blazejewski, Appl. Phys. Lett. 52(19), 1614 (1988).

3. C.J.L. Moore, J. Hennessey, J. Bajaj, and W.E. Tennant, September 1988 issue of Photonics Spectra.

CURRENT APPROACHES TO PN JUNCTIONS IN WIDER BANDGAP II-VIs

J. O. McCaldin

California Institute of Technology
Pasadena, California 91125

Many wider bandgap semiconductors do not afford both p- and n-type doping, so that pn junctions cannot be obtained, a limitation that is especially restrictive for the II-VIs. Several rationale's for this difficulty have been advanced involving thermodynamics, structural problems and trace impurities. Two approaches currently being considered to overcome the limitation will be discussed in some detail: (1) use of heterojunctions and (2) attempts to increase the efficiency of dopants so as to extend the range over which the Fermi level, E_F, can be moved. Both approaches can be discussed in terms of a diagram predicting band edge energies of the common semiconductors, relative to a standard reference energy, plotted verses lattice parameter, as is illustrated in Fig. 1. The plotting scheme used in this figure shows, for any heterojunction, the band offsets, degree of lattice mismatch, and dopability of each material. For example, the figure indicates that the much-studied ZnSe/ZnTe heterojunction has moderate-sized band offsets of type I, is about 7% lattice mismatched and one component can be doped p-type and one n-type.

Unfortunately, there is no general agreement on values for the offsets in such figures. The widely-used values of Harrison and Tersoff[1], presented in fig. 1(a), tend to give a favorable prognosis for current injection under forward bias, such as one is accustomed to with pn homojunctions. For example, the ZnTe/AlSb heterojunction would be every bit as favorable as a pn homojunction, since both band offsets are "negative", ie injected carriers lose energy when crossing the interface. On the other hand, the more familiar ZnSe/ZnTe heterojunction would be less favored in that the valence band offset is positive, ie injected holes originating in the p-ZnTe face an uphill barrier. Such cases have been discussed[2] in more detail than is possible here with the conclusion that only a few heterojunctions involving wide band-gaps are interesting

prospects for current injection. This conclusion is even more compelling when band edge energy assignments besides those of Harrison and Tersoff are considered, eg those of ref. 3 shown in fig. 1(b).

Whereas the main difficulty with most heterojunctions can be seen in fig. 1 to be the barrier presented by band offsets, the problems in obtaining pn junctions by control of doping are a subject of controversy. The present experimental status is indicated in fig. 1, though even here it could be argued that the region enclosed by hatching should be expanded to include, for example, p-ZnSe. The substantial number of reports of p-ZnSe will be summarized and common features such as the frequent use of Li discussed.

Perhaps the most promising feature of contemporary experimental methods to overcome the historical problems in usefully doping the wide gap II-VIs is low processing temperatures, roughly 200C to 400C. Conventional Si processing causes dopants to "freeze-in" at about 850C, ie a metastable material is produced around 850C sufficient for many device uses. The corresponding temperature for wide gap II-VIs is undoubtedly much lower, but still hopefully within the range of 200 to 400C, at least for some dopants. Indeed the kinetics associated with processing in this temperature range appear to be crucial to resolving issues of dopability.

References

1. W. A. Harrison and J. Tersoff, *J. Vac. Sci. Technol.* **B4**, 1068 (1986).
2. J. O. McCaldin, *Proc. NATO-ARW Conf. on Wide Band-Gap II-VI Semiconductors* held in Regensburg, FRG, Aug 2-5 1988 (to be published 1989)
3. J. O. McCaldin, T. C. McGill and C. A. Mead, *Phys. Rev. Lett.* **36**, 56 (1976).

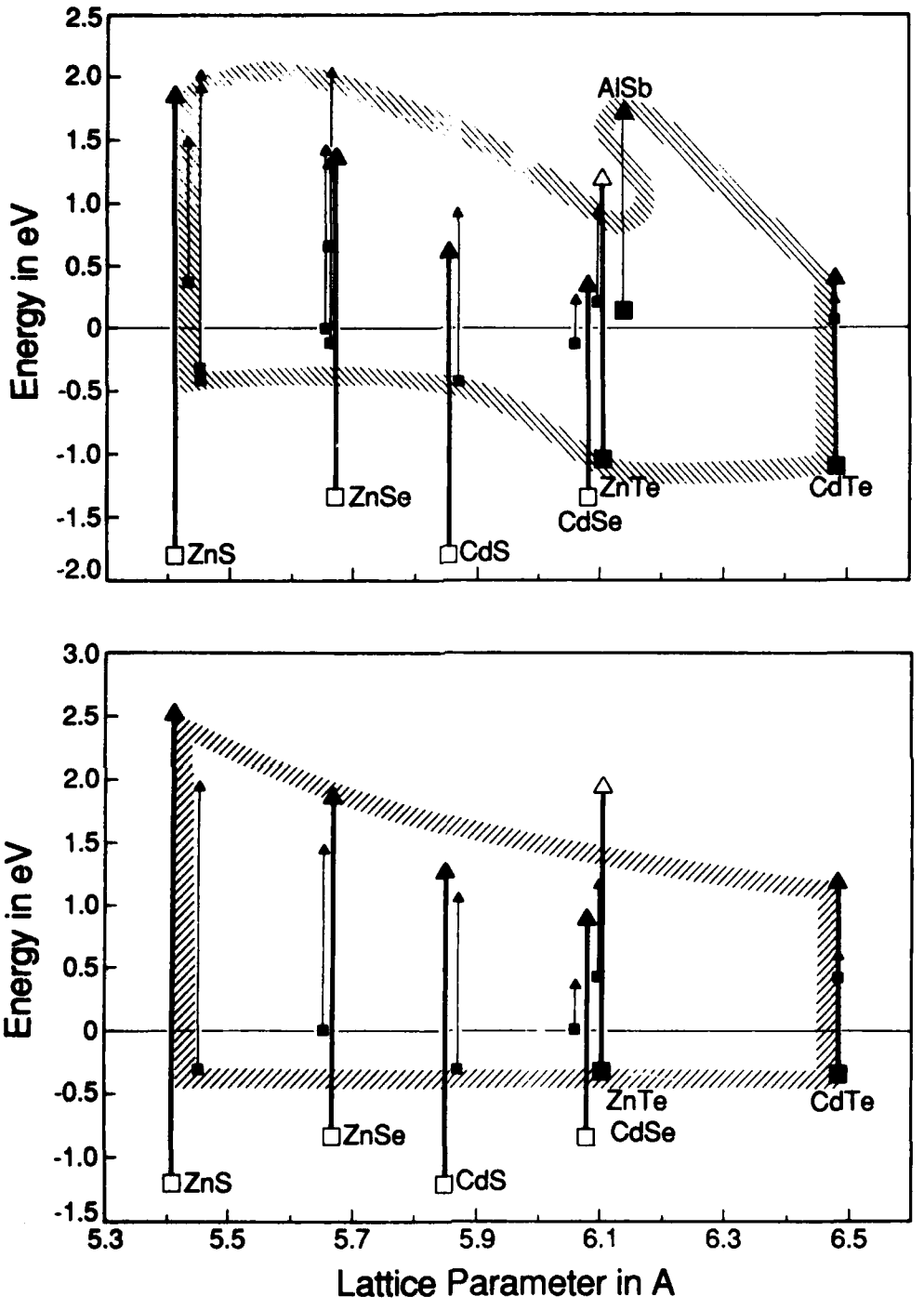

Fig 1. Energy relationships for band edges of common semiconductors according to (a) ref. 1 and (b) ref. 3. Squares represent valence and triangles conduction band edges, and vertical solid lines are band gaps. Material that conventionally cannot be made usefully p-type or n-type is denoted by the appropriate open symbol; otherwise filled symbols are used. Hatched lines enclose regions free of open symbols.

Room-Temperature Magnetoabsorption in $HgTe/Hg_{0.15}Cd_{0.85}Te$*

K.H. Yoo and R.L. Aggarwal
Francis Bitter National Magnet Laboratory and Department of Physics
Massachusetts Institute of Technology, Cambridge, MA 02139

L.R. Ram-Mohan
Department of Physics, Worcester Polytechnic Institute, Worcester MA 01609

O.K. Wu
Hughes Research Laboratories, Malibu, CA 92065

We report the observation of magnetoabsorption in $HgTe/Hg_{0.15}Cd_{0.85}Te$ superlattices at room temperature. Three samples grown along [100] axis with layer thicknesses of 80/40 Å (sample ML-25B), 64/40 Å (sample ML-28B), and 64/60 Å (sample ML-29B) were studied in this work. Three magnetoabsorption peaks were observed in the Faraday configuration in the spectral region between 6 μm and 21 μm, using magnetic field up to 15 T applied along the growth axis, as shown in Fig. 1. From the shift of the transition energy with temperature, the two higher energy peaks are identified as due to interband transitions, while the third as due to intraband transition.

A quantitative analysis of the data has been made using our transfer matrix method.[1] The input parameters were chosen after extensive review of the published literature on the subject. Considering (i) interband or intraband nature of the peaks, (ii) that the samples are n-type and (iii) the predicted pattern[2] of the transitions (Fig. 2), we have identified observed magnetoabsorption peaks labeled 1, 2, and 3 as due to $0'E_1/\text{-}1'H_1$, $\text{-}1'E/\text{-}2'H_1$ and $1E_1/0E_1$ transitions, respectively. In the following analysis we have primarily focused on peaks 2 and 3, since peak 1 is relatively weak and its identification is less certain. The best-fit valence band offset (V_p) values have been determined to be 730 meV and 850 meV for samples ML-25B and ML-28B, respectively, as illustrated in Fig. 3.

We have examined the effect of changes in the input parameters such as energy gap and light-hole effective mass of HgTe on the transition energies. The light-hole effective mass is determined by E_p and modified Luttinger parameters denoted by γ's for a given E_g. For each set of

input parameters we determined the range of V_p that fit each absorption peak, considering (i) the experimental error, and (ii) zone-center as well as zone-edge transitions. The plots in Fig. 4 illustrate determination of the lower limit on V_p, and similar plots for zone-edge transitions provide the upper limit on V_p. The overlap range in V_p is then obtained from a comparison of the V_p ranges for the two peaks. The best-fit V_p and overlap range for V_p is summarized in Table I for various combinations of input parameters. V_p changes over ~250 meV with lower values of 500-600 meV, still larger than the widely accepted value of 350 meV.[3]

Table I. Variation in E_g(HgTe) and E_p(HgTe) and the resulting best-fit V_p and overlap range of V_p in parenthesis in meV. The upper one for ML-25B and the lower one for ML-28B. The last column is for a different set of modified Luttinger parameters of HgTe.

E_g(eV) / E_p(eV)	17	18	19	E_p=18 eV another γ set.
-0.11	(I) 720 (180) 840 (150)	(IV) 730 (100) 850 (30)	(VII) --- ---	(X) --- ---
-0.13	(II) 610 (60) 730 (210)	(V) 610 (200) 760 (120)	(VIII) 640 (90) ---	(XI) 650 (80) ---
-0.15	(III) --- 620 (160)	(VI) 530 (80) 670 (220)	(IX) 550 (210) 690 (100)	(XII) 560 (190) 700 (100)

References

*Work supported by SDIO-ISTO (NRL, Agent) Contract No. N00014-88-K-2132.

1. L.R. Ram-Mohan, K.H. Yoo, and R.L. Aggarwal, Phys. Rev. B38, 6151 (1988).
2. K.H. Yoo, R.L. Aggarwal, and L.R. Ram-Mohan, J. Vac. Sci. Technol. A7, 415 (1989).
3. S.P. Kowalczyk, J.T. Cheung, E.A. Kraut, and R.W. Grant, Phys. Rev. Lett. 56, 1605 (1986); T.M. Duc, C. Hsu, and J.P. Faurie, Phys. Rev. Lett. 58, 1127 (1987).

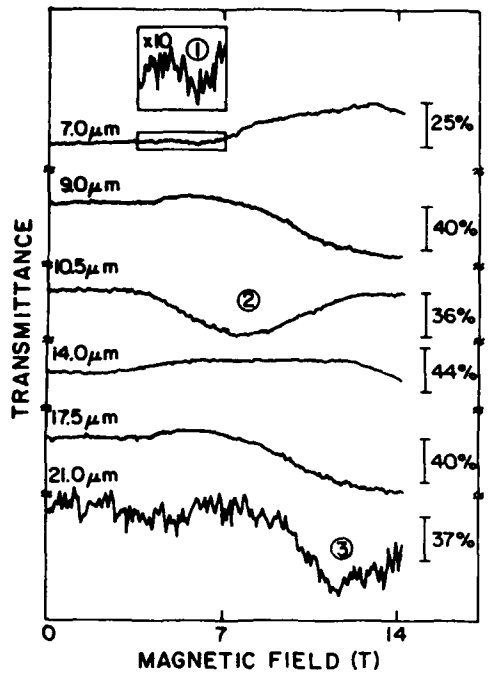

Fig. 1. Magnetotransmission spectra for sample ML-28B.

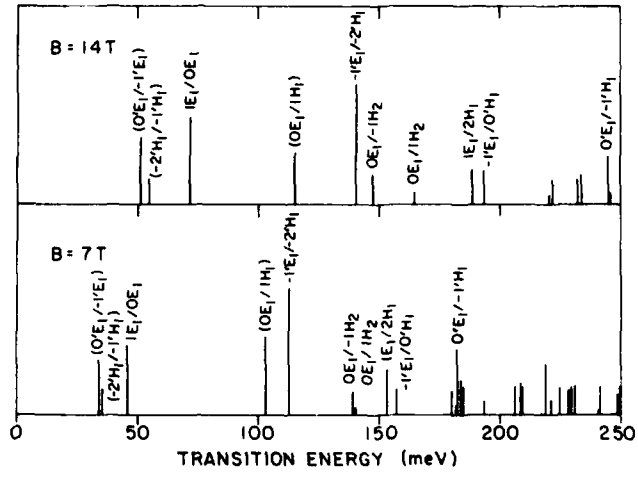

Fig. 2. Squares of the transition matrix elements for the transitions between Landau levels at B=7 T and 14 T for sample ML-28B.

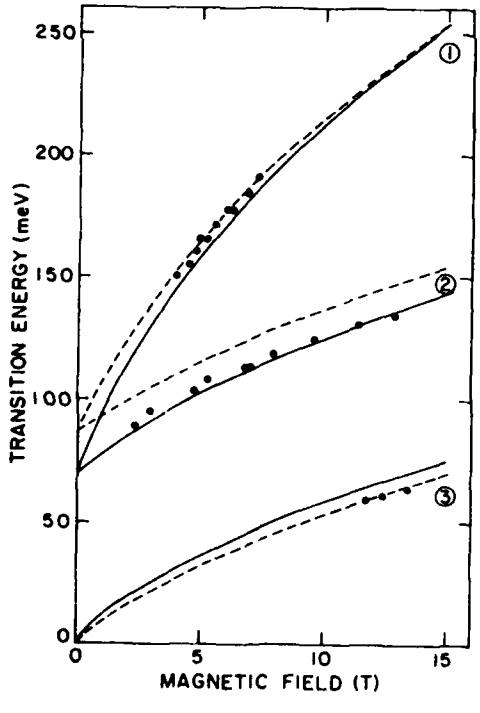

Fig. 3. Comparison of the observed (dots) and calculated transition energies for sample ML-28B using V_p=850 meV. Solid and dotted lines represent calculated energies for zone-center and zone-edge transitions, respectively.

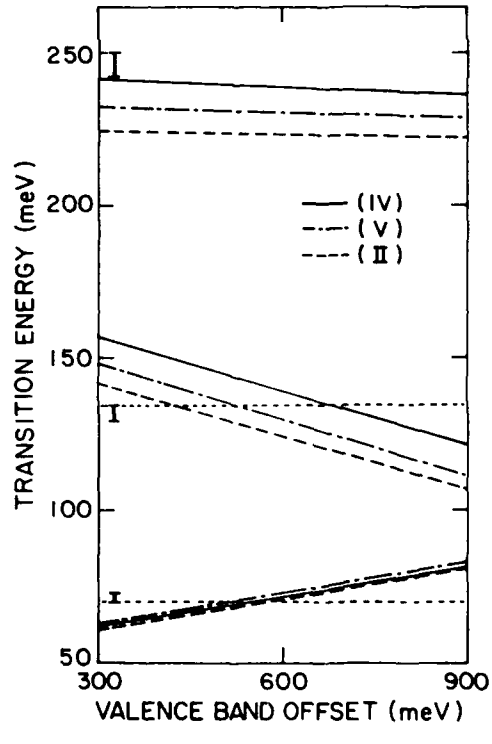

Fig. 4. Calculated zone-center transitions as a function of V_p for three sets of input parameters at 15 T for sample ML-25B. The observed energies are indicated by the bars. The crossing point corresponds to the lower limit of allowable V_p range of each transition peak for a given set of input parameters.

Electron Transport and Cyclotron Resonance in [211]-Oriented HgTe-CdTe Superlattices

C. A. Hoffman, J. R. Meyer, R. J. Wagner, and F. J. Bartoli
Naval Research Laboratory, Washington, D. C. 20375

X. Chu and J. P. Faurie
Univeristy of Illinois at Chicago, Chicago, IL 60680

L. R. Ram-Mohan and H. Xie
Worcester Polytechnic Institute, Worcester, MA 01609

We discuss a magneto-transport and magneto-optical investigation of [211]-oriented HgTe-CdTe superlattices, along with the first theoretical band structure treatment for that orientation. Measurements were performed on seven n-type samples with well widths spanning the range 41 to 125 Å. Energy gaps between 0 and 128 meV were determined from the temperature dependences of the intrinsic carrier densities. Semimetallic samples showed evidence for more than a single species of high-mobility electron, which is consistent with the theoretical prediction that the in-plane electron mass should be intrinsically broadened. Furthermore, the magneto-transport measurements indicated the presence of an additional electron species, whose density and mobility remained nearly constant between 4.2 and 300 K. These electrons are believed to result from a transfer of charge from the CdTe buffer layer into the superlattice [Berroir et al., Phys. Rev. Lett. 62, 2024 (1989)]. Magneto-optical measurments in Faraday geometry (cyclotron orbits in the plane) yielded multiple cyclotron resonance lines. When the magnetic field was rotated to Voigt geometry, one line in a semiconducting sample and two lines in a semimetallic sample displayed anisotropic 3D behavior. In agreement with theory, the superlattice electron mass anistropy is found to be greater in the semimetallic sample. Additional higher-field cyclotron resonance lines, which may correspond to the charge-transfer carriers, showed a complicated dependence as a function of magnetic field orientation. Although the behavior was clearly not 3D, neither could the data be interpreted in terms of a simple 2D model. Energy gaps and effective masses obtained from the band structure calculations are compared with the experimental results.

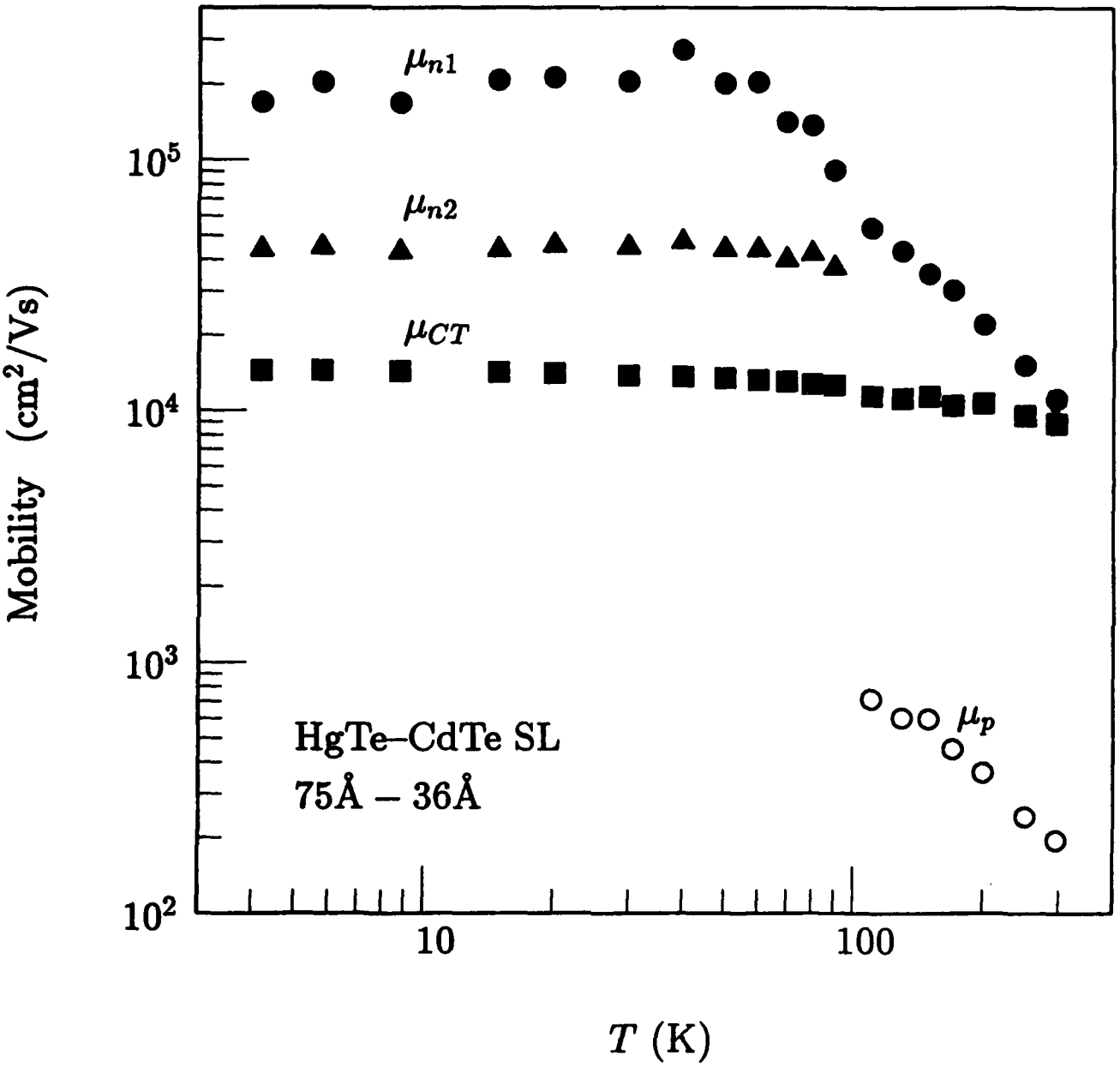

Figure 1. Mobilities vs T for mass-broadened electrons (μ_{n1} and μ_{n2}), holes (μ_p), and charge-transfer electrons (μ_{CT}) in a semimetallic HgTe-CdTe superlattice.

Stimulated Emission at 2.8 μm from Hg-Based Quantum Well Structures Grown by Photoassisted Molecular Beam Epitaxy

N.C. Giles, Y. Lansari, Jeong W. Han, J.W. Cook, Jr., and J.F. Schetzina
Department of Physics, North Carolina State University
Raleigh, North Carolina 27695-8202

We report the first observation of stimulated emission from Hg-based double heterostructures in which the active region is a superlattice. The laser structures were grown at NCSU on (100) substrates by photoassisted molecular beam epitaxy. The active region in these structures (Fig. 1) is a superlattice composed of 30 double layers of $Hg_{0.63}Cd_{0.37}Te$ (L_z ~ 166 Å) alternating with $Hg_{0.15}Cd_{0.85}Te$ (L_b ~ 60 Å). The superlattice is sandwiched between two wide-band-gap $Hg_{0.15}Cd_{0.85}Te$ layers as shown, thus forming a double-heterojunction. At the 1988 MCT Workshop, structures of this type were reported to emit bright photoluminescence (PL) at low temperatures at wavelengths in the range from 2.5 - 3.5 μm.

In the experiments reported here, the samples were chemically removed from the substrates using a selective etch and cleaved to form rectangular parallelepipeds. The cleaved cavities were then pressed into indium and cooled to liquid helium temperatures (T ~ 5 K). The laser cavities were optically pumped using the 1.06 μm output from a cw Nd:YAG laser. Power densities employed ranged from 1 to 7 kW/cm^2 at the sample surface. The PL emission spectrum was collected and analyzed using a Nicolet FTIR spectrometer.

Stimulated emission cavity modes were seen at cw laser power densities as low as 3.4 kW/cm^2. For a 65 μm wide cavity (Fig. 2), the PL emission at 5 K is centered at ~2.8 μm (FWHM = 48 meV). Under increased optical pumping, laser action is observed and many (> 10) cavity modes appear superimposed on the PL background (Fig. 2b). The spacing between adjacent laser modes is measured to be $\Delta\lambda$ = 0.02 μm. There is excellent agreement between the observed mode spacing ($\Delta\lambda$) and that predicted theoretically from the equation

$$\Delta\lambda = \lambda^2/[\, 2\, l\, (n - \lambda(dn/d\lambda))\,],$$

where λ = output wavelength, l = cavity width, and n = index of refraction. Using n = 3 and assuming $dn/d\lambda \approx 0$, we find the theoretical laser mode spacing also to be 0.02 μm.

The observation of stimulated emission from these double heterojunction structures is especially important since structures of this type are also appropriate for fabricating injection lasers by doping the two HgCdTe cladding layers on either side of the active superlattice region n-type and p-type, respectively. Both n-type and p-type doping of HgCdTe by photoassisted MBE has already been demonstrated at NCSU and elsewhere. Thus, fabrication of injection lasers may soon be possible.

Additional experiments involving HgCdTe laser structures are currently underway at NCSU. The results of these experiments will also be discussed at the 1989 MCT Workshop.

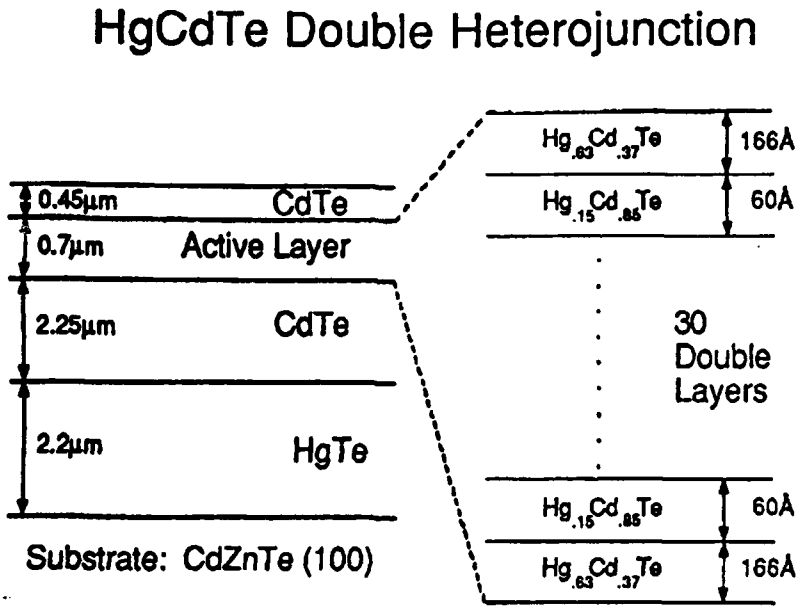

Figure 1. Schematic of the double heterojunction laser structures grown by photoassisted MBE; the active region is a 30 period superlattice.

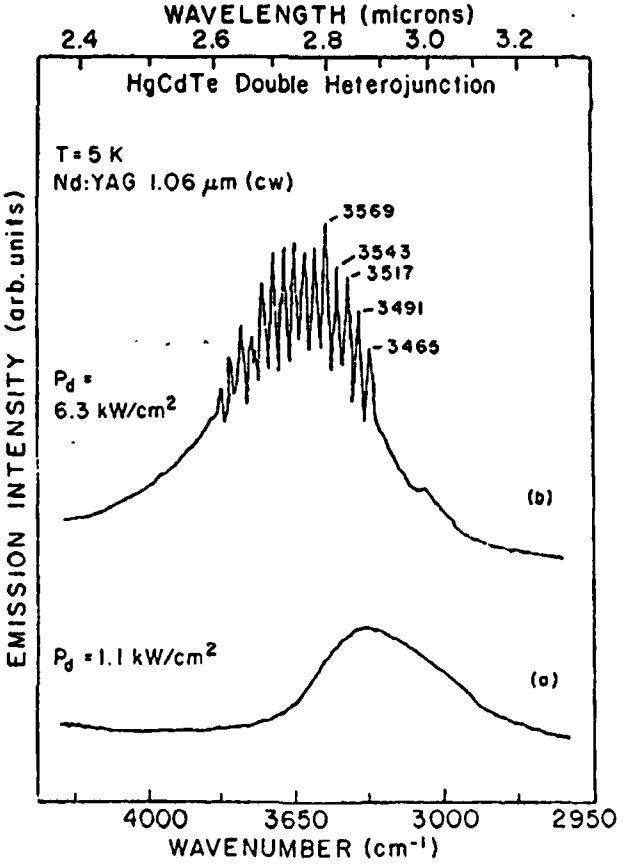

Figure 2. Stimulated emission from a 65 μm wide cleaved cavity: (a) PL emission spectrum at 5 K measured below threshold (1.1 kW/cm^2); (b) Stimulated emission cavity modes superimposed on PL background (6.3 kW/cm^2).

Stimulated Emission from $Hg_{1-x}Cd_xTe$ Epilayers and $CdTe/Hg_{1-x}Cd_xTe/CdTe$ Double Heterostructures Grown by Molecular Beam Epitaxy

K.K. Mahavadi, J. Bleuse, X. Chu, M. D. Lange,
S. Sivananthan and J.P. Faurie

Dept. of Physics, University of Illinois at Chicago,
Chicago, IL 60680

There is a considerable technological interest in mercury based II-VI semiconducting alloys and their microstructures as laser sources in the mid-infrared (2-5μm) region. We report the results of stimulated emission obtained *on* $Hg_{1-x}Cd_xTe$ (100) epilayers and $CdTe/Hg_{1-x}Cd_xTe/CdTe$ (100) double heterostructures grown by molecular beam epitaxy.

The intense low temperature photoluminescence (PL) and the minority carrier lifetimes of the order of 1 to 5μs showed the epilayers to be of high quality. The cleaved epilayers were optically pumped by a Nd:YAG laser and were found to lase continuously at 2.4μm up to 40K.

The growth of double heterostructures is complicated by the fact that the top CdTe layer has to be grown initially at a lower temperature to prevent the mercury diffusion from the active layer. Then the temperature can be ramped slowly to improve the CdTe layer quality. This procedure can create both graded x value layer and some defects at this interface. The low temperature PL spectra from these structures were intense and very broad, indicating the presence of a graded x value layer. The strong PL implies relatively fewer defects at the interface. The cleaved double heterostructures were found to lase continuously at 14K.

We are currently working on separate confinement heterostructures to achieve laser action at lower thresholds.

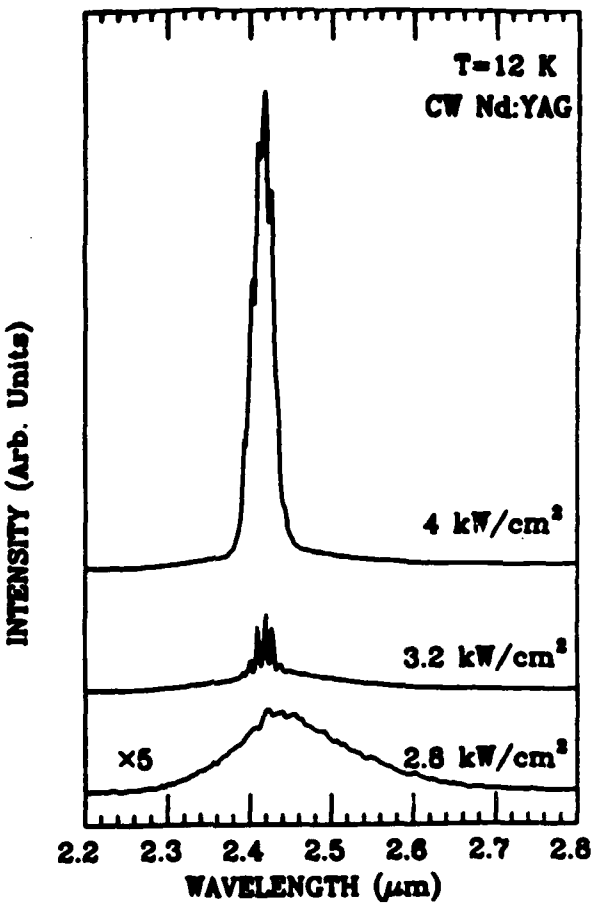

FIG 1. CW emission spectra from a cleaved 500 × 1500 μm $Hg_{0.54}Cd_{0.46}Te$ MBE grown epilayer under different incident powers.

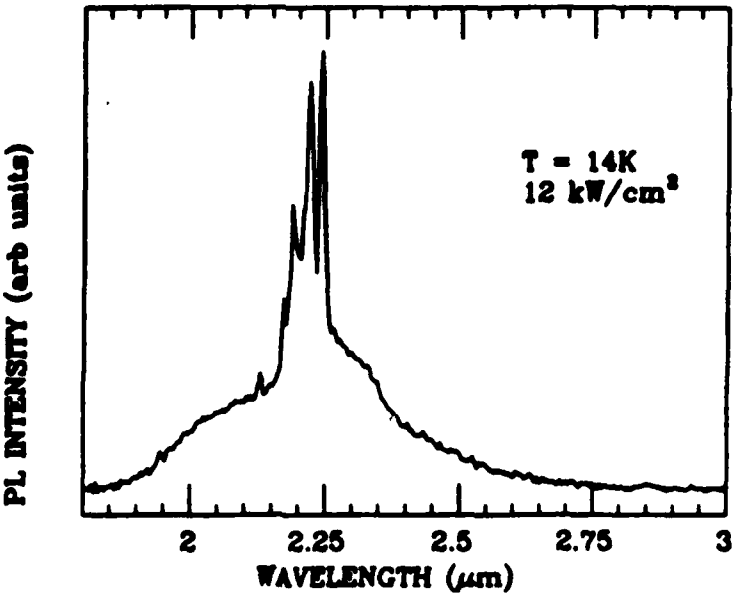

FIG 2. CW emission spectrum from a cleaved 480 × 1000 μm $CdTe/Hg_{1-x}Cd_xTe/CdTe$ double heterostructure.

Nonlinear Optical Coefficients of Narrow-Gap Semiconductors

E. R. Youngdale, C. A. Hoffman, J. R. Meyer, and F. J. Bartoli
Naval Research Laboratory, Washington, D. C. 20375

J. W. Han, J. W. Cook, Jr., and J. F. Schetzina
North Carolina State University, Raleigh, NC 27695

N. A. Engelhardt, E. W. Niles, and H. Höchst
Synchrotron Radiation Center, University of Wisconsin-Madison 53589

We discuss an experimental study of optical nonlinearities in Hg-based superlattices and MBE layers of $\alpha - Sn_{1-x}Ge_x$. Previous work has shown that these systems are attractive candidates for nonlinear optical applications. While both materials have very light electron effective masses in the regime near zero bandgap, the α-Sn layers have the additional feature that the energy separation between the Γ_8 (zone center) and L_6 electron valleys is small. Measurements have been performed on a series of samples well-characterized by magneto-transport measurements. $\chi^{(3)}$ has been determined by the non-degenerate four-wave mixing technique, using a pair of grating tuned, Q-switched CO_2 lasers. For the HgTe/CdTe superlattices, values of $\chi^{(3)}$ at 300 K and $\Delta\omega = 1.8$ cm^{-1} of up to 3.0×10^{-5} esu were obtained. The dependence of $\Delta\omega$ on $\chi^{(3)}$ was measured to determine the relaxation time, τ, for the dominant nonlinear mechanism. τ was found to decrease with increasing band gap, yielding $\tau \approx$ 1ps for the wider gap materials. The finite-gap samples also show stronger dependencies of $\chi^{(3)}$ on laser power and temperature than do the zero-gap superlattices, in agreement with a theoretical calculation based on optical heating of carriers. In addition, a series of MBE-grown α-Sn and $Sn_{1-x}Ge_x$ ($x < 0.02$) alloy layers have been studied. At $\Delta\omega$=1.8 cm^{-1} and 300°K , $\chi^{(3)} \approx 2 \times 10^{-5}$ esu is attained for pure α-Sn, and the nonlinearity shows no evidence of saturation for laser intensities up to 400 kW/cm^2. The pure α-Sn samples show $\tau \approx$ 1ps, while $\tau >$ 3ps in the $Sn_{1-x}Ge_x$ alloy layers. Theoretical calculations show that in addition to carrier heating, intervalley electron transfer also contributes to the nonlinearity in Sn-based layers.

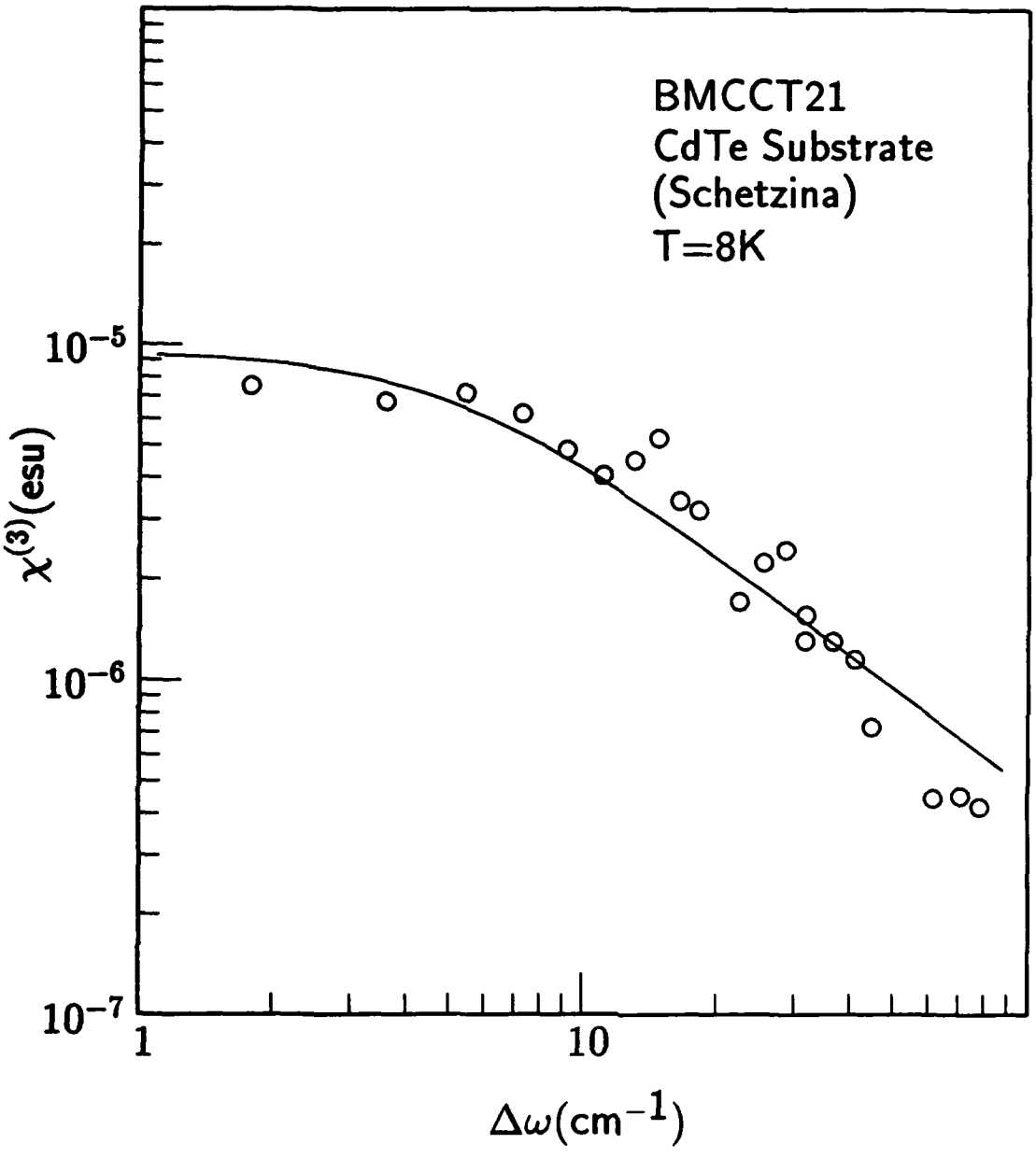

$\chi^{(3)}$ as a function of $\Delta\omega$ for a HgTe/CdTe superlattice with a helium-temperature bandgap of 80meV. The points are experimental, and the line is the result of a fit to the theoretically predicted shape of the curve. The roll-off in the curve indicates that the nonlinear response time is 1.1ps.

Field-effect transistors in $Hg_{1-x}Cd_xTe$ grown by photoassisted molecular beam epitaxy

D. L. Dreifus and R. M. Kolbas
Department of Electrical and Computer Engineering

Jeong W. Han, J. W. Cook, Jr. and J. F. Schetzina
Department of Physics

North Carolina State University
Raleigh, North Carolina 27695-8202

We report the first demonstration of $Hg_{1-x}Cd_xTe$ metal-insulator-semiconductor field-effect transistors (MISFETs) prepared using n-type layers grown by photoassisted MBE and processed by means of a new low-temperature (<60°C) semiconductor device processing technology developed at NCSU. Our transistor structures differ significantly from other $Hg_{1-x}Cd_xTe$ MISFET structures previously reported [1-4]. In particular, 1) a depletion region instead of a surface inversion layer is used as the principle for device operation, 2) high x-value $Hg_{1-x}Cd_xTe$ is employed as the active region of the device, and 3) the transistor structures are fabricated without the use of damaging processing steps(such as ion implantation and annealing, which can introduce defects into the material). In addition, the low-temperature processing technology developed at NCSU is compatible with the future development of superlattice and multilayer device structures in the Hg-based alloys.

The MISFET devices were fabricated using n-type, indium doped $Hg_{1-x}Cd_xTe$ films grown at 170°C by photoassisted MBE on (100) CdTe substrates. Epitaxial layers with x-values in the range from x=0.55 to x=0.60, carrier concentrations in the range from 1×10^{15} cm^{-3} and 5×10^{16} cm^{-3}, and mobilities as large as 5300 cm^2/V-s (300 K) were used. The devices were fabricated using a four-step processing sequence similar to that previously reported for CdTe metal-semiconductor field effect transistors[5,6], but with all processing steps performed below 60°C. For the gate insulator, a low-temperature MBE deposition of ZnS was employed.

Depletion-mode transistor action for a MISFET (5 μm gate length and 25 μm gate width) is illustrated in Fig. 1(a). The device shown has a transconductance of 0.54 mS/mm , and exhibits a pinch-off voltage of 500 mV with no appreciable gate current at a gate voltage of 20 V as shown in Fig. 1(b). MIS depletion-mode channel modulation has been observed for many devices on each of the four wafers processed to date. Optimization of the low-temperature (<60°C) processing and MBE growth technologies has increased device yields to greater than 80% across a 5mm x 7mm wafer. Photographs of the processed device structures are shown in Figs. 2(a) and 2(b).

These new transistor structures demonstrate that photoassisted MBE can be used to obtain high quality n-type $Hg_{1-x}Cd_xTe$:In epilayers suitable for the fabrication of integrated optoelectronic devices. This work has important implications for the development of monolithically-integrated HgCdTe focal plane detector array s, in which the electronic read-out circuitry is lattice-matched to the substrate and insensitive to the incident infrared radiation. Of equal technological importance is the low temperature (< 60°C) processing technology developed at NCSU. This technology, which does not employ damaged-junction approaches in the fabrication of devices, is also suitable for the processing of heterojunctions and superlattices of Hg-based alloys without significant Hg interdiffusion at the heterointerfaces.

1] A. Kolodny, Y.J. Shacham-Diamond and I. Kidron, IEEE Trans. Elect. Dev., ED-27, 591 (1980).

2] Y. Nemirovsky, S. Margalit and I. Kidron, Appl. Phys. Lett. 36, 466 (1980).

3] R. A. Schiebel, IEDM Technical Digest, 711 (1983).

4] R.A. Schiebel, IEDM Technical Digest, 132 (1987).

5] D.L. Dreifus, R.M. Kolbas, K.A. Harris, R.N. Bicknell, N.C. Giles and J.F. Schetzina, Appl. Phys. Lett. 51,931 (1987).

6] D.L. Dreifus, R.M. Kolbas, K.A. Harris, R.N. Bicknell, R.L. Harper, J.R. Tassitino, and J.F. Schetzina, J. Vac. Sci. Technol. A 6, 2722 (1988).

Fig. 1(a). Photograph of the Drain-to-source current vs drain-to-source voltage for a 5μm gate length by a 200μm gate width MISFET. The gate voltage, starting at 0.0 V, is varied by -100.0 mV steps. This device has a maximum transconductance of 0.54 mS/mm.

Fig. 1(b). Current-voltage (I-V) characteristics for 1.0x10 $^{-5}$cm^2 area MIS gate. The looping in the I-V curve is due to probe capacitance.

Fig. 2. Photographs of processed MISFETs: (a) 5μm gate length by 200μm gate width device; (b) large area photograph showing the uniformity of the processed device structures.

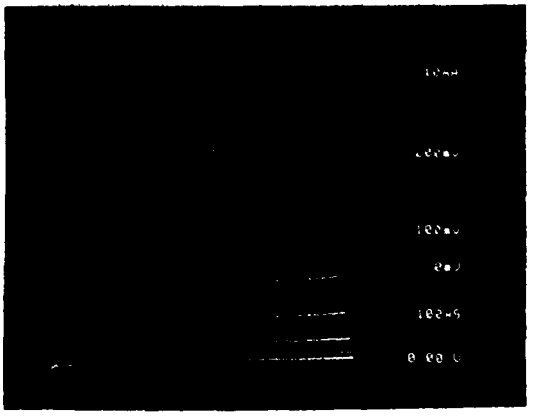

Figure 1 (a).

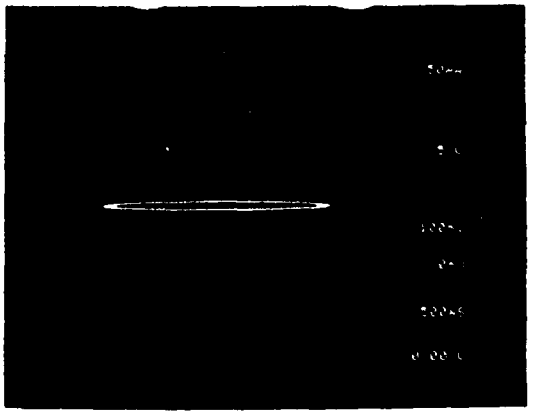

Figure 1 (b).

Figure 2 (a)

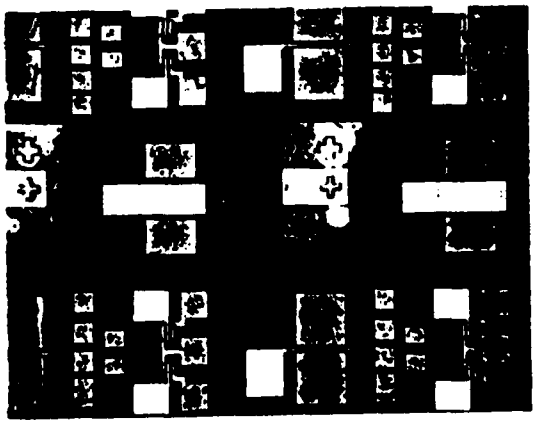

Figure 2 (b).

MIS PROPERTIES OF MBE GROWN HETEROSTRUCTURES*

M. W. Goodwin, M. A. Kinch, and R. J. Koestner
Texas Instruments Inc.
Central Research Laboratories
Dallas, Tx 75227

New infrared material systems composed of heterostructures have been proposed as a way of overcoming some of the problems inherent in single layer HgCdTe devices. Two of the major limiting problems in current HgCdTe infrared detectors are dark and tunnel currents caused by a number of effects such as defects, impurities, and interface states due to surface passivation. By utilizing a heterostructure concept in an MIS approach these problems can be significantly reduced.

We have studied the MIS properties of HgCdTe heterostructures grown by MBE. MBE offers the best growth technique, because of the precise control of the individual layers needed to fabricate this type of structure. The heterostructures studied consist primarily of a thin (~ 1 um) n-type wide-bandgap layer (X ~ .3) on top of a thicker (~ 5 um) n-type narrow-bandgap layer (X ~.22), all of which were grown on CdZnTe substrates. The measurements were made from MIS devices which were fabricated on top of the structure. The results show a factor of 2 reduction in dark currents for cutoff wavelengths between 9.2 and 11.2 um for the narrow-bandgap layer. In addition the breakdown fields are increased from .6 V/um typically found in material with this cutoff wavelength to 1.4 V/um. From a dark current analysis of the heterostructures we do not observe a significant problem of dark current generation at the hetero-interface between the top and bottom layers. We also find that the valence band offset between the top and bottom layers appears to be small, thus diffusion dark currents and optically generated minority carrier currents from the narrow-bandgap layer can flow into the inversion layer of the MIS device in the wide-bandgap layer.

*Work supported by DARPA contract no. N00014-86-C-2389 (Option)

The authors prefer an oral presentation.

MBE GROWTH OF HgCdTe HETEROSTRUCTURES

R.J.Koestner and H.F.Schaake
Texas Instruments, Inc.
Central Research Laboratories
Dallas, Tx 75265

HgCdTe heterostructures consisting of a thin n-type widegap layer deposited on an n-type narrowgap layer offers the promise of very high performance MIS photocapacitors for LWIR detection. Molecular Beam Epitaxy (MBE) is a candidate growth technology for these two layer films due to its fine control in composition, thickness and doping concentration. The critical materials issues are achieving low net donor concentrations in the widegap layer, reducing the defect content associated with compound twins present in the grown layers and avoiding the formation of misfit dislocations at the HgCdTe heterointerface.

For MBE grown HgCdTe(001) films, net donor densities of 1-2 x 10^{15} cm^{-3} for the widegap layer (x = 0.30) and 2-3 x 10^{15} cm^{-3} for the narrowgap layers (x = 0.22) are reproducibly measured in MIS test structures. A further reduction of the net donor density in the widegap layer to 5-10 x 10^{14} cm^{-3} is necesaary for optimal heterostructure performance. The net donor concentration in HgCdTe(001) layers with x = 0.22-0.30 does not show any significant change in MIS test structure and Hall transport measurements before or after a 200°C postanneal under Hg saturated conditions. This suggests that the as-grown HgCdTe(001) layers have a Hg vacancy concentration less then 1 x 10^{15} cm^{-3}. In fact, only n-type films are grown over the composition range of x = 0.22-0.33 at our substrate temperature of 195°C.

Surprisingly, the net donor concentration in the HgCdTe(001) layers rises to the low 10^{16} cm^{-3} range when the Hg flux is less than two times the minimal flux necessary for single crystalline growth. Figure 1 illustrates the change in surface hillock morphology that occurs at increasing Hg flux. In Figure 1(a), a Hg flux ~20% above the minimum value was employed; a triangularly shaped hillock results with a measured net donor density in the low 10^{16} cm^{-3}. In Figure 1(b), a Hg flux ~40% above the minimum value was used; in this case, a surface pyramid with a square base and smooth faces results with a measured net donor density of 8 x 10^{15} cm^{-3}. As the Hg flux is increased to ~100% above the minimum, Figure 1(c) shows the surface pyramids develop a rectangular base and textured faces. The measured net donor concentration falls to our lower limit for HgCdTe(001) layers at x = 0.29 of 1-2 x 10^{15} cm^{-3} and at x = 0.22 of 2-3 x 10^{15} cm^{-3}.

In Figure 1(d), the surface hillocks now appear polycrystalline since a Hg flux ~350% above the minimum was used, yet the net donor density again falls to the low 10^{15} cm^{-3} range. Although the dislocation density for the film in Figure 1(d) is two orders of magnitude (1×10^7 cm^{-2}) higher than that in Figure 1(c), the net donor density is not significantly different. In fact, we have not seen any correlation between defect density (dislocations and twins) and net donor density in the HgCdTe(001) films that we have grown to date.

The compound twins that lead to surface pyramids on MBE HgCdTe(001) layers are primarily caused by Hg rich clusters on the HgCdTe growth front. At present, the density of these surface hillocks falls in the $1\text{-}3 \times 10^4$ cm^{-2} range. Since these hillocks may cause higher tunnel currents in HgCdTe layers, reduction in their density on the (001) surface is required. By removing Te vacancies from the CdZnTe substrate surface prior to buffer layer growth, the hillock density in our HgCdTe(001) layers is found to drop from the low 10^5 to the low 10^4 cm^{-2} range. In addition, Hg pressure bursts that occasionally happen due to condensation of Hg at the effusion cell lip leads to the nucleation of additional hillocks during growth. The lateral dimension of the surface pyramids provides a measure of their nucleation depth. We find that less than 5×10^3 cm^{-2} hillocks nucleate at or near the substrate or buffer layer interface; the balance are nucleated during HgCdTe layer growth.

Due to the low substrate temperature (195°C) employed in MBE HgCdTe growth, a kinetic barrier appears to effectively block the formation of misfit dislocations that are predicted to occur at equilibrium. This permits the growth of a 1-2 μm thick widegap layer ($x = 0.30$) on a narrowgap layer ($x = 0.22$) without the addition of Zn to the widegap layer. For example, a 530 ÅHgCdTe ($x = 0.85$) on 1.2 μm HgCdTe ($x = 0.295$) on 6.3 μm HgCdTe ($x = 0.205$) heterostructure that was grown at 195°C by MBE showed a threading dislocation density through the HgCdTe layers of 2×10^5 cm^{-2}. This density is very close to the CdZnTe substrate dislocation density and suggests that few, if any, misfit dislocations were produced at the HgCdTe heterointerface. Double Crystal Rocking Curves (DCRC) indicate a lattice mismatch of 3.7×10^{-4} at 200°C between the two HgCdTe layers. At equilibrium, ~50% of this mismatch should be accommodated by misfit dislocations; yet DCRC analysis indicates that no misfit dislocations are formed within the experimental error (~ 5%).

Acknowledgments

We thank Don Todd for his technical assistance. This work was performed under DARPA contract No. N00014-86-C-2379.

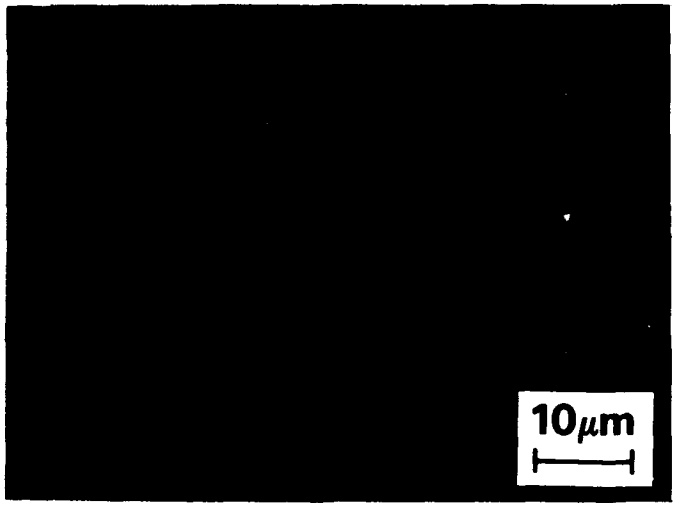

(a)

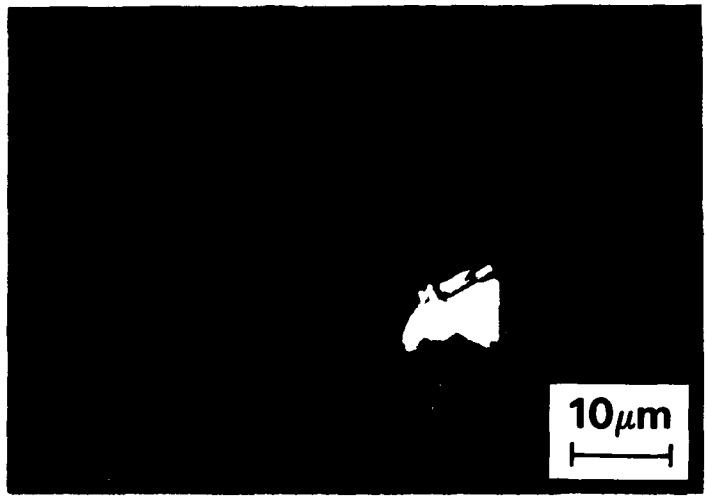

(b)

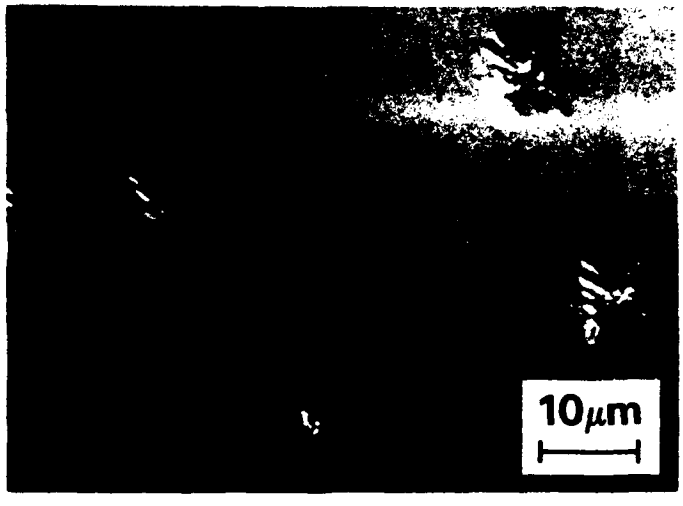

(c)

(d)

Figure 1. The surface hillock morphology of MBE grown HgCdTe(001) films is shown for increasing Hg flux. The Hg fluxes relative to the minimum flux required for single crystalline growth are (a) 1.2, (b) 1.4, (c) 2.0 and (d) 4.5.

The Spreading Resistance technique applied to MCT Heterojunctions

M. Boukerche and J.P. Faurie
Dept. of Physics, University of Illinois at Chicago, Chicago, IL 60680

One of the fundamental difficulties of II-VI materials is the control of their doping properties. One of the most exciting possibilities of the MBE growth technique is to be able to realize sharp in situ doping and compositional changes while the crystal is being grown. To be able to design sophisticated (unannealed) device heterostructures we face the problem of first characterizing them along the growth axis. The spreading resistance measured between two sharp electrodes closely spaced is a well known technique for profiling resistivity in silicon structures. Elaborate numerical techniques have been developed during the last twenty years to correct for non-uniform doping or multilayer configurations. This technique (SR) has also been used more recently to characterize GaAs device structures. Reproducible measurements could be obtained for n-type doping levels exceeding $10^{17}cm^{-3}$. To our knowledge, the profiling of mercury cadmium telluride structures by spreading resistance has not been reported yet. Apart from the well known limitations associated with SR (bias between probes less than kT, spatial resolution limited by tip radius and splitting distance between probes, sensitivity to surface states), the application to MCT profiling faces very specific problems. MCT is recognized as a very soft material where piezoelectricity and irreversible electrically active dislocations can be generated very easily. For silicon the growth technology and material understanding have reached such a maturity that the mobility and carrier concentration can be reasonably well predicted from resistivity thanks to well accepted tabulations. Such is obviously not the case for MCT even for a fixed cadmium composition . The problem gets even more complicated if we consider the sharp electron mobility variation with composition in the narrow bandgap range.

Our approach was to consider two independent measurements made at room temperature and cryogenic temperature respectively. The first made in the intrinsic region would give information related to the Cd composition profile. The latter made in the extrinsic temperature region would on the contrary provide information connected to the doping profile of the sample. The splitting distance between probes was 50um and the force .5 gm/probe. The samples were beveled etched by linear

dipping versus time in Br/HBr solutions producing etching rates close to 2um/min. The samples were subsequently loaded in the vacuum chamber and measured as fast as possible. Successful measurements could be achieved even at cryogenic temperature. Our experience is that when the sample is cooled the measurement is feasible during a limited time only due to unpredictable barrier formation by progressive adsorption of the residual gases on the sample. We could resolve profiles of n on p homojunctions produced by low energy ion sputtering at 400eV showing a junction depth of .6um and a low mobility surface layer, as well as more complicated in situ indium doped structures in agreement with SIMS profiling. Measurements of HgCdTe/CdTe interfaces will be presented as well as results on HgCdTe/HgTe heterojunctions showing unexpected resistivity variations close by the interface which will be discussed.

A New, Accurate Relationship of $E_g(x,T)$ for $Hg_{1-x}Cd_xTe$ Alloys*

D. G. Seiler and J. R. Lowney
Semiconductor Electronics Division
National Institute of Standards & Technology
Gaithersburg, MD 20899
and
C. L. Littler and M. R. Loloee
Department of Physics
University of North Texas
Denton, TX 76203

The dependence of the energy gap, E_g, of $Hg_{1-x}Cd_xTe$ (MCT) on temperature T and alloy composition x is one of the most important fundamental relationships of this alloy system. Once known accurately, it provides a convenient means to determine x from measurements of E_g. Recently[1,2] two-photon magneto-optical (TPMO) spectra have been obtained and used to determine values for E_g that are more accurate than those obtained by any other means. In this paper we present systematic and comprehensive TPMO data at various temperatures on seven different samples (both n- and p-type, $0.21 < x < 0.31$). Results reported here were carried out on both single crystal samples grown by solid-state recrystallization and the traveling-heater methods. The output of a grating-tunable cw CO_2 laser, mechanically chopped at a low duty cycle, was focused onto the samples placed in a 12T superconducting magnet. TPMO spectra were observed in the photoconductive response of the samples and recorded by boxcar averager techniques. Our results provide an accurate new formulation of the relationship for $E_g(x,T)$. The results definitely show that at low temperatures (< 100K), a linear $E_g(T)$ relationship is unsatisfactory and should not be used.

Our results will be compared with pertinent thermodynamic principles and with the known experimental dependencies of $E_g(x,T)$ for other semiconductors such as PbTe and InSb. Both PbTe and InSb have nonlinear dependencies of E_g versus T. We review the types of measurement techniques involving different physical processes that have been used in the past to determine values for E_g for $Hg_{1-x}Cd_xTe$. Various different relations for $E_g(x,T)$ used in the past are presented and discussed. The determination of the band gap by two-photon absorption techniques has significant advantages over the more traditional methods.

1. D. G. Seiler, M. R. Loloee, S. A. Milazzo, A. J. Durkin, and C. L. Littler, Solid State Commun. 69, 757 (1989).
2. D. G. Seiler, C. L. Littler, M. R. Loloee, and S. A. Milazzo, J. Vac. Sci. Tech. A7, 370 (1989).
*Work supported in part by the Center for Night Vision and Electro-Optics, Fort Belvoir, VA and a grant from Texas Instruments, Inc.

Temperature Dependence of Phonons in $Hg_{1-x}Cd_xTe$ and the Implications on its Electronic Properties

P.M. Amirtharaj,
U.S. Army Center for Night Vision and Electro-Optics
Fort Belvoir, VA-22060

A detailed Raman scattering (RS) investigation of the temperature dependence of the phonons in HgTe, CdTe and $Hg_{1-x}Cd_xTe$ (x=0.2) was conducted in the range of 10 to 300K. A clear softening of the HgTe like transverse optical (TO) phonon by ~2 cm^{-1} was established, for the first time, in the binary HgTe as well in the alloy $Hg_{1-x}Cd_xTe$ with x=0.2. Indirect evidence of the softening of a Brillouin zone (BZ) boundary accoustic phonon was also obtained from the two-phonon--difference process. This leads to the suggestion that the accoustic branch could be undergoing a similar downshift with reducing temperature.

Softening of phonon frequencies in HgTe may be understood qualitatively in terms of the inverted ordering of the bonding Γ_8 and the antibonding Γ_6 electronic states; promotion of an electron from Γ_8 to Γ_6 results in a net softening of the lattice.[1,2] The relationship between the shift in the phonon and the fundamental gap energies will be discussed using the Heine and Van Vechten theory.[1,2]

The CdTe TO phonon, on the contrary, hardens by ~4 cm^{-1}. $Hg_{1-x}Cd_xTe$ with x=0.2 exhibits a mixed behavior where the HgTe-like TO softens but at the same time the CdTe-like TO hardens slightly (<1 cm^{-1}). Hence, the temperature induced perturbations of the Hg-Te and the Cd-Te bonds are qualitatively similar to the constituent binaries.

1. M.L. Cohen and D.J. Chadi, Handbook on Semiconductors, Vol. II, ed., M. Balkanski, (North-Holland, NY, 1980), p. 155.
2. V. Heine and J.A. Van Vechten, Phys. Rev. B 13, 1622 (1976).

THE EXCESS CARRIER LIFETIME IN VACANCY AND IMPURITY DOPED HgCdTe

R.Fastow and Y. Nemirovsky

Microelectronics Research Center, Dept. of Electrical Engineering,
Technion-Israel Institute of Technology, Haifa, 32000, Israel

The excess carrier lifetime in HgCdTe is a basic physical parameter which governs the magnitude and frequency response of devices. One of the outstanding questions relating to the excess carrier lifetime of p-type HgCdTe is whether this parameter can be increased by doping with impurity atoms rather than Hg vacancies. At the present time, only a small number of papers have been published dealing with this topic. Two works have suggested that As doping improves the lifetime by at least a factor of three[1,2], while a third has found no differences in the lifetimes of impurity doped and vacancy doped material[3].

In this work, the excess carrier lifetimes of numerous vacancy and impurity doped bulk p-type HgCdTe crystals are measured using the techniques of steady state photoconductivity and photoconductive decay. It is shown that the steady state minority carrier lifetimes of impurity doped crystals can be significantly larger than those of vacancy doped crystals. However, the steady state and the transient lifetimes of the same specimen are generally not equal. For $Hg_{1-x}Cd_xTe$ wafers with x~0.225 and $N_a \sim 1\times10^{16}/cm^3$, the steady state minority carrier lifetimes of impurity doped crystals ranged from 1.6 to 62 ns, while those of vacancy doped

crystals ranged from 1.4 to 28 ns.

Measurements of the steady state minority carrier lifetime of a Au doped $Hg_{0.775}Cd_{0.225}Te$ crystal are shown in figure 1. The steady state lifetime was extracted from the magnitude of the photoconductive signal, which is proportional to $\mu_n\tau_n$, and from separate measurements of the minority carrier mobility. In this crystal, the steady state lifetime was 6 ns, and the minority carrier mobility was 49,000 $cm^2/V\text{-}s$ at 77 K. Photoconductive decay curves for the same Au doped crystal are shown in figure 2. The transient lifetime, as determined by the 1/e point, is seen to be 62 ns at 77 K.

Results for a number of crystals in this study, both vacancy and impurity doped, are summarized in Table 1. In this table, the growth methods, heat treatments, acceptor ionization energies, carrier concentrations, minority carrier mobilities, transient and steady state minority carrier lifetimes, and calculated diffusion lengths are listed. It is seen that there is a wide variation in the steady state lifetimes (from 1.4 to 62 ns). However, the largest lifetimes occurred in the impurity doped material, reaching values greater than 45 ns in a few cases. Significantly, a large fraction of the impurity doped samples had steady state minority carrier lifetimes between 2-10 ns, as in the case of vacancy doped material.

References

1. C.E. Jones, K. James, J. Merz, R. Braunstein, M. Burd, M. Eetemadi, S. Hutton, J. Drumheller, J. Vac. Sci. Technol. A3, 131(1985).

2. Tse Tung, M.H. Kalisher, A.P. Stevens, P.E. Herning, Materials Research Soc., vol. 90, edited by R.F.C. Farrow, J.F. Schetzina, J.T. Cheung (Materials Research Society, Pittsburg, Penn, 1987).

3. D.E. Lacklison and P. Capper, Semicond. Sci. Technol. A1, 1700(1983).

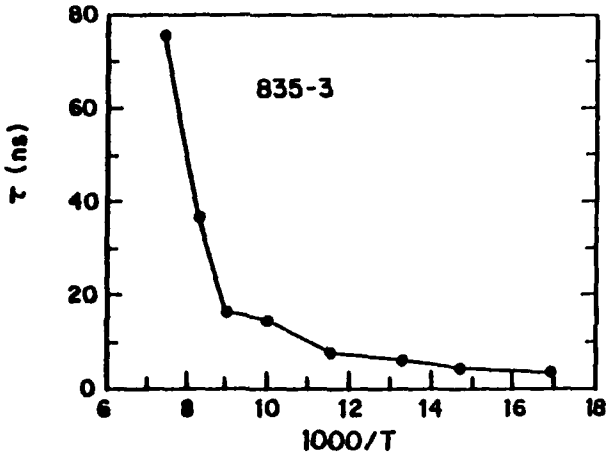

Fig. 1. The steady state minority carrier lifetime of a Au doped $Hg_{0.7}Cd_{0.3}Te$ specimen. The solid lines are for visual aid.

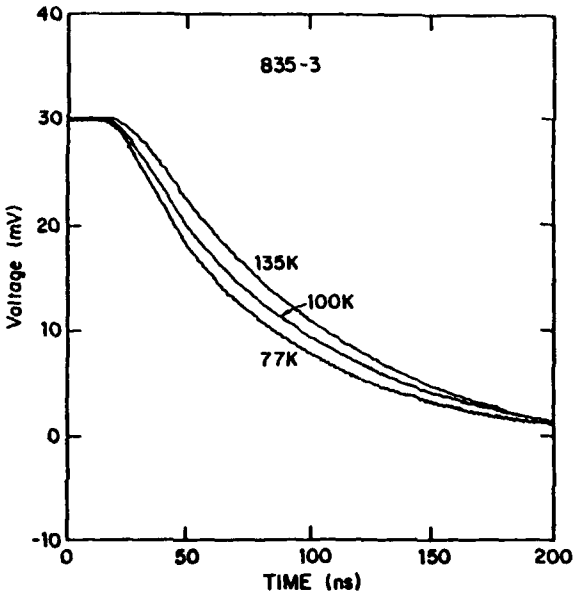

Fig. 2. Photoconductive decay curves from a Au doped $Hg_{0.7}Cd_{0.3}Te$ specimen, taken at 135, 100, and 77 K.

TABLE I - CRYSTAL PARAMETERS

Sample #	Growth Method	Dopant	Anneal (°C)	N_{a1} E_{a1}	N_{a2} E_{a2}	N_a	$u_a \times 10^4$ $cm^2/V\text{-}s$	τ_{ao} (ns)	τ_c (ns)	D_L (um)
P1637	Slush	None	400	2.3×10^{16} 14.5 meV	5.0×10^{14} 5.5 meV	1.5×10^{16}	6.7	1.4	23	7.9
THM6-36	THM	None	400	4.6×10^{15} 15.0 meV	2.0×10^{15} 2.0 meV	4.4×10^{15}	6.7	10	90	21
855-1	SSR	As	270	8.0×10^{15} 7.0 meV	1.0×10^{15} 3.0 meV	9.0×10^{15}	5.2	8	36	17
861-3	SSR	As	270	1.0×10^{16} 7.0 meV	3.5×10^{15} 2.7 meV	1.2×10^{16}	5.5	62	90	47
809-1	SSR	Au	270	6.5×10^{15} 10.5 meV	4.0×10^{14} 3.0 meV	6.2×10^{15}	4.5	49	220	38
835-3	SSR	Au	350	1.5×10^{15} 18.0 meV	5.5×10^{15} 2.2 meV	6.4×10^{15}	4.9	6	62	14

RADIATIVELY LIMITED MWIR PHOTOVOLTAIC DETECTORS FABRICATED ON SAPPHIRE SUBSTRATES

August 1989

R.E. DeWames, J.G. Pasko, D.L. McConnell, J.S. Chen, J. Bajaj, L.O. Bubulac, E.S. Yao, G.L. Bostrup, R. Zucca, G.M. Williams and A.M. Blume

Rockwell International Science Center
Thousand Oaks, CA 91360

and

T.P. Weismuller
Rockwell International Optical Center Anaheim, CA 92803

The capability to grow device quality epitaxial HgCdTe on Al_2O_3 substrates has been long demonstrated, and it has impacted the IR imaging technology. Advantages of Al_2O_3 substrates are the availability of large substrates and workability in a manufacturing environment. Current attempts to grow device quality epitaxial HgCdTe on GaAs, GaAs/Si and Si have the potential to extend the spectral region to long wavelengths and the possibility to integrate sensors and the associated signal processing circuitry in a single chip. However, such parameters as lattice mismatch, thermal expansion coefficient mismatch and substrate cross-doping can induce a diversity of flaws which limit the quality of the material. In addition, non-equilibrium growth conditions are used for synthesis and such parameters as sticking coefficients, ion mobility and crystal orientation can impact the microstructure content of the semiconductor layer. Therefore, to realize the benefits of the use of the above substrates for IR imagery, the role of microstructure on devices must be assessed in order to quantify the conditions for which these features will be limited and to identify the need for further improvements in material quality.

The purpose of this work is to carry out a comprehensive study of the properties of high performance (MWIR) devices fabricated on CdTe/Sapphire substrates by ion implantation, with the goal to start identifying layer properties and junction formation characteristics which are needed to bring about the highest possible MWIR array performance. These photovoltaic devices are limited by radiative processes at temperatures above 200K. This condition represents the upper theoretical limit performance for such parameters as the zero-bias resistance-area, (R_oA product). At lower temperatures Shockley-Reed processes limit device performance. At 120K, R_oA

values of $3x10^5\Omega$-cm^2 with cut-off wavelength $\lambda co(120) = 4.64\ \mu m$ are observed. Device uniformity is considered good down to 80K, where R_oA values are $>10^7\ \Omega$-cm^2. The I/f noise values measured at 1Hz and 20mv reverse bias at 120K are $\approx 10^{14}$ A/$\sqrt{Hz}$. Such performance represents an improvement of at least a factor of five over what is typically observed on devices fabricated on CdTe/Sapphire sub-strates. C-V data yield a carrier concentration in the range of $3x10^{14}$ cm^{-3} over a relatively large region of the device. Avalanche breakdown is observed in these devices, and the breakdown voltage is on the order of 11.5V. The electron multipli-cation factor is $M_n = 4$, at 5V reverse bias. The electron ionization coefficient is $\alpha = 8x10^4 \exp 3x10^4/E$, where E is the electric field. At sufficiently high reverse bias, with voltages still below breakdown, avalanching mechanisms are dominant, and band-to-band tunneling is not observed. In this voltage region, breakdown is mostly associated with localized regions which have a lower breakdown voltage than the breakdown voltage of the whole junction. An important observation is that the layer used for device fabrication had no sub-grain structure and a relatively low content of dislocations, $\sim 5x10^5$ cm^{-2}.

It is proposed that the high performance is associated with the reduction of the microstructure and dislocation content of the layer and the low carrier concentration. In addition, it is proposed that these flaws are electrically active and p-type. This work points to the need for further assessments of effects on devices and layers of both microstructure and residual doping, to bring about the highest possible MWIR array performance.

REVERSE BREAKDOWN IN LONG WAVELENGTH LATERAL COLLECTION CMT DIODES

C.T. Elliott, N.T.Gordon and R.S. Hall
Royal Signals and Radar Establishment, Malvern, Worcs, England

G Crimes
Philips Components Limited, Southampton, Hants, England

CMT diodes show large deviations from ideality in their reverse characteristics. The excess currents are attributed in many published papers to band to band tunneliing at high reverse bias and to trap assisted tunnelling at low reverse bias[1,2]. New evidence is presented that in long wavelength loophole diodes[3], the breakdown is due to impact ionisation by electrons in the depletion region.

Measurements have been made of the multiplication of a photo-signal as a function of bias and the results are plotted in Fig. 1. The solid line in this figure is a fit to Shockley's "lucky electron" equation[4], assuming that electrons only mutliply. The measured multiplication can be used to predict the reverse IV characteristics assuming that avalanching is the only breakdown mechanism. Figure 2 shows the predicted reverse characteristics (crosses) and the measured characteristic (solid line) in a room temperature background flux. The correspondence between the measured and predicted characteristic is evidence that in this case, the reverse breakdown is due to avalanching.

The IV characteristics of these diodes have also been measured under a cold shield to exclude the background flux. In this case, however, the dark current is found to increase with bias by a greater factor than the photocurrent multiplication. At low voltages (in this case less than one volt)the dark current multiplication is proportional to the photocurrent

multiplication (Fig. 3). A possible explanation is that the dark current contains a greater proportion of electron current. Assuming that only electrons multiply, this would lead to a greater dark current multiplication. Figure 3 shows that above a threshold voltage, the dark current increases more rapidly than can be explained by the measured multiplication. This is due to an additional leakage mechanism, possibly tunnelling.

Figure 4 shows that the white noise, measured above the 1/f knee, is approximately proportional to the multiplication. This result is consistent with the assumption that multiplication is predominantly by one carrier (electrons)[5].

References

1. R.E. DeWames, J.G. Pasko, E.S. Yao, A.H.B. Vanderwyck and G.M.Williams, J.Vac.Sci Technol. A6 (4), 2655 (1988)
2. Y. Nemirovsky, D. Rosenfeld, R.Adar and A. Kornfeld, CMT Workshop, Orlando 1988
3. I.M. Baker, I.D. Jenner, J. Parsons and R.A. Ballingall, SPIE Conference on IR Technology and Systems (1984)
4. W. Shockley, Solid State Electronics, 2, 35 (1961)
5. R.J. McIntyre, IEEE Trans.Elect.Dev., ED-13 (1), 164 (1966)

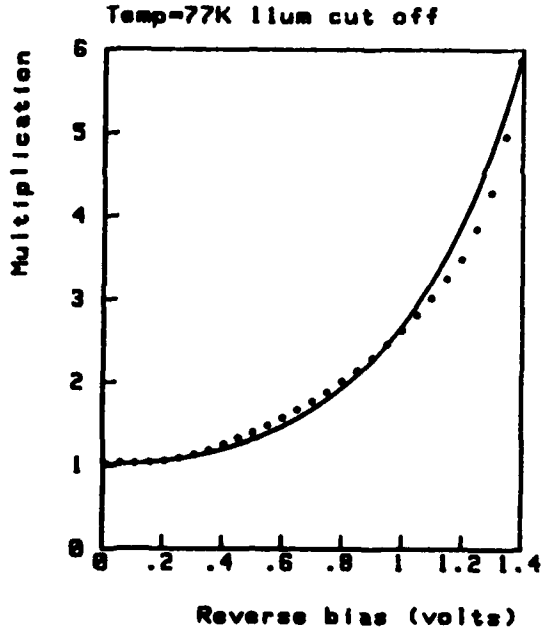

Fig 1 Photo-multiplication vs voltage

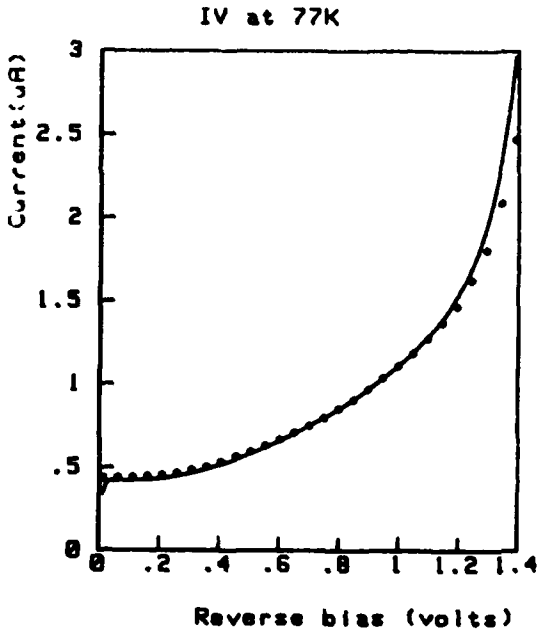

Fig 2 Actual (solid line) and predicted (crosses) IV

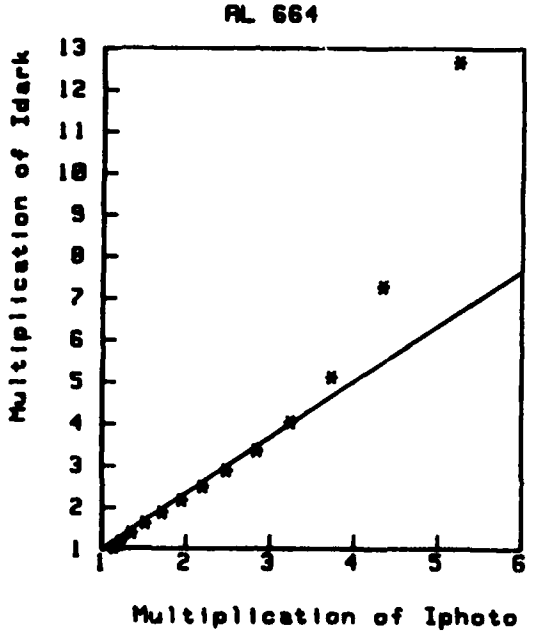

Fig 3 Dark current vs photo-multiplication

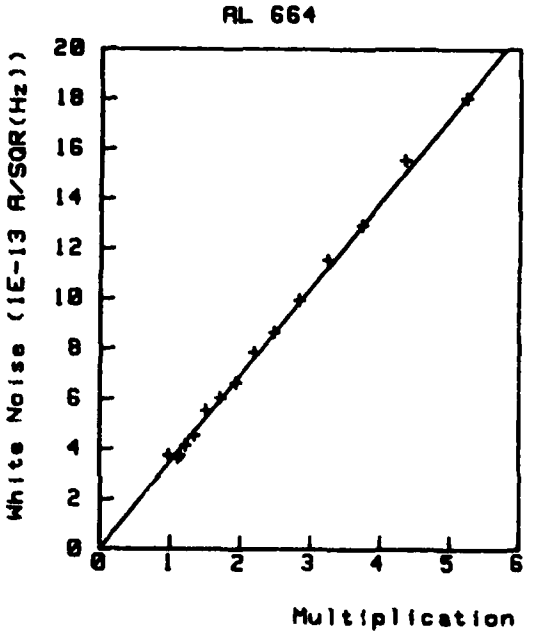

Fig 4 Multiplication of white noise

INFLUENCE OF BARRIERS ON CHARGE TRANSPORT ACROSS HgCdTe HETEROJUNCTIONS

K. Kosai and W. A. Radford

Santa Barbara Research Center
Goleta, CA 93117

The effects of various parameters on potential barrier height in graded $Hg_{1-x}Cd_xTe$ heterojunctions have been previously calculated at equilibrium.[1-3] In this paper we discuss the nonequilibrium situation with photogeneration and the influence of heterojunction barriers on charge transport in wide bandgap p^+ on narrow bandgap n diodes that are illuminated from the n side. We have performed one-dimensional numerical simulations which solve Poisson's equation coupled with the transport and continuity equations for electrons and holes. The model (HET III) is a modification of Stanford University's device simulator SEDAN[4], and contains Fermi-Dirac statistics. Other model capabilities are incomplete impurity ionization and valence band offset, but these were not incorporated in the calculations. Parameters in the modeling include the composition of the p^+ cap layer (x_{cap}), the composition grading width (W_{HJ}), the doping of the base layer (N_d), temperature and detector bias.

The simulated devices are abrupt p^+-n junctions centered on a graded composition profile that is proportional to a complementary error function with the argument $2y/W_{HJ}$, where y is the depth. The thickness of the cap layer is 2 μm and the acceptor concentration is 2×10^{17} cm^{-3}. The thickness of the n-type base is 15 μm, and the cut off wavelength is 10.5 μm at 80 K. As W_{HJ} is increased a minority carrier barrier on the n side forms and becomes larger in height, impeding collection of holes by the junction. Figure 1 plots the internal quantum efficiency at 8.6 μm and zero diode bias for two different values of donor concentration and hole Shockley-Read-Hall lifetime parameter. For both cases calculations are shown with the CdTe mole fraction in the p-type cap layer equal to 0.3 and 0.42. The quantum efficiencies for the case with higher N_d are lower overall because of the shorter hole lifetime.

Figure 2 replots the data in Figure 1 as a function of barrier height E_B. The modeling predicts that a barrier height of $2kT$ reduces hole collection from the no-barrier case by a factor of

0.95, while a $4.5kT$ barrier causes a decrease by 0.5. This is much less degradation than the naive prediction that transport across the barrier is proportional to $\exp(-E_B/kT)$, where the barrier height E_B is determined from a solution of only Poisson's equation. The simple Boltzmann expression gives much smaller degradation factors of 0.14 and 0.011. A barrier also causes the collection process to become significantly dependent on both detector bias and temperature.

The model predictions have been qualitatively confirmed by experimental measurements of x=0.42/0.23 and x=0.30/0.23 heterojunctions grown by liquid phase epitaxy from Hg solutions. These devices also used various doping concentrations to adjust the heterojunction potential barrier. The experimental and model results agree qualitatively in both the bias and temperature dependence of the collection efficiency. Figure 3 compares the calculated and measured dependence of quantum efficiency on inverse temperature where Figure 3a is for N_d=2×10^{15} cm^{-3} and 3b, 5×10^{15}. In both plots the calculations are the lines without symbols and represent various values of cap composition and grading width, while the experimental data are plotted as circles. In Figure 3a the experimental device has a cap composition of 0.3 and a base layer donor concentration of 2×10^{15} cm^{-3}, while in Figure 3b, x_{cap}=0.42 and N_d=4×10^{15}. The heterojunction grading width and barrier heights of the samples were not measured, but comparison with the simulations indicate a barrier height slightly larger than 9 meV for the lower doped case, and between 30 and 45 meV for the higher. Measurement of other heterojunction layers produced with similar techniques gives typical grading widths of 0.6 μm, in agreement with the plots of Figure 3 which imply W_{III} is between 0.4 and 0.8 μm. The modeling confirms the measured sensitive dependence of quantum efficiency on base layer doping and cap composition.

REFERENCES

[1]P. Migliorato and A. M. White, *Solid State Electronics* **26**, 65 (1983).
[2]P. R. Bratt and T. N. Casselman, *J. Vac. Sci. Technol. A* **3**, 238 (1985).
[3]F. L. Madarasz and F. Szmulowicz, *J. Appl. Phys.* **62**, 3267 (1987); **64**, 6373 (1988).
[4]Z. Yu and R. W. Dutton, *SEDAN III–A Generalized Electronic Material Device Analysis Program*, Integrated Circuits Laboratory, Stanford University, 1985 (unpublished).

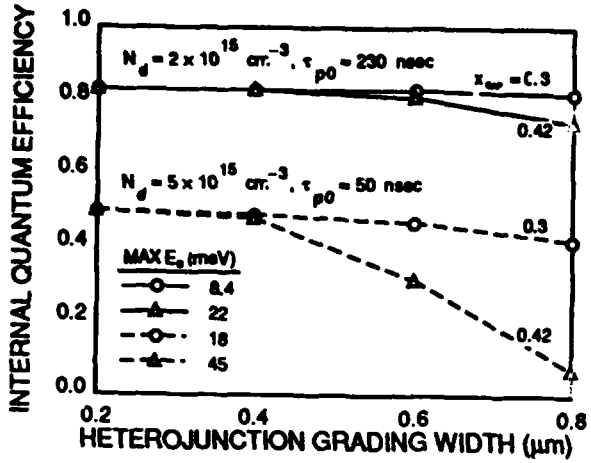

Figure 1. Dependence of internal quantum efficiency on heterojunction grading width in p^+-n HgCdTe detector as modeled in one dimension. Quantum efficiencies of the dashed curves are lower because of the lower lifetimes assumed. The legend lists the barrier heights at W_{HJ} = 0.8 μm

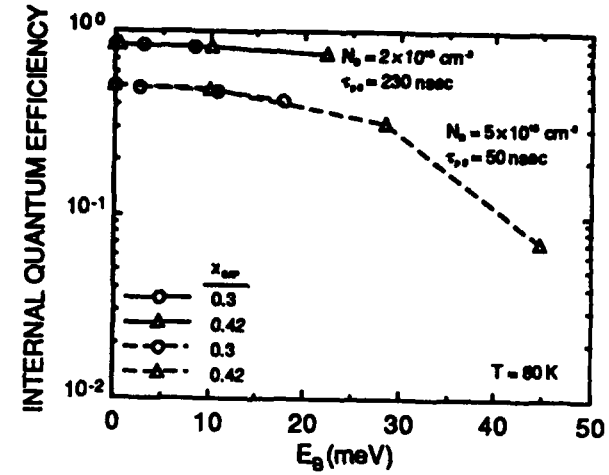

Figure 2. Internal quantum efficiency data of Figure 1 plotted as a function of heterojunction barrier height.

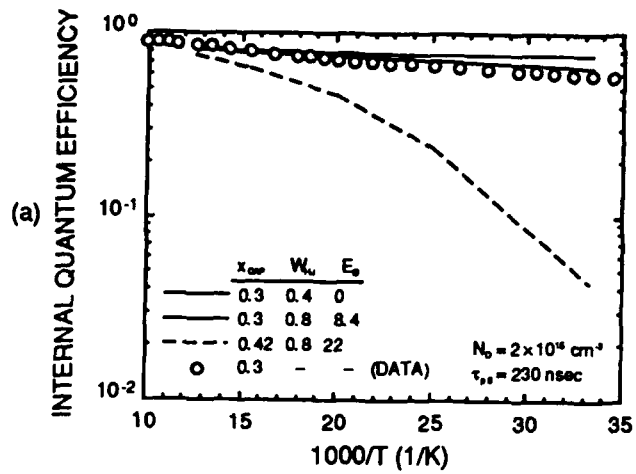

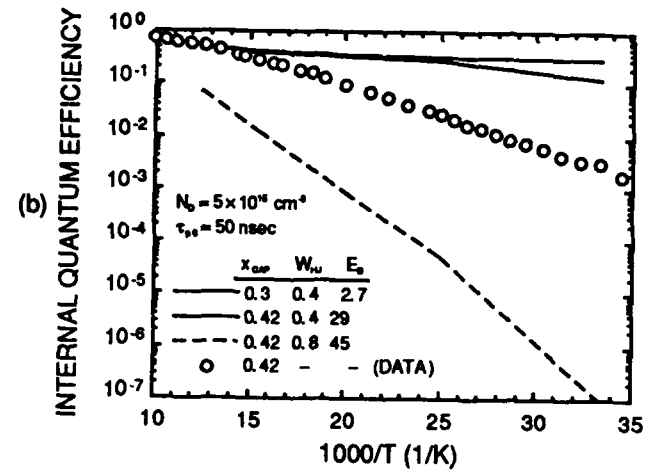

Figure 3. Dependence of internal quantum efficiency on temperature for modeled and experimental detectors with cap composition and heterojunction grading width in μm as parameters. Modeled data are lines without symbols, while experimental devices are denoted by circles. (a) $N_d = 2\times10^{15}$ cm^{-3} for calculations and experimental device. (b) $N_d = 5\times10^{15}$ cm^{-3} for calculations and 4×10^{15} for sample.

NATIVE OXIDE INTERFACES

C. R. Helms

Department of Electrical Engineering
Stanford University
Stanford, CA 94305

The properties of native oxide/semiconductor systems are of obvious importance for all semiconductor technologies in use today. The starting surface onto which devices are always fabricated invariably is composed of native oxide compounds. In a few cases, the formation of native oxide/semiconductor interfaces can lead to superior device structures--MOS devices in Si are a key example. In other cases, the native oxides formed lead to pathological behavior, such as the case for GaAs.

Restricting ourselves for the moment to insulating oxides, we ask the question: what properties of the oxides are desirable? Such properties as band gap, band line up, dielectric constant, breakdown properties, and electrically active interface defects (fixed charge and interface traps) come to mind.

Of equal, if not more, importance, however, are the chemical properties of the oxide/semiconductor system, as well as the chemical stability of the oxide in other processing environments (such as H_2O). Germanium, for example, can be oxidized much the way Si can; however, the instability of the germanium oxide in the presence of H_2O makes it unsuitable for device fabrication.

The chemical stability of the oxide semiconductor system itself is of equal importance. It is, of course, conceivable that a thermochemically unstable structure may find technological use if the reactions are slow enough. The small number of interface defects necessary to affect the electrical properties usually dictates that a stable interface is necessary, however. In GaAs, for example, it has been shown that oxidized forms of As are unstable in the presence of the Ga in GaAs via

$$As_2O_3 + GaAs \rightarrow Ga_2O_3 + 3As \quad (1)$$

forming excess As which leads to unacceptable electrically active states.[1] As first shown by Rhiger and Kvaas[2], $Hg_xCd_{1-x}Te$ can also exhibit these types of instabilities through reactions such as

$$3/2\ TeO_2 + CdTe \rightarrow CdTeO_3 + 3/2\ Te \quad (2)$$

or

$$HgTeO_3 + CdTe \rightarrow CdTeO_3 + HgTe \quad (3)$$

Looking at the right hand side of these reactions, it is clear that the reaction products can cause disastrous electrical effects.

In addition to the above chemical concepts, this paper will review the kinetics of the oxide $Hg_xCd_{1-x}Te$ reactions[3] and the dynamics of subsequently formed electrically active defects (excess Te or Hg). A discussion of the chemical basis for superior properties of sulfides and halogen based passivations will also be presented.

The author would like to acknowledge his former student, Carl Stahle, whose thesis led to many of the conclusions upon which this paper is based, as well as my colleagues from Texas Instruments, including Art Simmons, Roger Strong, Kent Carson, and Grady Roberts. This work was supported by gift funds from Texas Instruments, Inc.

References

1. C. D. Thurmond, G. P. Schwartz, G. W. Kammlott, and B. Schwartz, J. Electrochem. Soc. 127, 1366 (1980).
2. D. R. Rhiger, and R. E. Kvaas, J. Vac. Sci. Technol. A 1, 1712 (1983).
3. C. M. Stahle, C. R. Helms, and A. Simmons, J. Vac. Sci. Technol. B 5, 1092 (1987).

CHARACTERISTICS OF CHEMICALLY ETCHED HgCdTe

David R. Rhiger
Santa Barbara Research Center
75 Coromar Dr.
Goleta, CA 93117
805-562-2786

An understanding of the chemically etched surface of HgCdTe is essential, because etching is commonly used to prepare for many critical operations, including growth of another epitaxial layer, growth of a native oxide or sulfide film, deposition of metal contacts, and deposition of a dielectric film, as well as optical and electrical measurements to characterize the HgCdTe. Often the outcome may be strongly influenced by the characteristics of the etched surface.

The chemistry and physics of the HgCdTe surface are complicated because (1) it is a ternary compound; (2) the elements have dissimilar chemistries; (3) there are four oxidation states available to the Te; (4) Hg is weakly bound in oxides, sulfides, and tellurides; (5) defects migrate easily between the bulk and the surface of the HgCdTe; (6) surface defects exert a major influence on the surface chemistry; and (7) practical processes often introduce impurities to the surface. This presentation will assemble a picture of the chemically etched HgCdTe surface based on a review of the available data concerning these issues.

For example, it is known, in brief, that etching with Br_2 in an organic solvent can produce an altered surface layer more than 50 Å thick, having a modified stoichiometry and significant disorder. This layer itself should be considered as a stack of still thinner layers, each having its own thickness, composition, and degree of disorder. Before air exposure, at least three are likely. Innermost would be a layer whose principal difference from the unaltered material is a loss of Cd and an increase in point defect density. Next would be 5 to 10 Å of mostly elemental Te. Outermost would be a 5 to 15 Å carbon-rich layer composed of fragments of the solvent molecules due the attack of the Br_2 on the solvent itself. Characteristics of the altered layers, approaches to manipulate them, and applicable principles will be reviewed.

ARO 26911.1-EL-CF

MCT ATTENDEES LIST
OCTOBER 3-5, 1989
SAN DIEGO, CA

Frank W.	Adams, Jr.	Lockheed, Palo Alto, CA
Roshan L.	Aggarwal	MIT, Cambridge, MA
Jeff	Aldridge	Eagle-Picher Ind., Inc., Miami, OK
Worth P.	Allred	Galtech Semicon. Mat. Corp., Mt. Pleasant, UT
Paul M.	Amirtharaj	A(CNVEO), Ft. Belvoir, VA
Philip L.	Anderson	Texas Instruments, Dallas, TX
Jose M.	Arias	Rockwell International, Thousand Oaks, CA
Jan W.	Baars	Fraunhofer IAF, WEST GERMANY
Gad	Bahir	Technion Israel Inst. of Technology, ISRAEL
Jagmohan	Bajaj	Rockwell International, Thousand Oaks, CA
Fil J.	Bartoli	NRL, Washington, DC
Piotr	Becla	MIT, Cambridge, MA
Rudo ı G.	Benz II	Georgia Tech Research Institute, Atlanta, GA
Marcy A.	Berding	SRI International, Menlo Park, CA
Sergio S.	Bernardi	C.S.E.L.T., ITALY
Malcolm J.	Bevan	Westinghouse R&D Center, Pittsburgh, PA
Edward R.	Blazejewski	Rockwell International, Thousand Oaks, CA
Gary	Bostrup	Rockwell International, Thousand Oaks, CA
Marc	Boukerche	University of Illinois, Chicago, IL
Robert C.	Bowman, Jr.	The Aerospace Corp., Los Angeles, CA
Maurice J.	Brau	Colorado Research Laboratory, Walsenburg, CO
Robert F.	Brebrick	Marquette University, Milwaukee, WI
Kenneth W.	Brown	The Aerospace Corp., Albuquerque, NM
Lynette E.	Brown	WRDC/MLPO, Wright-Patterson AFB, OH
Margaret	Brown	Grumman Space Systems Division, Irvine, CA
Jack F.	Butler	San Diego Semiconductors, Inc., San Diego, CA
Griff	Carpenter	Emcore Corp., Somerset, NJ
Tom N.	Casselman	Santa Barbara Research Center, Goleta, CA
John-Sea	Chen	Rockwell International, Thousand Oaks, CA
Jenkon	Chen	Rockwell International, Thousand Oaks, CA
Jeffrey T.	Cheung	Rockwell International, Thousand Oaks, CA
Joan K.	Chia	Santa Barbara Research Center, Goleta, CA
Muren	Chu	Fermionics Corp., Simi Valley, CA
Gidon	Cinader	Soreq Nuclear Research Center, ISRAEL,
Eun-Hee	Cirlin	Hughes Research Labs, Malibu, CA
Donald E.	Cooper	Rockwell International, Thousand Oaks, CA
William J.	Dateno	A(CNVEO), Ft. Belvoir, VA
Brian E.	Dean	II-VI, Inc., Saxonburg, PA
Robert L.	Denison	WRDC/MLPO, Wright-Patterson AFB, OH
Neil F.	Deutscher	Arizona State University, Tempe, AZ
Roger E.	DeWames	Rockwell International, Thousand Oaks, CA
Ron S.	Dickson	Monash University, AUSTRALIA
David L.	Dreifus	North Carolina State University, Raleigh, NC

Carolyn B.	Dubberley	Texas Instruments, Dallas, TX
Dennis D.	Edwall	Rockwell International, Thousand Oaks, CA
Jerry	Elkind	Texas Instruments, Dallas, TX
James	Elliott	Raytheon Co., Lexington, MA
Richard M.	Fastow	Technion Israel Inst. of Technology, ISRAEL
Jack K.	Furdyna	Notre Dame University, Notre Dame, IN
Edward R.	Gertner	Rockwell International, Thousand Oaks, CA
Sorab K.	Ghandhi	Rensselaer Polytechnic Institute, Troy, NY
Nancy C.	Giles	West Virginia University, Morgantown, WV
Arvid	Goldberg	Martin Marietta Labs, Baltimore, MD
Michael W.	Goodwin	Texas Instruments, Dallas, TX
Neil T.	Gordon	RSRE, UNITED KINGDOM
Ronald D.	Graft	A(CNVEO), Ft. Belvoir, VA
Gordon H.	Griffith	AFWAL, Wright-Patterson AFB, OH
Theodore C.	Harman	MIT Lincoln Lab, Lexington, MA
Karl A.	Harris	General Electric Co., Syracuse, NY
Richard H.	Hartley	Def. Science & Tech. Organ., SO. AUSTRALIA
William G.	Hatton	The Aerospace Corp., Los Angeles, CA
James E.	Hawkey	Keystone Crystal Corp., Butler, PA
Tony	Heim	Johnson Matthey Electronics, CANADA
C. R.	Helms	Stanford University, Stanford, CA
John	Hennessy	Waterloo Scientific, CANADA
Craig A.	Hoffman	NRL, Washington, DC
Yu	Huang	NASA Langley Research Center, Hampton, VA
Cho	Huang	Santa Barbara Research Center, Goleta, CA
Stuart J.	Irvine	RSRE, UNITED KINGDOM
John E.	Jensen	Hughes Research Labs, Malibu, CA
Scott	Johnson	Santa Barbara Research Center, Goleta, CA
Colin E.	Jones	Santa Barbara Focalplane, Goleta, CA
Leon Y.	Juravel	Rockwell International, Anaheim, CA
Holger	Jurgensen	Aixtron GmbH, WEST GERMANY
Murray H.	Kalisher	Hughes Aircraft Co., Goleta, CA
Sanjiv G.	Kamath	Hughes Research Labs, Malibu, CA
Nasser H.	Karam	Spire Corp., Bedford, MA
James J.	Kennedy	A(CNVEO), Ft. Belvoir, VA
Stephen W.	Kennerly	A(CNVEO), Ft. Belvoir, VA
Donghwan	Kim	Stanford University, Stanford, CA
Young	Kim	AT&T Bell Labs, Holmdel, NJ
Jae-Mook	Kim	Agency for Defence Development, KOREA
Michael A.	Kinch	Texas Instruments, Dallas, TX
David E.	Koegel	A(CNVEO), Ft. Belvoir, VA
Toivo	Koehler	New England Research Center, Sudbury, MA
Roland J.	Koestner	Texas Instruments, Dallas, TX
Ralph	Korenstein	Raytheon Co., Lexington, MA
Kenneth	Kosai	Santa Barbara Research Center, Goleta, CA
Albert	Koury	Emcore Corp., Somerset, NJ
Vilnis	Kreismanis	Raytheon Co., Lexington, MA

V.	Krishnamurthy	Stanford University, Stanford, CA
Eric E.	Krueger	Honeywell EOD, Lexington, MA
Martha R.	Krueger	Honeywell EOD, Lexington, MA
Daniel	Laser	Ministry of Defence, ISRAEL
Seung Bae	Lee	Stanford University, Stanford, CA
Myung B.	Lee	Grumman, Bethpage, NY
Sang-Don	Lee	Agency for Defence Development, KOREA
Lee	Li	Johnson Matthey Electronics, CANADA
Long-Xia	Li	Cleveland Crystals, Inc., Cleveland, OH
Lawrence	Lichtmann	Aerojet Electrosystems, Azusa, CA
Chris L.	Littler	University of North Texas, Denton, TX
Dennis S.	Lo	Rockwell International, Thousand Oaks, CA
Dieter J.	Lohrmann	A(CNVEO), Ft. Belvoir, VA
Vincent C.	Lopes	Texas Instruments, Dallas, TX
Terry	Lovis	Aixtron, Inc., Wilsonville, OR
Stian	Lovold	Norwegian Defence Res. Est., NORWAY
Jeremiah R.	Lowney	NIST, Gaithersburg, MD
J. D.	Luttmer	Texas Instruments, Dallas, TX
Paul	Mackett	Philips Components Ltd., UNITED KINGDOM
K. K.	Mahavadi	University of Illinois, Chicago, IL
James O.	McCaldin	CALTECH, Pasadena, CA
Paul A.	McDonald	Honeywell EOD, Lexington, MA
Thomas C.	McGill	CALTECH, Pasadena, CA
Philip E.	McGraw	Morton International, Alta Loma, CA
William V.	McLevige	Rockwell International, Thousand Oaks, CA
Salini	Menezes	Rockwell International, Thousand Oaks, CA
Jerry R.	Meyer	NRL, Washington, DC
Caroline G.	Morgan-Pond	Wayne State University, Detroit, MI
Natalija	Nabajova-Gabain	SCD Semiconductor Devices, ISRAEL
Yael	Nemirovsky	Technion Israel Inst. of Technology, ISRAEL
Peter Q.	Ngo	Fermionics Corp., Chatsworth, CA
Donald R.	Nichols	II-VI, Inc., Saxonburg, PA
Paul R.	Norton	Santa Barbara Research Center, Goleta, CA
Ryoicho	Ohno	Stanford University, Stanford, CA
Joseph P.	Omaggio	NRL, Washington, DC
Peter J.	Orders	Def. Science & Tech. Organ., SO. AUSTRALIA
Geoff N.	Pain	Telecom Australia Research Labs, AUSTRALIA
John G.	Pasko	Rockwell International, Thousand Oaks, CA
Libby A.	Patten	Santa Barbara Research Center, Goleta, CA
Michel	Picault	Instruments SA, Inc., Edison, NJ
Dennis L.	Polla	University of Minnesota, Minneapolis, MN
Paul M.	Raccah	University of Illinois, Chicago, IL
Alan D.	Raisinen	University of Minnesota, Minneapolis, MN
Emmanuil	Raiskin	San Diego Semiconductors, Inc., San Diego, CA
Damodaran	Rajavel	Georgia Tech Research Institute, Atlanta, GA
Gregory B.	Raupp	Arizona State University, Tempe, AZ
John L.	Reno	Sandia National Labs, Albuquerque, NM

Keith E.	Ritala	Johnson Matthey Electronics, Spokane, WA
C. Grady	Roberts	Texas Instruments, Dallas, TX
Ronald J.	Roedel	Arizona State University, Tempe, AZ
Jeffrey E.	Roller	Texas Instruments, Dallas, TX
William H.	Rolls	Infrared Associates, Cranbury, NJ
John A.	Roth	Hughes Research Labs, Malibu, CA
David G.	Ryding	Mercury LPE Co., Inc., Cheswick, PA
Herbert F.	Schaake	Texas Instruments, Dallas, TX
Samuel E.	Schacham	NASA Lewis Research Center, Cleveland, OH
Rolf	Schettler	Preussag Pure Metals GmbH, WEST GERMANY
Jan E.	Schetzina	North Carolina State University, Raleigh, NC
Thomas R.	Schimert	LTV Missiles & Electronics Group, Dallas, TX
William A.	Schmidt	NRL, Washington, DC
Joseph L.	Schmit	Honeywell EOD, Lexington, MA
Joel N.	Schulman	Hughes Research Labs, Malibu, CA
Susan K.	Scott	Eagle-Picher Ind., Inc., Miami, OK
David G.	Seiler	NIST, Gaithersburg, MD
Robert L.	Seliger	Hughes Research Labs, Malibu, CA
Curt	Shannon	Johnson Matthey Electronics, Spokane, WA
Ariel	Sher	Soreq Nuclear Research Center, ISRAEL
Arden	Sher	SRI International, Menlo Park, CA
Ilan	Shilo	SCD Semiconductor Devices, ISRAEL
Soo H.	Shin	Rockwell International, Thousand Oaks, CA
Lee R.	Shiozawa	Cleveland Crystals, Inc., Cleveland, OH
S.	Sivananthan	University of Illinois, Chicago, IL
Mark R.	Skokan	Texas Instruments, Dallas, TX
Lesley M.	Smith	GEC Hirst Res. Center, UNITED KINGDOM
I. K.	Sou	University of Illinois, Chicago, IL
William E.	Spicer	Stanford University, Stanford, CA
John E.	Stannard	Santa Barbara Research Center, Goleta, CA
David A.	Stevenson	Stanford University, Stanford, CA
Roger L.	Strong	Texas Instruments, Dallas, TX
Sang-Hee	Suh	Korea Inst. of Science & Tech., KOREA
Chris J.	Summers	Georgia Tech Research Institute, Atlanta, GA
A. J.	Syllaios	Texas Instruments, Dallas, TX
Hiroshi	Takigawa	Fujitsu Laboratories Ltd., JAPAN
Yoshiteru	Taniguchi	Nippon Mining Co., Ltd., Cupertino, CA
William E.	Tennant	Rockwell International, Thousand Oaks, CA
Sevag	Terterian	Fermionics Corp., Simi Valley, CA
James E.	Thomas	Eagle-Picher Ind., Inc., Miami, OK
Gary S.	Tompa	Emcore Corp., Somerset, NJ
John J.	Vajo	Hughes Research Labs, Malibu, CA
Istvan K.	Varga	Def. Science & Tech. Organ., SO. AUSTRALIA
John T.	Viola	Rockwell International, Thousand Oaks, CA
Honnavalli	Vydyanath	Aerojet Electrosystems, Azusa, CA
Robert J.	Wagner	NRL, Washington, DC
Brent K.	Wagner	Georgia Tech Research Institute, Atlanta, GA

Anita	Wahi	Stanford University, Stanford, CA
James R.	Waterman	NRL, Washington, DC
Margaret H.	Weiler	Honeywell EOD, Lexington, MA
Eliezer	Weiss	Stanford University, Stanford, CA
Marc	Wigdor	Nichols Research Corp., Vienna, VA
George M.	Williams	Rockwell International, Thousand Oaks, CA
Horst	Wittmann	AFOSR, Washington, DC
Owen K.	Wu	Hughes Research Labs, Malibu, CA
Zhi-Yu	Yang	North Carolina State University, Raleigh, NC
Takafumi	Yao	Electrotechnical Laboratory, JAPAN
Keon-Ho	Yoo	MIT, Cambridge, MA
Eric R.	Youngdale	NRL, Washington, DC
John P.	Ziegler	Rockwell International, Anaheim, CA
Peter H.	Zimmerman	Honeywell EOD, Lexington, MA
Ricardo	Zucca	Rockwell International, Thousand Oaks, CA
Alex	Zunger	SERI, Golden, CO